Detailed Analysis of Recent Acoustic Reflection Data on the Texas Shelf

Authors:
Carson Miller
John A. Goff
Sean P.S. Gulick
Christopher M. Lowery

U.S Department of the Interior
Bureau of Ocean Energy Management
Marine Minerals Program
Gulf of Mexico Regional Office

DISCLAIMER

REPORT AVAILABILITY

To download a PDF file of this report, go to the U.S. Department of the Interior, Bureau of Ocean Energy Management Marine Minerals Program Marine Minerals Resource Evaluation Research webpage (https://www.boem.gov/marine-minerals/marine-mineral-research-studies/marine-mineral-resource-evaluation-research) and use the Browse Library tools to search report title, region (state), or year.

CITATION

Miller, CB, Goff, JA, Gulick, SPS, Lowery, CM (UTIG, Austin, TX). 2024. Detailed Analysis of Recent Acoustic Reflection Data on the Texas Shelf. Austin, TX: U.S. Department of the Interior, Bureau of Ocean Energy Management. 64 p. Agreement No.: M22AC00008.

ACKNOWLEDGMENTS

Contents

List of Figures

List of Tables

List of Abbreviations and Acronyms

BOEM	Bureau of Ocean Energy Management
BP	Before Present
CEPRA	Coastal Erosion Planning and Response Act for the State of Texas
GLO	General Land Office of Texas
GMT	Generic Mapping Tools
ky	Kilo-years
LGM	Last Glacial Maximum
MIS	Marine Isotope Stage
ms	Milliseconds
NOAA	National Oceanic and Atmospheric Administration
OCS	Outer Continental Shelf
RESTORE	Resources and Ecosystem Sustainability, Tourist Opportunities, and Revived Economies
TWT	Two-Way Traveltime
TT	Time Thickness
USGS	United States Geological Survey
UTIG	University of Texas Institute for Geophysics

1   Introduction

This report details work conducted by the University of Texas Institute for Geophysics (UTIG) utilizing RESTORE (Resources and Ecosystem Sustainability, Tourist Opportunities, and Revived Economies) Act funding provided by the Bureau of Ocean and Energy Management (BOEM). This overall project was comprised of two separate efforts. The first sought to reconcile a number of discrepancies that have been discovered between core data bases compiled by UTIG and the Texas General Land Office (GLO). These discrepancies are inherent in data mining projects and their existence provides an opportunity to identify issues with these processes and formulate better protocols in the future. This work directly benefitted BOEM interests by improving the accuracy of database records for marine mineral identification and classification as well as improve data available through TXSed, the GLO's state database. The core reconciliation effort was concluded earlier in the project timeline, and was detailed in a separate report to BOEM (https://www.boem.gov/sites/default/files/mm-research/2023-10/M22AC00008_Core_Reconciliation_Report_FINAL.pdf).

The second component of this project, and the subject of this report, sought to conduct a detailed stratigraphic interpretation and analysis, using available chirp and sparker data (Figure 1.1), in the outer Trinity River and Sabine River paleovalleys, as well as Sabine, Heald and Shepard Banks. As part of cooperative agreement M16AC00020 (https://www.boem.gov/sites/default/files/mm-research/2022-10/BOEM_2022-035_rpt_02.pdf) and GLO CEPRA (Coastal Erosion Planning and Response Act) project 1706/BOEM M21AC00005 (https://www.boem.gov/sites/default/files/mm-research/2024-06/TGLO_OCS_Central_508_FinalReport_Rev3.pdf), these regions were surveyed at ~1 nm track spacing. In 2020, APTIM , with ~1100 nm of chirp track line, focused on the Sabine, Heald and Shepard banks but also covered major portions of the Sabine River paleovalley (Figure 1.1). The 2021, UTIG focused survey and analysis on the outer Trinity River paleovalley and confluence with the Sabine River paleovalley, connecting with the APTIM survey (Figure 1.1). It included ~260 nm of chirp data and ~180 nm of sparker data, as well as 3 successful cores. Major sedimentary units were mapped as part of a preliminary, or "first order" regional stratigraphic interpretation. These included: total valley fill (Figure 1.2), Heald/Shepard bank unit (Figure 1.3), and Sabine Bank unit (Figure 1.4). The internal stratigraphic structure of these units is complex and records a rich sedimentary history of response of both the sand banks and estuarine valleys to past sea level rise and shoreline retreat. The prior preliminary interpretation did not investigate these important details of the sedimentary record; the existing data are thus in need of a far more thorough stratigraphic interpretation and analysis than has been accomplished thus far. Specifically, key questions involve the origin of these sand bodies (marine sand sheets from after the shoreline transgressed or drowned barrier islands) to assess resource utilization, any archeological assessments needed, and identification of geological and geophysical characteristics that identify origins of these sand bodies and processes that lead to barrier island submergence. The results will have direct relevance to BOEM interests and stakeholders in the State of Texas in seeking to identify new potential sand resources on the outer continental shelf as well as conduct research into formation, modification, and ultimate preservation of these mineral resources on continental shelves.
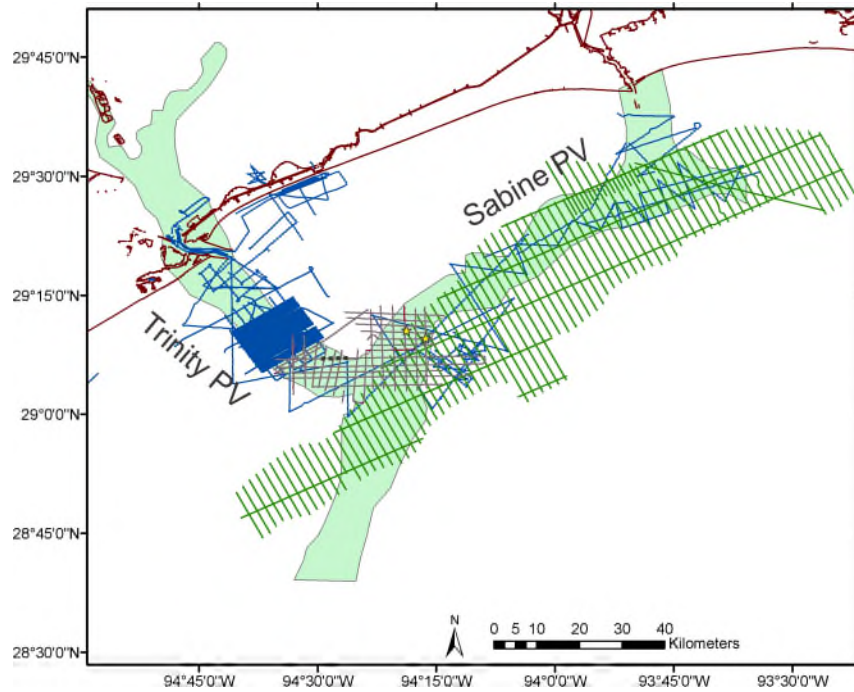
Figure 1.1 Chirp and sparker track locations
APTIM (green) and UTIG (gray) chirp track lines in the OCS area collected in 2021. Sparker track lines are a subset of the UTIG chirp lines. Blue lines indicate prior UTIG chirp data. Green shaded area is location of Trinity and Sabine paleovalleys (PVs) as mapped by Thomas and Anderson (1994).
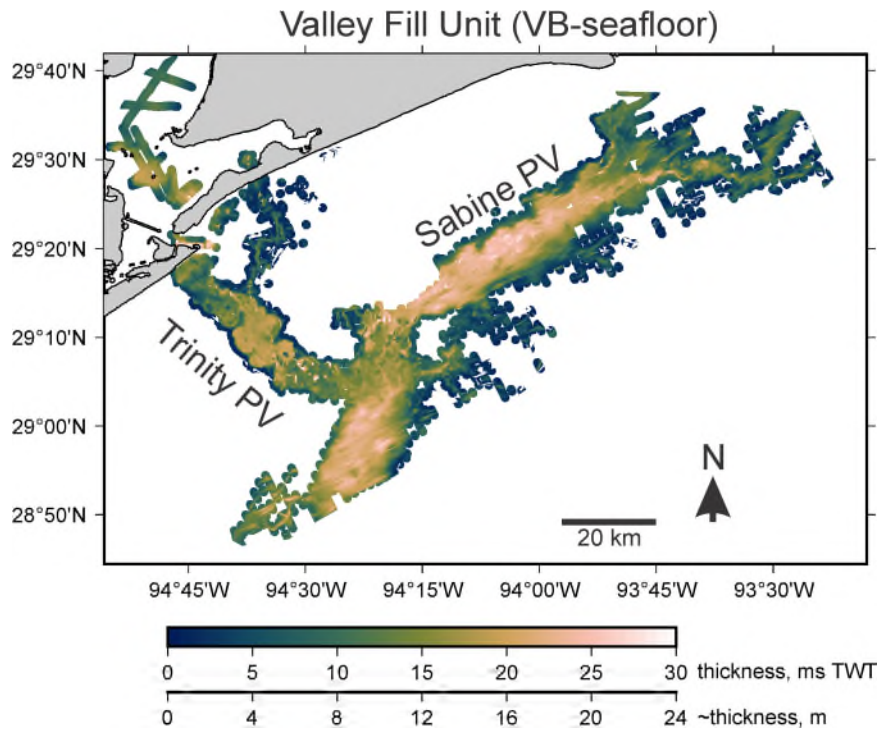
Figure 1.2. Isopach map of the valley fill unit
Preliminary isopach map of the valley fill unit (seafloor to the top of the fluvial section) of Trinity and Sabine River paleovalleys, along with important tributaries, based on new and archival data in both State and Federal waters.
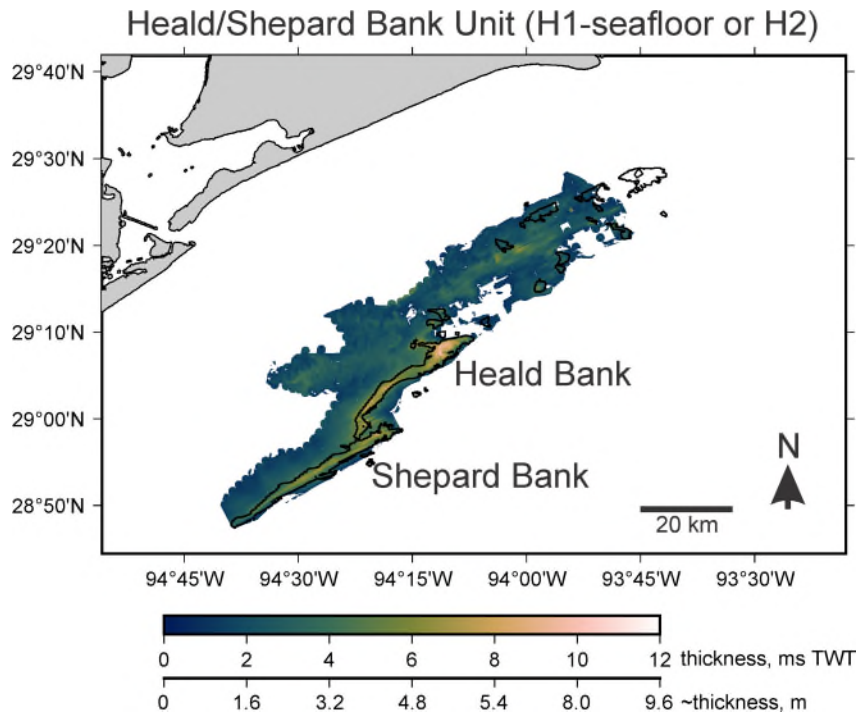
Figure 1.3. Isopach map of the Heald/Shepard Bank unit
Preliminary isopach map of Heald/Shepard Bank unit over the APTIM/UTIG survey areas. Black outlines indicate extent of modeled shoals by Pickens et al. (2021) based on topographic considerations.
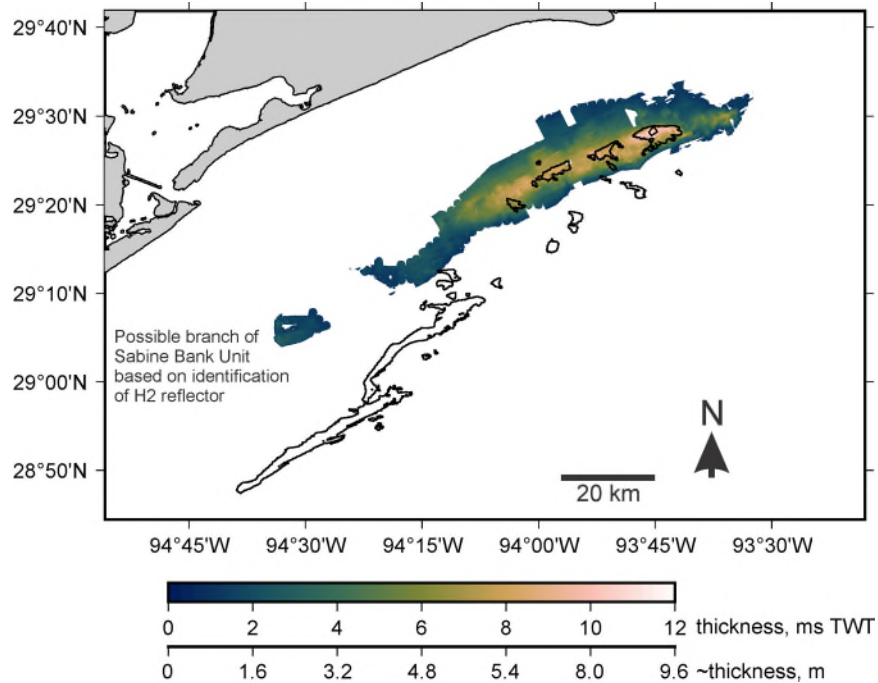
Figure 1.4. Isopach map of the Sabine Bank unit
Preliminary isopach map depicting the full extent of the Sabine Bank unit over the APTIM/UTIG survey areas. Black outlines indicate extent of modeled shoals by Pickens et al. (2021) based on topographic considerations.

2 Stratigraphic Analysis of Texas Sand Banks

2.1 Introduction

Barrier islands comprise ~10% of the global shorelines, protecting low-lying coastal regions from sea-level rise and storms (Stutz and Pilkey, 2011). Accommodation, or the space available for sediment accumulation (Jervey, 1988), and sediment supply force barrier islands to evolve and migrate over centennial to millennial time scales. Antecedent lows, subsidence, and sea-level rise can increase accommodation, whereas longshore currents, tides, storms, and climate change alter sediment supply (Jervey 1988; Milliken et al., 2008a; Simms et al., 2013; Milliman and Syvitski, 1992; Fruergaard et al., 2015). Sediment supply decreases through bypassing longshore currents or reducing fluvial input during climatic changes (Nordt et al., 1994; Toomey et al., 1993). Three patterns of barrier island evolution have been recognized, based on the direction of barrier movement: aggradation (vertical, stable, or no movement), transgression (landward movement), and regression (seaward movement; Galloway and Hobday, 1983). Transgression typically occurs when the island migrates landward, decreasing the barrier width and ultimately causing drowning if sediment supply is less than accommodation (Emery et al., 2019; Cooper et al., 2016; Galvão et al., 2023; Lorenzo-Trueba and Ashton, 2014; Nichols, 1989; Fisher, 1961; Swift 1975).

Barrier islands are typically not preserved on continental shelves nor in the geologic record, because these landforms usually keep up with sea-level rise by migrating landward, via backstepping (e.g., Thorne et al., 1991). Thus, rare occurrences of a drowned barrier island or associated facies present important opportunities to examine the processes and conditions (accommodation and sediment supply) that lead to preservation of these sediments on the continental shelf. Here we report on stratigraphic analysis of Heald and Sabine Banks, located on the east Texas continental shelf, based on high-resolution chirp sub-bottom data collected from multiple cruises between 2008 and 2021 (Figure 2.1). These banks were hypothesized first to be post-transgressive marine deposits (Thomas and Anderson, 1994), and then later to be drowned barrier island remnants (Rodriguez et al., 2004). This project provides a valuable case study to examine under what conditions a barrier island or related sediments can be preserved in the geologic record, enabling improved ability to observe coastal sedimentary systems dynamics during sea-level rise and storm impacts. We seek to understand (1) the internal seismic stratigraphy that can be used to identify paleo-barrier island associated facies in the geologic record, and (2) determine the conditions that are conducive to barrier island or barrier island remnant drowning and preservation. The high-resolution seismic imaging, paired with previously published core stratigraphy can greatly improve identification of coastal facies that can be used to establish regional and local processes responsible for coastal change.

Offshore sand bodies are also potentially valuable resources for shoreline restoration projects, which will be increasingly more important as sea-level rise and storms continue to threaten vulnerable coastal populations, as barrier islands are the first line of coastal defense against these hazards. Understanding the nature of these deposits is essential for evaluating their sand resource potential. Mapping and evaluating sand bodies on the continental shelf was a primary goal for this project. 80% of the Texas coast is considered critically eroding (Coastal Erosion Planning and Response Act, 2020-2021), and a comprehensive plan with multiple lines of defense has been constructed by the Texas General Land Office (GLO) alongside the Federal government to minimize storm impacts, like erosion of the coast and surge flooding and damage (Texas Coastal Resiliency Master Plan, 2023). Within this plan, ecosystem restoration will be implemented to control erosion on both the Gulf and bay shorelines by adding sand to the beach front of degrading islands, as well as restoring existing dunes and constructing a second dune line and planting vegetation to provide a buffer during hurricanes and winter storms. These projects require a large volume of sand that is costly to supply from terrestrial sources (Jones and Mangun, 2001;

Dobkowski, 1998). Heald and Sabine banks are both potential sand resources because these deposits are easily accessible at the seafloor; if both banks are remnant barrier islands (Rodriguez et al., 2004), they could contain sand that is close in grain size, composition, and color to modern day beaches.
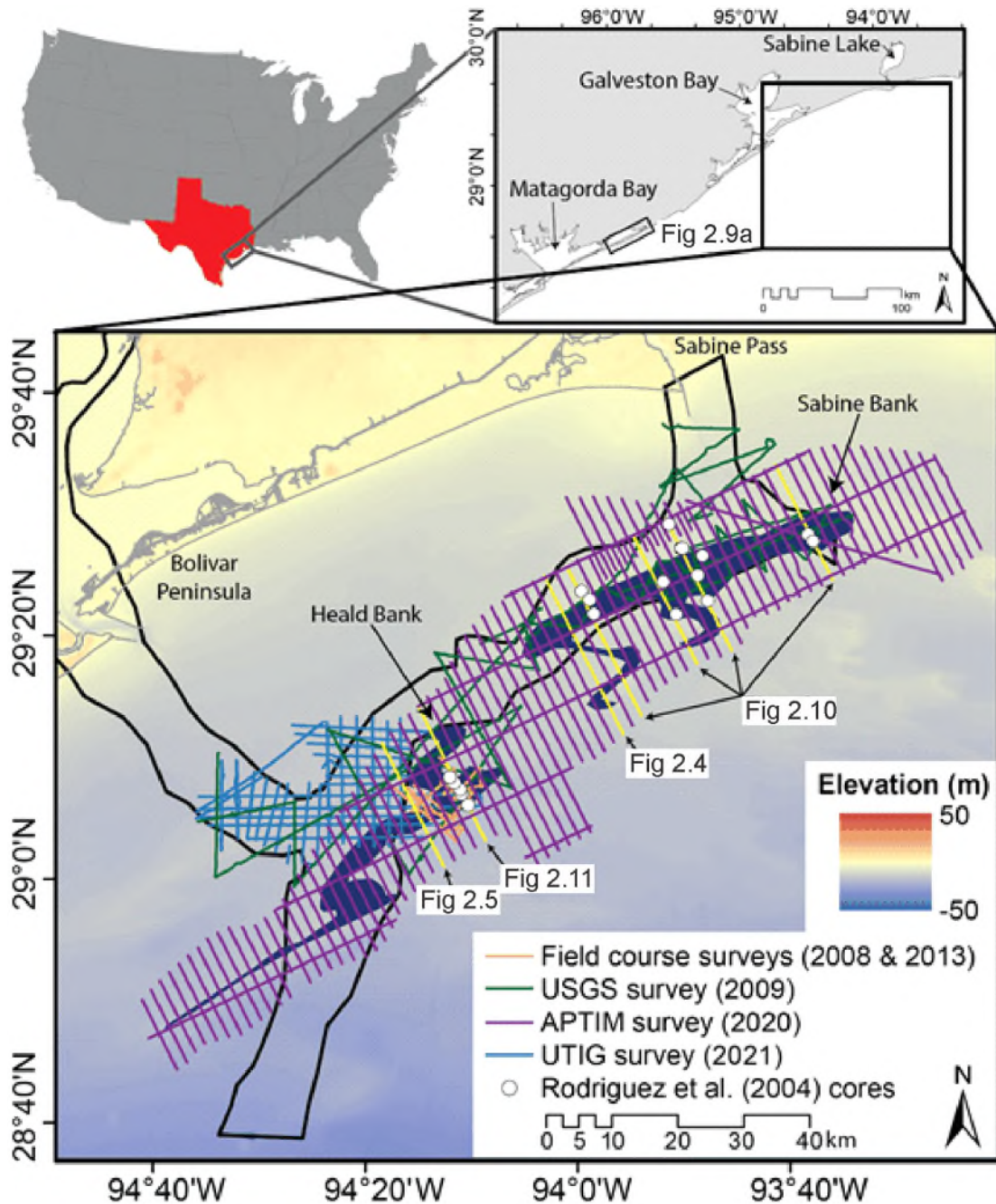
Figure 2.1. Location of Field Area

Study area map of the Trinity-Sabine incised valley extent, chirp surveys, and Rodriguez et al. (2004) core locations. The black outline is the paleo-Trinity-Sabine River valley from Thomas and Anderson (1994). The dark blue polygons show the extent of Heald Bank to the south and Sabine Bank to the NE. Background elevation data was obtained from: https://www.gmrt.org/GMRTMapTool/.Yellow lines are figure locations as indicated.

2.2 Study Area

2.2.1 Coastal Geologic Setting

The paleo-Sabine River valley, on the northeast Texas continental shelf (Figure 2.1), exhibits a basic infilling sequence of fluvial sands overlain by estuarine and finally open marine deposits (Anderson et al., 2008). The dominant antecedent topography on the east Texas shelf is the Sabine River marine isotope stage (MIS) 2 paleovalley, which has a shore-parallel orientation adjacent to Sabine Bank and has been thought to provide accommodation for the paleo-barrier island remnant sediments of the bank (Rodriguez et al., 2004). Additionally, shallow sediment compaction of the estuarine sediments, typically organic rich, can increase local accommodation within the valley; in some areas, accommodation increases 10% of the total sediment thickness (Simms et al., 2013; Paul and Barras, 1998).

The east Texas coast also consists of a lower shelf gradient than the rest of the state (Rodriguez et al., 2001). Shelf gradients impact transgression based on the amount of back barrier accommodation that sediments would need to infill (Rodriguez et al., 2001). Low shelf gradients have longer transgression distances and more back-barrier accommodation than higher shelf gradients (Shawler et al., 2020). While the low gradient might make barrier island survival more difficult, it could also provide enough accommodation for preservation of barrier island related facies.

2.2.2 Sea-level History

Sea-level on the Texas coast fluctuated throughout the Holocene and Pleistocene. Between MIS5, the last interglacial period ~ 120 ka, and MIS2, the Last Glacial Maximum (LGM) ~20 ka, sea-level fell ~120 m (Shepard, 1956). During this period, rivers along the Texas coast incised the continental shelf and terminated near the present-day shelf break (Anderson et al., 2016). At the beginning of the Holocene, the sea-level curve shows rapid, episodic rise (4.2 mm/yr), which slowed to a more continuous rise during the middle (7,000-4,000 years BP; 1.4 mm/yr) to late (4,000-100 years BP; 0.4-0.6 mm/yr) Holocene (Milliken et al., 2008a). Modern rates of sea level rise are substantially higher than sea-level rise rates during the late Holocene. Globally, tide gauge and satellite records document an acceleration in the sea-level rise rate since the 20th century, from an average of ~1.4 mm/yr to the current rate of ~4.0 mm/yr (Oppenheimer et al., 2019; Wang et al., 2021). Along the Gulf Coast, the rate was approximately 10.0 mm/yr during the last decade (Dangendorf et al., 2023; Yin, 2023). These changes in modern sea-level rise rates have led to a Gulf-wide increase in rates of shoreline retreat relative to the past ~5 ka (Anderson et al., 2023).

2.2.3 Sediment Supply: Longshore Currents

Sediment supply also varies along the Texas coast and is influenced by longshore currents (Watson, 1968). The east Texas shelf has higher wave and current energy than elsewhere in the state, driven by strong predominately southeast winds interacting with the shoreline orientation. High angle waves cause excess erosion and longshore currents transport sediment from the east and south towards the central Texas coast (McGowen et al., 1977).

2.2.4 Sediment Supply: Fluvial Sources

Sediment supply to the coast operates on both short (yearly to decadal time scales) and long (centennial to millennial) time scales. Changes in fluvial input are driven by changes in climate, like precipitation and storminess; watershed characteristics, like slope and relief; and underlying lithology (Milliman and Syvitski, 1992). During warm/dry periods fluvial input decreased as there was less runoff bringing sediment into the watershed that propagates downstream (Fraticelli, 2006; Weight et al., 2011). Prior to

3500 yBP, sedimentation rates in Calcasieu and Sabine Lakes kept pace with sea-level rise, indicating an overfilled valley with an abundance of sediment (Milliken et al., 2008b, Milliken et al., 2008c; Simms et al., 2006).

The Mississippi River transports terrigenous sediment that dominates the Texas-Louisiana-Mississippi shelf and the average discharge across the Holocene has not significantly changed (Doyle and Sparks, 1980; Van Andel and Poole, 1960; Roberts, 1997). Fine grained sediment from the Mississippi River has been found as far west as the south Texas coast (Basalm and Beeson, 2003). Around 90% of the annual sediment discharge from the Mississippi is fine sand (Roberts, 1997). Adams et al. (1984) showed very fine sand could be transported during cold fronts towards the ESE and offshore, however during mean flows, sediment moved westward with the direction of longshore transport (McGowen et al., 1977). Galveston Island is composed of a relatively large proportion of Mississippi River sand (Cole and Anderson, 1982).

Over the past ~7 ky, the Mississippi has built 6 major delta complexes and 18 subdeltas (Frazier, 1967; Penland et al., 1988; Coleman et al., 1998; Roberts, 1997). These delta complexes have a regressive phase where the delta rapidly builds into the estuary, supplying locally eroding environments with sediment (Roberts, 1997; Coleman et al., 1998; Penland et al., 1988). Once discharge begins decreasing because of the infilling of the basin with sediment, the delta goes into an abandonment phase (Roberts, 1997; Penland et al., 1988). During this phase, the delta loses fluvial input and subsides, and marine processes begin reworking the sandy delta front (Roberts, 1997; Penland et al., 1988). These large delta complex cycles operate on a ~1-2 ky time scale, whereas the smaller subdeltas operate over 150-200 years (Roberts, 1997; Coleman, 1998). For example, local shorelines downdrift of the Atchafalaya River delta experienced growth as the delta was prograding (Roberts, 1998).

2.3 Methods

2.3.1 Seismic Data Collection

This study is based primarily on analysis of ~3260 km of 2D high resolution acoustic chirp data gathered during four different surveys over the Texas sand banks and the Trinity and Sabine paleovalleys (Figure 2.1). These surveys include: (1) ~2040 km of data collected by APTIM in 2020 under contract to the Texas GLO and BOEM (M21AC00005; https://www.boem.gov/sites/default/files/mm-research/2024-06/TGLO_OCS_Central_508_FinalReport_Rev3.pdf), with 1 nm line spacing in a shore-normal orientation, with several more widely spaced shore-parallel tracks acquired as crossing lines (Figure 2.1); (2) ~620 km of data collected by the United States Geologic Survey (USGS) and Texas A&M Galveston over Sabine and Heald banks in multiple diagonal cross-cutting orientations, collected in 2009 (Forde et al., 2010; https://pubs.usgs.gov/ds/526/); (3) ~480 km of data collected by the University of Texas Institute for Geophysics (UTIG) in 2021 over a ~1.9 km (1 NM) grid; (BOEM Coop M16AC00020 (https://www.boem.gov/sites/default/files/mm-research/2022-10/BOEM_2022-035_rpt_02.pdf) and (4) ~126 km of data, oriented primarily shore-perpendicular, collected in 2008 and 2013 as part of the University of Texas Marine Geology and Geophysics field courses (data archived with the Academic Seismic Portal; https://www.marine-geo.org/collections/#!/collection/Seismic#summary. The APTIM, USGS, and field course chirp data were collected using an Edgetech 512i sub-bottom profiler using a 20 ms, 0.7-12 kHz swept-frequency pulse, whereas the UTIG survey used an Edgetech 216s with a 20 ms, 2-10 kHz pulse. Both envelope and full-waveform data were recorded for all lines for the APTIM and field course surveys, whereas only envelope data were recorded for the USGS and UTIG surveys. Full-waveform data are higher in vertical resolution at ~10 cm, and include both positive and negative amplitudes, which is useful for viewing the detailed internal stratigraphy of sediment packages. Envelope

data are a derivative of the full-waveform record and only include positive amplitudes but are useful for looking at regional patterns of stratigraphy.

2.3.2   Seismic Data Processing

Chirp data processing, described in detail in Saustrup et al. (2019), was conducted using Paradigm Echos software. Corrections were made for tow depth, and heave, and a layback correction was applied to the navigation. Additional processing of the full waveform data included a secondary deconvolution, using the seafloor return as a proxy for the source, to correct for inaccuracies in the initial match-filtering performed in the chirp topside. This processing resulted in sharper seismic reflections resolved at a decimeter scale. Seismic interpretation was performed with Landmark DecisionSpace software. A static mis-tie correction was also applied using the seafloor, which empirically corrects for tidal variations. While this correction helped align the seafloor across the four surveys, the merged surveys still contain slight offsets from differences in vertical resolution of the full-waveform and envelope data. The offset can still be seen in some structure maps presented here and should be disregarded.

2.3.3   Seismic Data Interpretation

Seismic facies were classified based on geometry and reflection amplitude and may be present in multiple units. After identifying the facies present, we interpreted seismic horizons that are laterally continuous and thus mappable as well as horizons observed to bound distinct seismic facies or groups of facies. For example, a single, high-amplitude, continuous reflection could define a horizon, or a horizon could designate the boundary between a facies consisting of low-amplitude horizons, and a facies consisting of high-amplitude horizons. Amplitude, geometry, continuity, and stratigraphic position helped define seismic horizons. Once horizons and seismic facies were identified, horizons were used as upper and lower bounds of sedimentary units and subunits. Within each unit, observed facies helped characterize and identify coastal and marine environments that the units represent.

Horizons were converted into time-structure maps and units were turned into gridded time-thickness maps using a combination of Python and Generic Mapping Tools (GMT) scripts. This process involved interpolating between tracks using a triangulation algorithm and an 800 m grid cell size, while masking any parts of the resulting grid that exceeded 600 m from any data control point. Time-thickness (TT), or isopach maps were created by subtracting the two-way traveltime (TWT) in milliseconds of the bottom from the TWT of the top boundaries for each unit.

2.3.4   Core-Seismic Integration

Stratigraphy, depositional environment, and age can be correlated to the seismic horizons and units using radiocarbon dates and sedimentological analysis from cores taken on Heald and Sabine banks (Rodriguez et al., 2004). We recalibrated the radiocarbon ages from Rodriguez et al. (2004) using CALIB 8.20 (Stuiver and Reimer, 1993). We used the Marine20 calibration curve for all marine species reported in Rodriguez et al. (2004) and the IntCal20 curve for the 2 peat samples. Core penetration depths and contact depths were converted to TWT using 1,525 m/s as a conversion, which assumes no variation in velocity with depth (Abdulah et al., 2004). Variation in the velocity likely exists, however we do not account for it in our estimations. The TWT of the seafloor is added to the core to obtain meters below sea-level.

2.3.5   Paleo- and Modern Overwash Slope Measurements

Slopes of dipping reflectors were calculated using the equation, $(y_1-y_2)/\Delta x$, where y_1 and y_2 are depths in TWT that were converted to depth in meters using 1,525 m/s (Abdulah et al., 2004). The value for Δx was

measured in DecisionSpace using the ruler tool (Figure 2.2). Using full-waveform data, we measured both the steeper paleo-slopes in the SE portion of the unit, and the shallower paleo-slopes in the NW portion of the unit. Paleo-slopes were measured on every other line where the landward dipping unit exists. For the paleo-slopes of an individual reflection to be measurable, the reflection had to be continuous, and well-defined (mappable) for >2,000 m in length for SE paleo-slopes and >1,000 m for NW paleo-slopes, with at least 3 reflections for SE and 2 reflections for NW paleo-slopes in the unit. The paleo-slopes in the SE portion were mapped from the erosive horizon above, to the break in slope, where we began the measurement for the NW paleo-slope to the end of the seismic line (Figure 2.2). If we were unable to trace a reflection to these areas, it was not included in the analysis. The difference in criteria was due to data limitations on the SE side of Sabine Bank (seismic lines did not image more than 2,000 m distance on the SE side of the unit), and the NW portion of the unit is much thinner than the SE portion, containing fewer horizons overall.
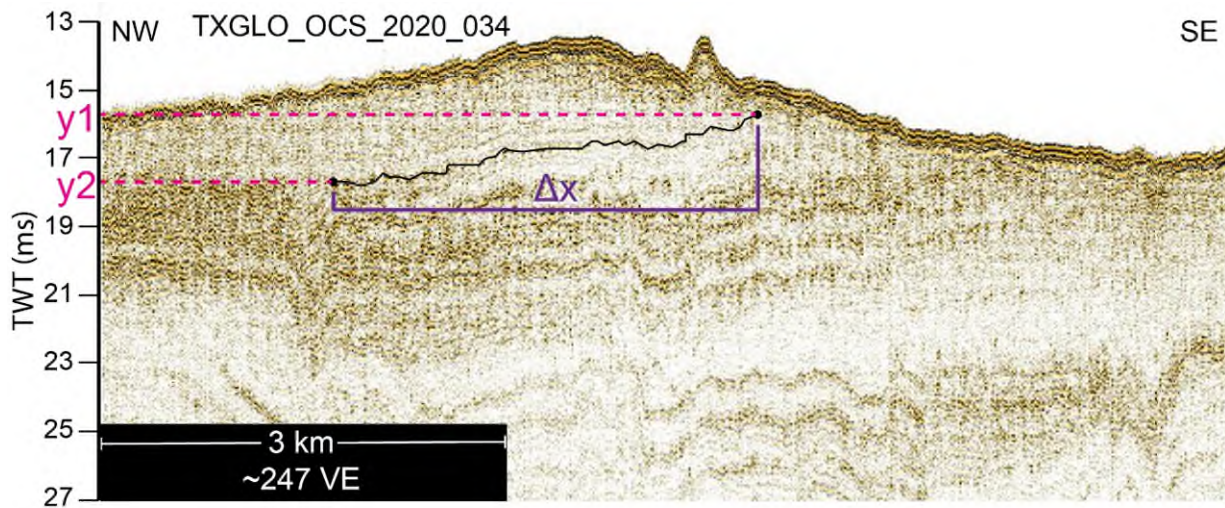
Figure 2.2. An example of an individual reflection that was measured for slope.
The individual reflector is shown in black, and depths in TWT are shown for y1 and y2 in pink, measurement of Δx is shown in purple. Location shown in Figure 2.4.
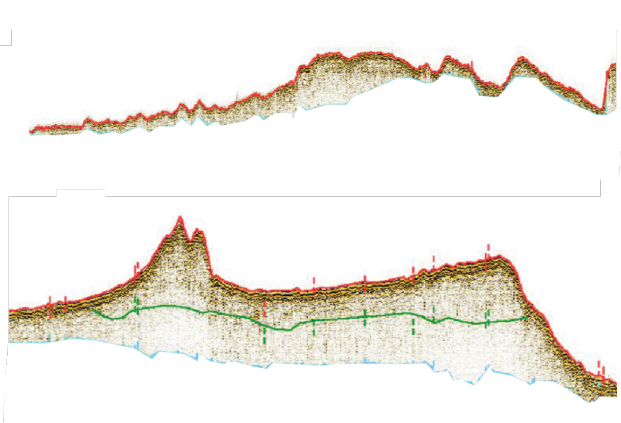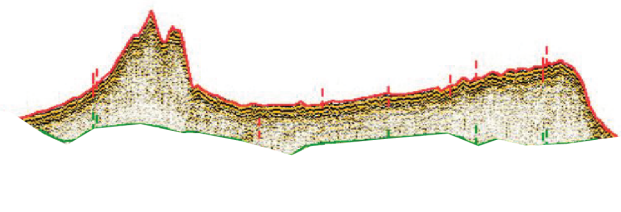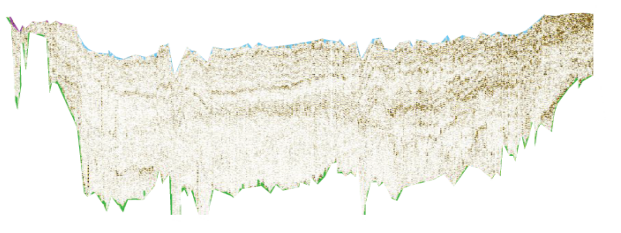
We estimated uncertainties for velocity, human picking, and vertical and horizontal resolution. We used ±25 m/s as an error for variability in velocity, leaving us with a range of 1,500-1,550 m/s as possible velocities. We assumed the human error of picking individual reflectors was $\lambda/4$ to $\lambda/2$, or the vertical resolution of our data, under the assumption that, when picking a reflector, the interpreter might erroneously go up or down by a single reflection. Using a median frequency of 6,350 Hz, the resultant vertical resolution is 6-12 cm; in this case, we use the median of 9 cm. The horizontal resolution is estimated as the width of the Fresnel zone, which is calculated using the formula $W_t = (2z\lambda)^{1/2}$. Once all uncertainties were calculated, the square root of the sum of squares method was used to estimate the final uncertainty (Table 2.1).

For modern comparison with paleo-slopes, we measured recent overwash slopes from Matagorda Peninsula using 1 m resolution LiDAR digital elevation model collected in 2018, processed by the Texas Water Development Board, Fugro Geospatial, Inc. and the Department of Information Resources. These data were obtained from the NOAA Data Access Viewer (https://coast.noaa.gov/dataviewer/#/). We chose Matagorda Peninsula because the island is largely undeveloped and consists of large, sheet-like overwash deposits that likely represent a similar environment of Sabine barrier island as it drowned (Wilkinson, 1975). Transects were placed approximately 1.9 km apart, while also avoiding human structures, like buildings, drainage ditches, etc. We avoided measuring transects within 300 m of inlets. Modern slopes

were calculated where an obvious break in slope exists landward of the highest point of the barrier island to the water's edge using linear regression. This break in slope represents the back-barrier environment where overwash is occurring and is located between 165-810 m landward of the tallest dune (average=418 m). We assume that modern slopes in the shallow subaqueous portion of the back-barrier are similar to those along the distal edges of the subaerial back-barrier.

Table 2.1: Seismic facies, horizons, units, and age summary

Unit	Example	Facies present	Upper bounding horizons	Lower bounding horizons	Age
1		SF1	H1	H3	<2.5 ka
1a		SF3	H1	H2	modern
2		SF2	H3	H4	7.2-2.5 ka
3		SF3	H4 when present, H3	H5	no data
4		SF4, SF5	H5 when present, H4 if present, H3	H6	9.6-4.4 ka

2.4 Results and Interpretation

Within the chirp data in this study, we observe 5 distinct seismic facies (Figure 2.3). Our seismic interpretation further identified 6 seismic horizons (Figure 2.4-6) bounding 5 seismic units (Figure 2.7).

2.4.1 Seismic Facies

Using reflection amplitude, geometry, and continuity, five seismic facies are present within and below Heald and Sabine banks:

Seismic Facies 1 (SF1): SF1 (Figure 2.3) consists of low-to-medium amplitude, chaotic and discontinuous reflections. This facies is mostly found near the surface of the section and has no internal truncations. This facies is found in U1a (Figures 2.4, 2.5).

Seismic Facies 2 (SF2): SF2 comprises high-amplitude, parallel to sub-parallel, unidirectional, dipping reflections with some internal truncations near the base of the facies (Figure 2.3). This facies is found in U2 (Figure 2.4).

Seismic facies 3 (SF3): SF3 is characterized by transparent-to low-amplitude, chaotic and discontinuous reflections (Figure 2.3). There is little definition in this facies to characterize the geometry. This facies is found in both U1 and U3 (Figures 2.4 and 2.5).

Seismic facies 4 (SF4): SF4 is composed of medium-to-high-amplitude, draping reflections with occasional truncations (Figure 2.3). This facies is found in U4 (Figures 2.4 and 2.5).

Seismic facies 5 (SF5): SF5 contains medium-to-high amplitude, unidirectional dipping reflections displaying lateral accretion (Figure 2.3). This facies is also found in U4 (Figures 2.4 and 2.5).

2.4.2 Horizons

We mapped six horizons based on their continuity and the facies bounded:

Horizon 1 (H1): H1 is a high amplitude, continuous horizon that is the modern seafloor. In the southern portion of the study area, the seafloor is ~33 ms TWT (~25 m) and gradually shallows towards the north, with the shallowest portions being the crests of Sabine and Heald Banks, ~9 ms TWT (~7 m; Figures 2.4, 2.5, 2.6a).

Horizon 2 (H2): H2 is a low-amplitude internal parallel reflection found within the banks and denotes a boundary between SF1 above and SF3 below. H2 is mostly restricted to Heald Bank and the most seaward portion of Sabine Bank. This horizon varies in depth between 16 and 29 ms TWT (12-22 m) with deeper depths within Heald Bank (Figures 2.4, 2.5, 2.6b).

Horizon 3 (H3): H3 is an erosive surface that truncates several major surfaces including H4, H5, and H6. This horizon designates the strong contrast between seismic facies beneath and seaward of the banks although is not always a strong reflector (Figures 2.4, 2.5, 2.6c). In some areas, landward of the banks, H3 is inferred based on geometric principles and must be above H4, or H5 and below H1. Above H3 is SF3, and below are SF2, SF3, and SF4. H3 is the shallowest (at ~13 ms, or 10 m) in the NE portion of the study area within Sabine Bank, and gradually increases in depth (to ~34 ms, or 26 m) underneath Heald Bank towards the southern corner.
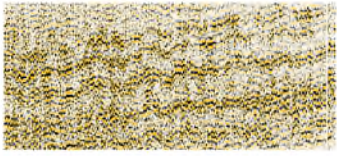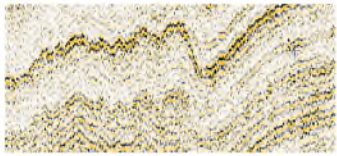
Facies	Example	Description
SF1		Low-to-medium-amplitude and discontinuous reflections
SF2		High-amplitude, parallel to sub-parallel, unidirectional, dipping reflections with some truncations near the base of the facies
SF3		Transparent-to-low-amplitude, chaotic and discontinuous reflections
SF4		Medium-to-high-amplitude, draping reflections with occasional truncations
SF5		Medium-to-high, unidirectional dipping reflections displaying lateral accretion

Figure 2.3. Examples of seismic facies found in this study with descriptions of each facies.
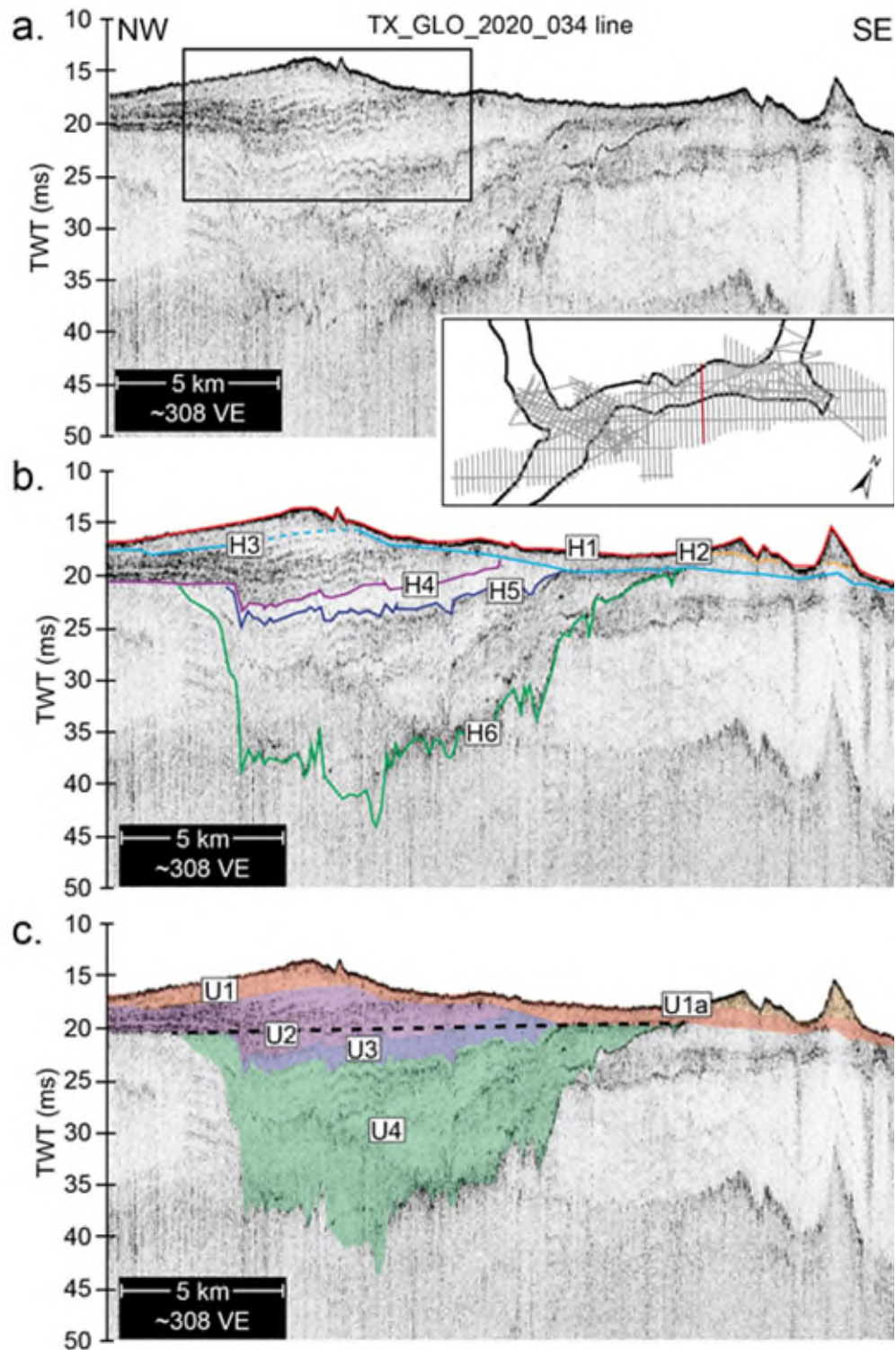
Figure 2.4. Chirp envelope record over Sabine Bank
(a) Uninterpreted data, (b) the interpreted horizons, and (c) interpreted units. The black dashed line in panel c indicates the hypothetical top of the paleovalley accommodation. Location shown in Figure 2.1 and in inset on this figure. H3 is dashed where definition is uncertain. Box in (a) indicates location of Figure 2.2.
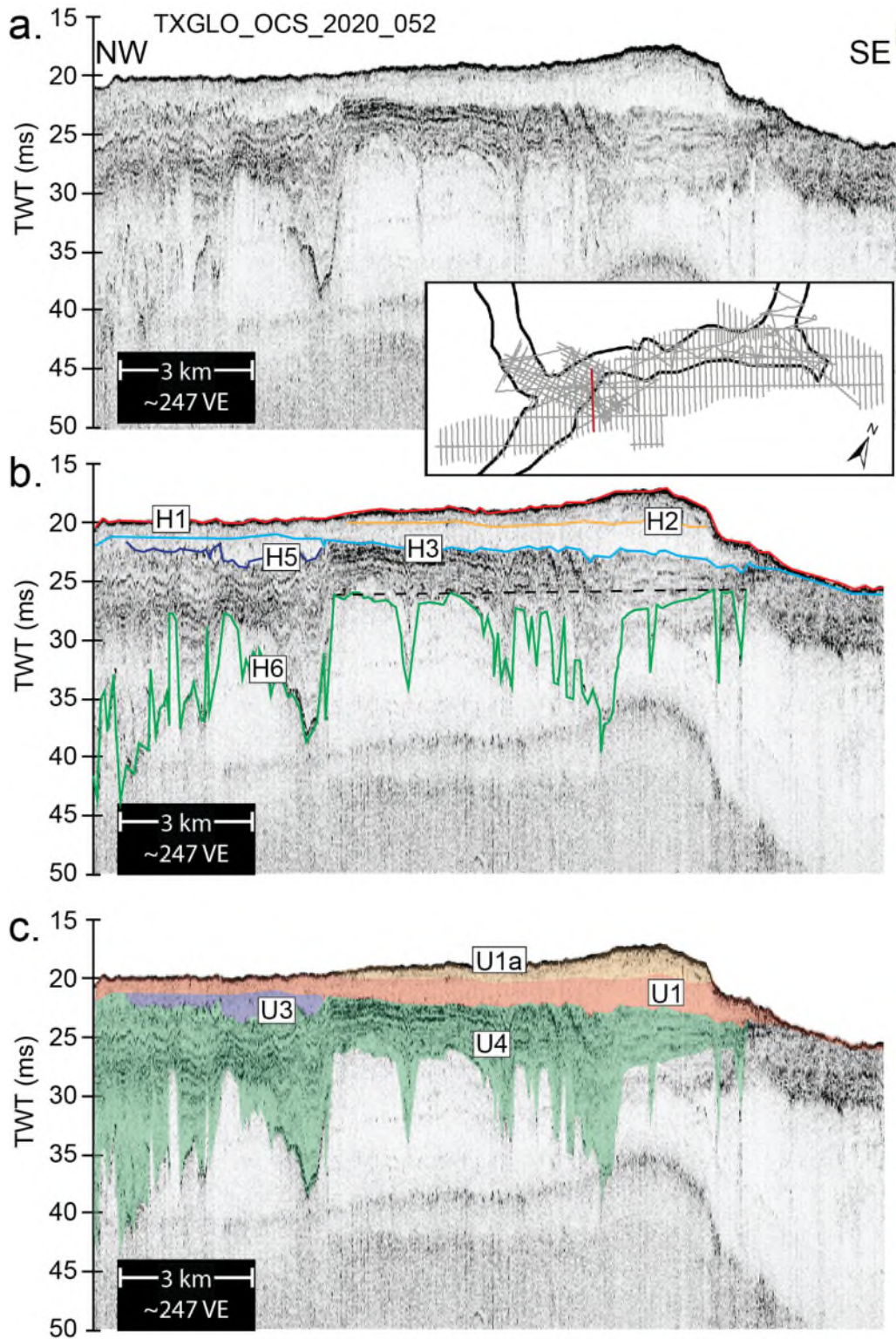
Figure 2.5. Envelope chirp record over Heald Bank
(a) The uninterpreted data, (b) interpreted horizons, and (c) units. The dashed black line on panel b indicates the top of the hypothetical accommodation from the valley edge to a terrace when the opposite valley edge is not imaged. Location shown in Figure 2.1 and in inset on this figure.
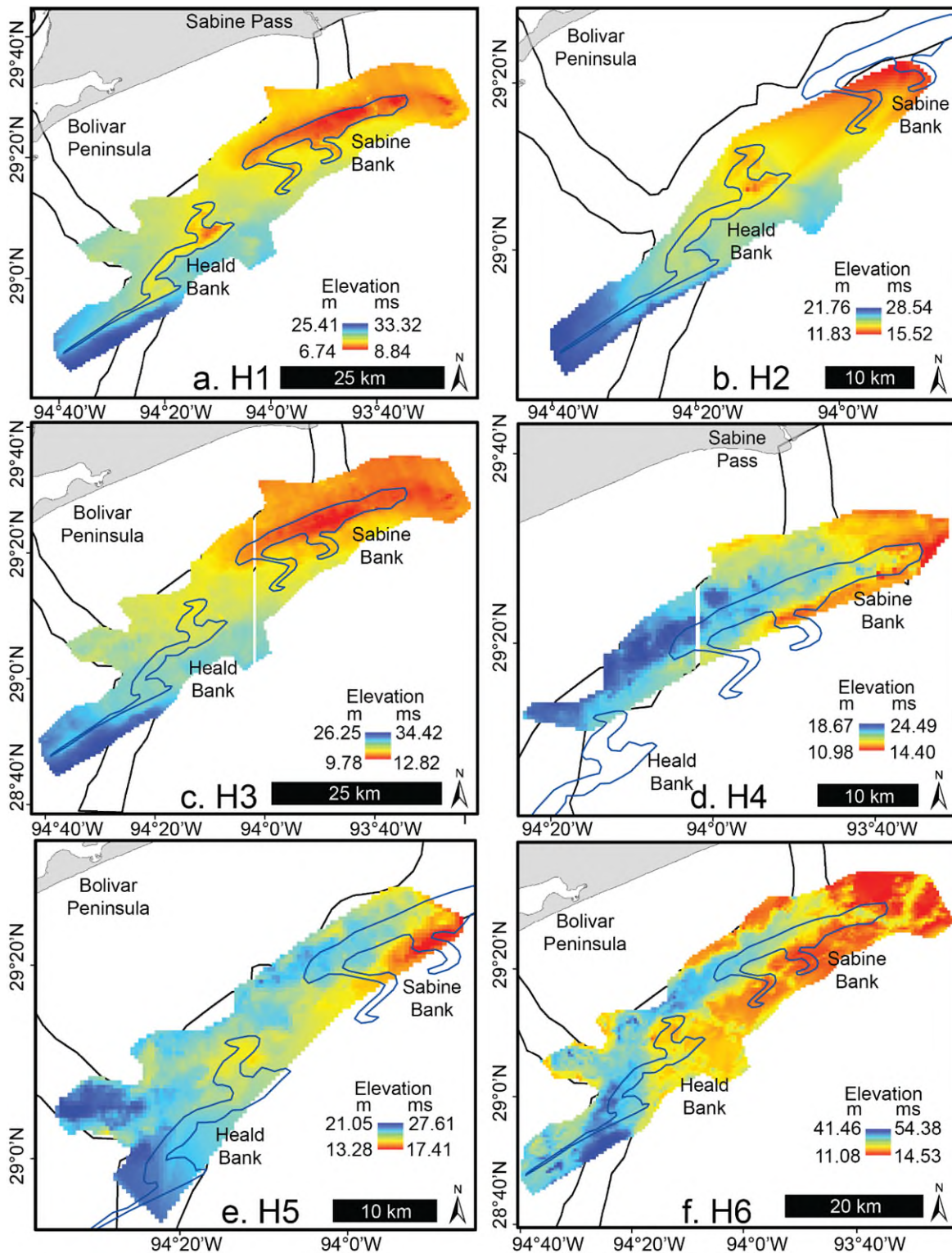
Figure 2.6. Structure maps for horizons.
Horizons are: H1 (a), H2 (b), H3 (c), H4 (d), H5 (e), and H6 (f). Refer to Figures 2.4 and 2.5 for the interpretation on the seismic lines. Depth is shown in both TWT (ms) and converted to meters. The black outline denotes the rough extent of the Trinity-Sabine paleo-river valley from Thomas and Anderson (1994).

15
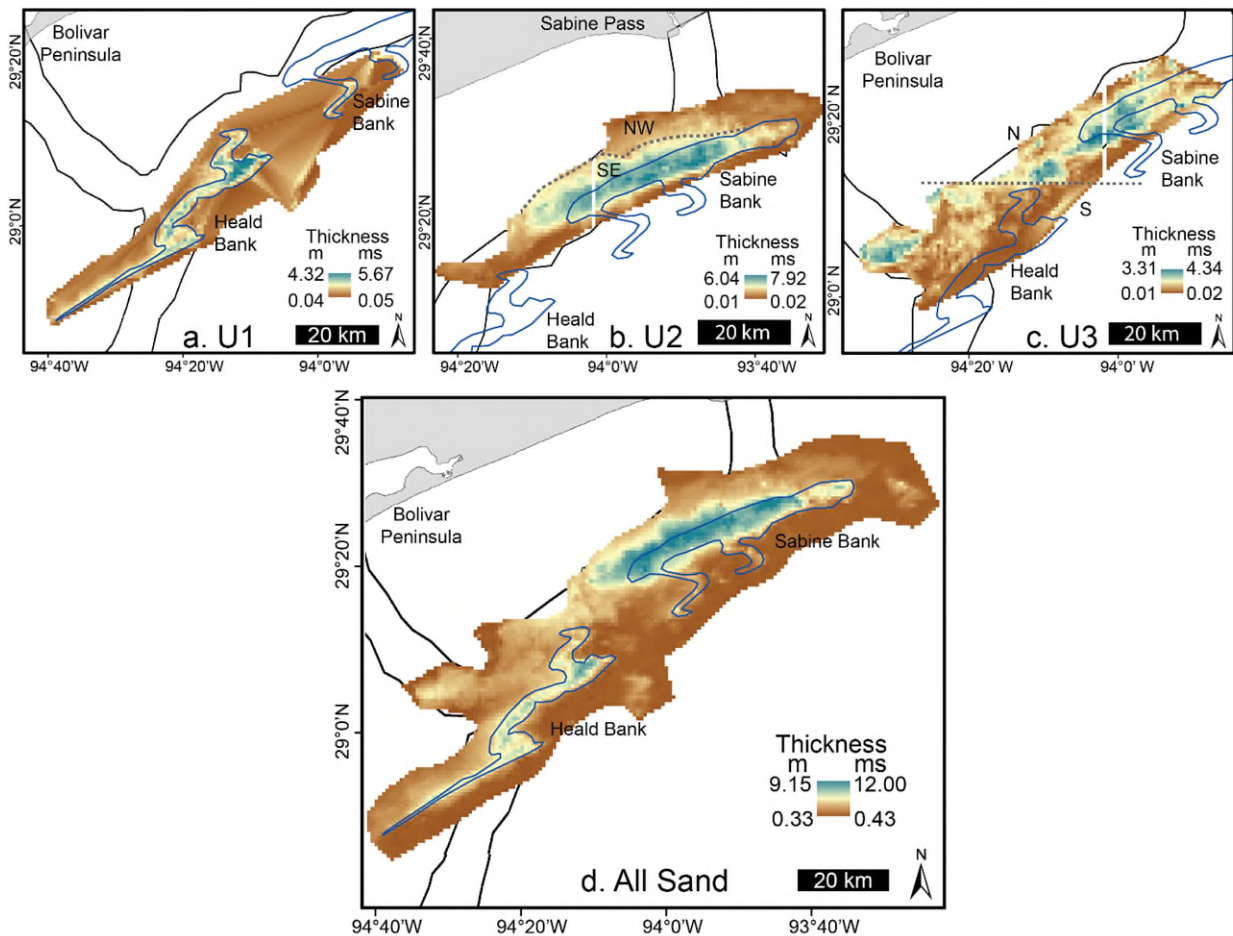
Figure 2.7. Isopach maps for interpreted sandy units
Units are U1 (a), U2 (b) and U3 (c). Panel d displays the combined thickness of all three. Thickness is shown in both TWT (ms) and converted to meters. Black outline denotes the approximate extent of the Trinity-Sabine paleovalley from Thomas and Anderson (1994).

Horizon 4 (H4): H4 is the boundary between SF2 above and SF3 below. SF2 downlaps onto H4, where truncations frequently characterize the surface. H4 is mostly present beneath and landward of Sabine bank. The TWT of H4 varies between 24 and 14 ms (19-11 m) with the deepest portion towards the west of Sabine Bank (Figures 2.3, 2.6d).

Horizon 5 (H5): H5 is the boundary between SF3 and SF4 and is generally a conformable surface. H5 is found under both banks and deepens towards the NE beneath Sabine Bank. The depth of H5 landward of Heald Bank is variable. H5 is deeper (~28 ms TWT, or 21 m) in the southern portion of the study area where the Trinity River valley joins the Sabine River valley. This surface mostly ranges between 28 and 21 ms TWT (21- 16 m; Figure 2.3, 2.4, 2.6e).

Horizon 6 (H6): H6 is an erosive boundary that incises into underlying strata. This horizon is a channelized feature that runs parallel to the modern-day shoreline with several smaller, and one large, perpendicular channelized feature joining the main parallel valley. The incision reaches a maximum 54 ms TWT (41 m) and shallows towards land and within the smaller channels (Figures 2.4, 2.5, 2.6f). H6 is interpreted to be the top of the fluvial deposits filling the valley, and contemporaneous floodplain deposits, pre-dating barrier island formation based on previous interpretations. In other words, it is the base of the estuarine section. Specifically, this surface is high impedance (consisting of bright reflections)

and where cores have sampled above and below H6 sedimentological data show estuarine and bayhead delta deposits overlying fluvial deposits (Burstein et al., 2023; Rodriguez et al., 2004; Thomas and Anderson, 1994). The chirp data are unable to acoustically penetrate below H6 to image the base of that unit, which is consistent with these being the top of fluvial deposits (e.g., Burstein et al., 2023). H6 can thus be viewed as the antecedent topography that coastal facies infill during transgression.

2.4.3   Units

We identified four main seismic units and one subunit based on the seismic facies analysis and mapped horizons that bound each unit (Figure 2.7):

Unit 1 (U1): U1 is bounded above by the seafloor (H1) and below by H3 and consists of low-to-medium (SF1) and transparent-to-low (SF3) discontinuous reflections. This unit is present through most of the study area, although it is typically relatively thin (<0.05 ms). This unit is relatively thick beneath Heald Bank and for a small region slightly seaward of Sabine Bank where in both cases it reaches 5.67 ms TT (4 m, Figure 2.4, 2.5, 2.7b, Table 2.1).

Unit 1a (U1a): U1a, subunit of U1, is bounded above by H1 and below by H2. This unit is relatively thin and geographically constrained to beneath Heald Bank with a small portion in front of Sabine Bank. This unit consists of SF1 (Figures 2.3 and 2.4, Table 2.1). U1a is a subunit because it is bounded by H2 and contains a slightly higher amplitude SF.

Unit 2 (U2): U2 is bounded above by H3 and below by H4 and consists entirely of SF2 (high-amplitude, dipping reflections). This unit is found below Sabine Bank, and is mostly absent under Heald Bank, except for a thin (<0.02 ms TT) portion near the NE portion of Heald Bank. The thickest portion (7.92 ms TT, 6 m) of U2 is concentrated in the seaward core of Sabine Bank and thins both landward and on the easternmost and westernmost flanks of Sabine Bank (Figure 2.7b). The SE portion of this unit consists of steeper dipping reflections that are lower amplitude. The NW portion consists of shallower dipping reflections that are higher in amplitude (Figures 2.4 and 2.7b, Table 2.1, location of the SE/NW portion of the banks is shown on Figure 2.7b).

Unit 3 (U3): U3 is bounded below by H5, and above by H4 if H4 is present, or by H3 if H4 is not present. This unit consists of SF3 and is thickest (4.64 ms TT) beneath Sabine Bank and near the junction of the Sabine and Trinity paleo-river valleys. This transparent, homogeneous unit fills the remaining accommodation above the estuarine fill (Figures 2.4, 2.5, 2.7c Table 2.1).

Unit 4 (U4): U4 is composed of medium-to-high, draping reflections (SF4) and medium-to-high dipping reflections (SF5). The top of U4 is bounded by H5, where present, H4, where present, and finally H3 if H4 and H5 are not present (Figure 2.4 and 2.5, Table 2.1). U4 is interpreted to be the estuarine unit, based on core borings 6 and 7 (Thomas and Anderson, 1994) that recovered stiff clays with organic material from the middle and upper bay units.

Units U1, U2, and U3 were combined to represent the extent of all likely sand resources (Figure 2.7d). An isopach map was created by differencing H5-H1, where H5 is present, H4-H1, where H4 is present, and finally H3-H1, where H3 is present. This composite unit is thickest (12 ms TT, 9 m) and covers the largest areal extent over Sabine Bank. This unit is also thick beneath Heald Bank (12 ms TT, 9 m) but covers a smaller areal extent. Landward of Heald Bank and near the confluence of the Trinity and Sabine paleovalleys, the unit thins to ~6 ms TT (4.5 m). A thin (0.43 ms TT, 0.3 m) layer of sand exists between the seafloor and H3 for the entire study area, which was verified by several cores that were ≤ 1m in length containing only sand.

2.4.4 Accommodation Estimation

The antecedent topography created by the Sabine River paleovalley provides accommodation for sediments to accumulate. We created a hypothetical boundary across the valley incision to assess the available accommodation that barrier sediments could infill. This boundary spans across the top of the valley from one valley edge to the other side, where below this line is potential available accommodation due to the antecedent topography of the paleo-Sabine River valley (Figures 2.4 and 2.5). Approximately half of the shore-perpendicular lines were used to calculate this conceptual boundary because many of the lines only imaged one edge of the valley, therefore we could not create the hypothetical boundary that extends across both valley edges. To incorporate more lines, if a topographic high, like a fluvial terrace, was present, we extended the boundary from the valley edge to the topographic high (Figure 2.5). Available accommodation was then calculated by subtracting the hypothetical "top of the valley" horizon from the base of the "all sand" unit (a combination of all units above H5, H4, and H3). The result is that available accommodation was concentrated beneath Sabine Bank and near the confluence of the Sabine and Trinity paleo-river valleys (Figure 2.8). There is little accommodation beneath Heald Bank; this result is apparent in the chirp data because U4, the estuarine unit, nearly completely fills the valley in this region (Figure 2.5). Beneath Sabine Bank, U4 fills most of the accommodation (Figure 2.4), U3 (the transparent, homogeneous unit) dips landward into the valley and below the hypothetical "top of valley" horizon (Figure 2.4) filling about half of the remaining accommodation, and finally, U2 fills the remaining accommodation and ultimately overfills the valley accommodation.
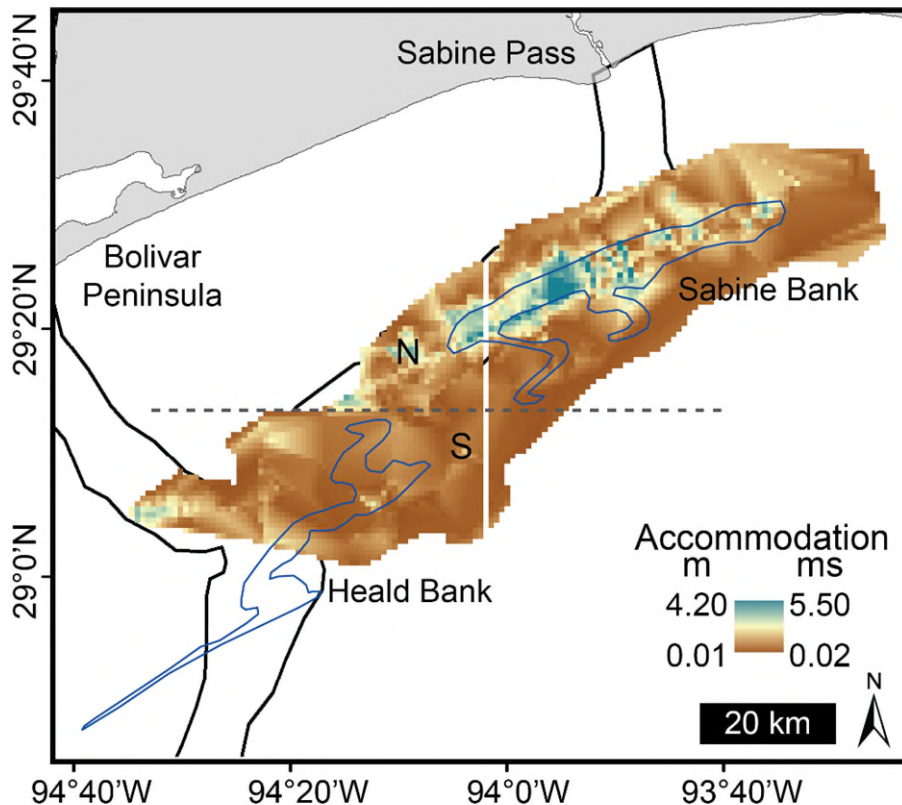
Figure 2.8. Extent and thickness of accommodation within the study area.
Black outline denotes the paleo Trinity-Sabine River valley from Thomas and Anderson (1994).

2.4.5 Paleo- and Modern Slopes

U2 contains many high-amplitude, landward-dipping, traceable internal reflections where paleo-slope could be measured to help characterize and identify this unit (Figure 2.4 and 2.7b). All paleo-slope measured, both NW and SE, were very low (Figure 2.9). NW paleo-slopes vary between -0.00010 and 0.00013 with an average of 0.00004 and a standard deviation of 0.00007. In this case, negative slopes indicate a seaward dipping reflection, whereas positive slopes indicate landward dipping reflections. SE paleo-slopes were higher than the NW paleo-slopes and vary between 0.00027 and 0.00123 with an average of 0.00065 and a standard deviation of 0.00032. The highest paleo-slopes were measured on lines 19, 22, 24, 26, and 28 beneath Sabine Bank in the SE portion of the bank (Figure 2.9). The NW paleo-slopes are consistently low, and do not vary much. The higher (SE) paleo-slopes have more variability and are over an order of magnitude higher than the lower (NW) paleo-slopes.
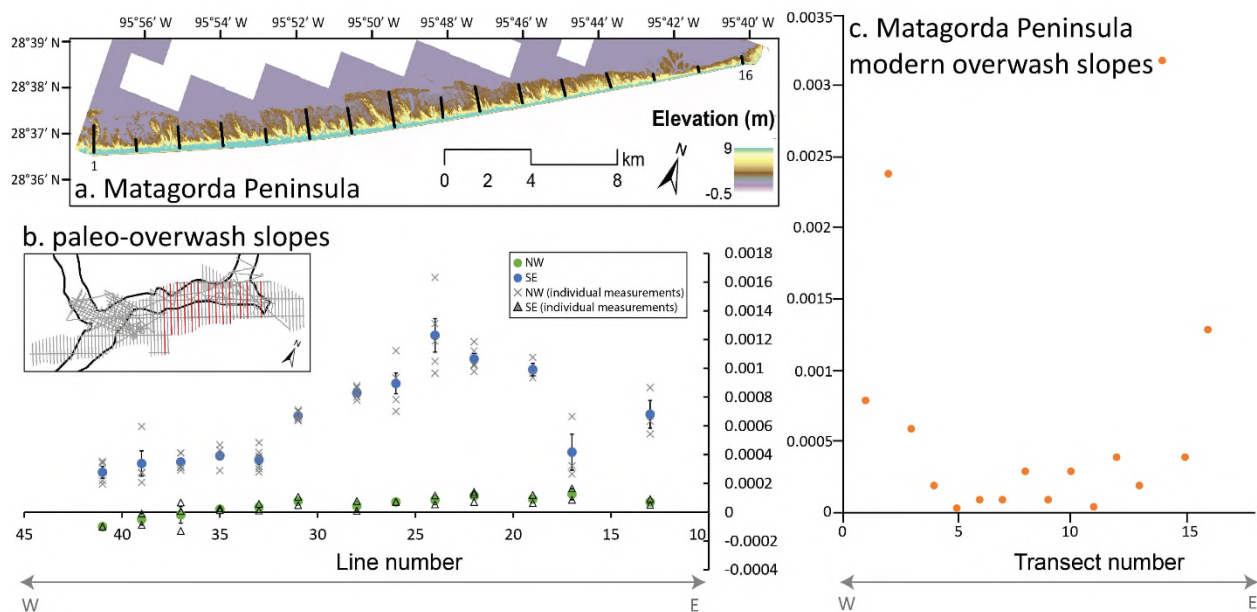
Figure 2.9. Comparison of landward dipping reflections slopes to modern overwash slopes
(a) Map of Matagorda Peninsula where modern day overwash slopes were calculated. Black lines indicate transect location. (b) Slopes measured for individual reflections in the washover deposit (U2). Values are computed from lines marked in red in inset map. The average landward slope for each line is designated with a green circle, and the black triangles represent all slope measurements calculated on that line. The average seaward slope for each line is denoted by a blue circle, and the individual measurements are represented by a gray x. An example of how slopes were measured can be found on Figure 2.2. (c) Modern day overwash slope measurements from each transect, plotted with same vertical scale as panel (b).

The modern slopes from East Matagorda Peninsula range from 0.00004 to 0.00320 with an average of 0.00066 (and a median of 0.00030) and standard deviation of 0.00091. The average slope from East Matagorda is 3.3 times lower than the average slope (average=0.0022) measured from a subaerial overwash fan internal stratigraphy on Matagorda Peninsula following Hurricane Ike (Shaw et al., 2015). The lower bound of these modern slopes are similar to the NW paleo-slopes preserved within Sabine Bank; however, the upper bound is higher than any of the paleo-slopes measured. The average (and median) is also higher than the paleo-slopes; however, these are all relatively low slopes. Only 2 of the 16 slope measurements from East Matagorda Peninsula are higher than any of the paleo-slope measurements, likely skewing the average and median higher even though the majority of slopes fall within the same range as the paleo-slopes. Without these two measurements, the average slope of East Matagorda

becomes 0.00035, which is 6.3 times lower than measurements from Shaw et al. (2015), 8.8 times higher than the NW paleo-slopes, and 1.9 times lower than the SE paleo-slopes. Most of the modern slopes fall between the NW and SE paleo-slopes (Figure 2.9). Therefore, the NW paleo-slopes are the lowest, followed by the modern slopes, and finally the SE slopes are the highest.

2.4.6   Core-Seismic Integration

Rodriguez et al. (2004) identified 3 key sedimentary facies from cores on Heald and Sabine banks: facies A, interbedded shell hash and sand that is acoustically chaotic, was interpreted to be inner-shelf sand; facies B, muddy sand with seaward prograding chaotic seismic reflections, was interpreted to be shoreface and/or tidal inlet (sands); and facies C, interbedded sand and mud with landward dipping seismic reflections, was interpreted as estuarine. They also identified Pleistocene sands and mud, saltmarsh peat, and inner-shelf muds within cores (Rodriguez et al., 2004). Rodriguez et al. (2004) collected 31 cores; of those, we projected the 17 containing radiocarbon dates onto the nearest APTIM seismic lines (Figures 2.10 and 2.11). On average, cores were located ~319 m (standard deviation= 274 m) from the chirp lines, with the largest deviation of ~915 m. Core penetration ranged from 461 cm to 179 cm, with an average of 341.5 cm (standard deviation = 76.9 cm).

Each sedimentary facies has a distinct shell assemblage that can be used as an environmental indicator. Facies A consists of a combination of bay/lagoonal (*Crassostrea virginica*), back-barrier/nearshore (*Crassinella lunulata, Mulinia lateralis, Natica pusilla, Anchis obesa*), and open marine species (*Plicatula gibbosa, Strigilla mirabilis, Semele bellastriata*). Facies B is composed of shoreface/inlet species (*Natica pusilla, Olivella dealbata, Ervilia concentrica, Caecum johnsoni, Anadara tranversa, Abra aequalis, Ensis minor*). Facies C contains bay/inlet species (*Ostrea equestris, Nassarius acutus, Nuculana concentrica, Mulinia lateralis, Rangia flexuosa*) (Table 2.2).

For three cores, two on Sabine and one on Heald banks, the core stratigraphy and seismic stratigraphy did not perfectly align. These cores are SB-93-4, SB-93-7, and HB-93-7, which are located 119 m W, 425 m E, and 610 m W, respectively, of their closest seismic lines. Each of these cores are located near the flanks of the bank edge where bathymetry can rapidly change over short distances. For instance, SB-93-7 records Holocene ages, but 425 m away, in the seismic line we interpret Pleistocene deposits at those depths. This suggests variability in the underlying antecedent geology on the scale of hundreds of meters. Bedforms on Heald and Sabine banks indicate recent modification by currents and storms. These bedforms were also seen in seismic data from Rodriguez et al. (1999). Between core collection and seismic collection, 28 years have elapsed, so we allow for variability in the height of the seafloor and lateral extent of the sand banks; therefore, the core and seismic stratigraphy still align generally well.
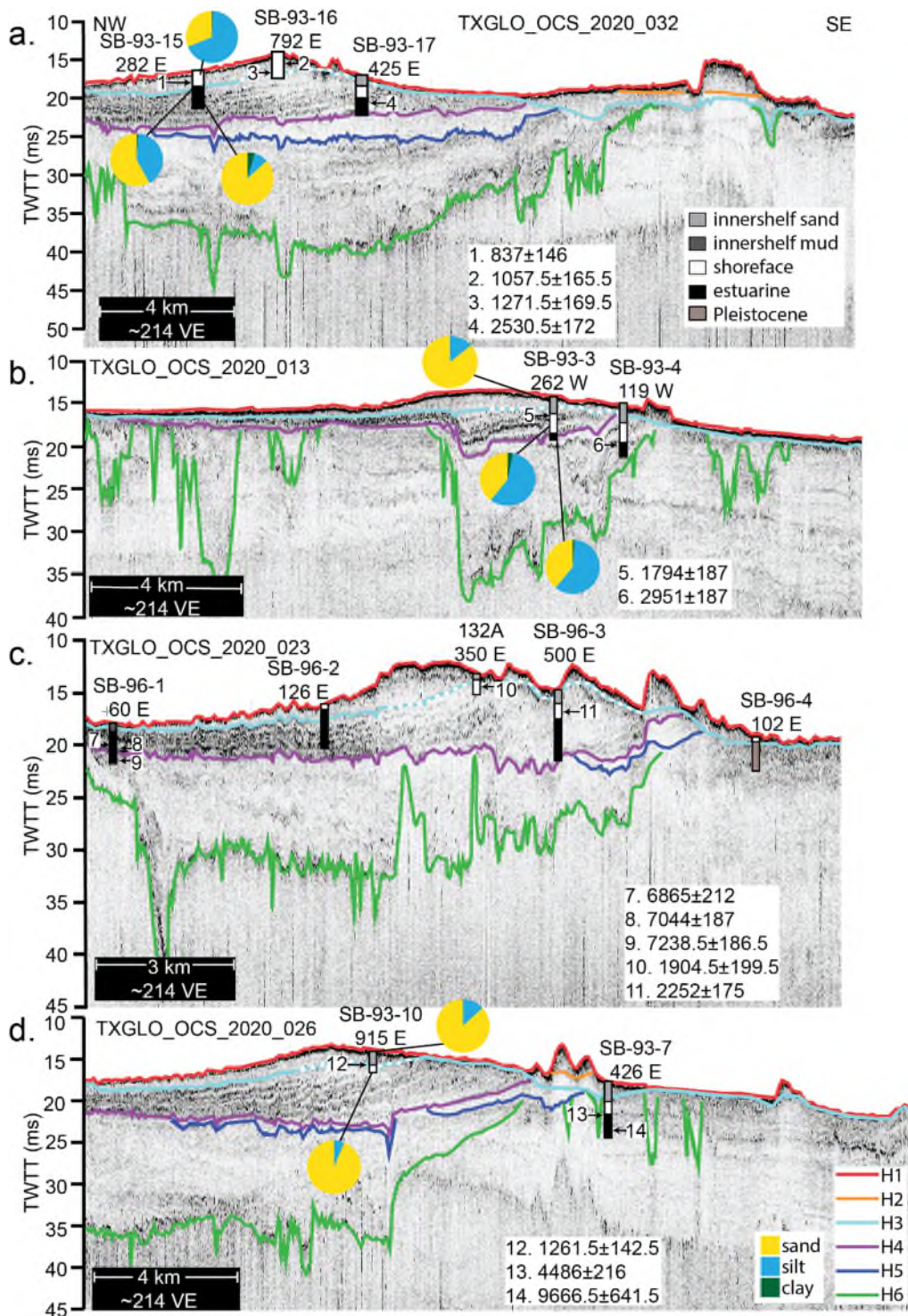
Figure 2.10. Core/seismic integration over Sabine Bank.
Four seismic lines collected by APTIM over Sabine Bank that correlate to locations of cores presented in Rodriguez et al. (2004); locations and depths of cores are represented by black rectangles. The approximate distance (m) and direction each core is located off of the seismic line is noted underneath the core name. Locations and depths of radiocarbon dates are shown with numbered arrows. Recalibrated radiocarbon dates (yr BP) are listed for the cores on each line. Line locations shown in Figure 2.1. H3 is dashed where definition is uncertain.
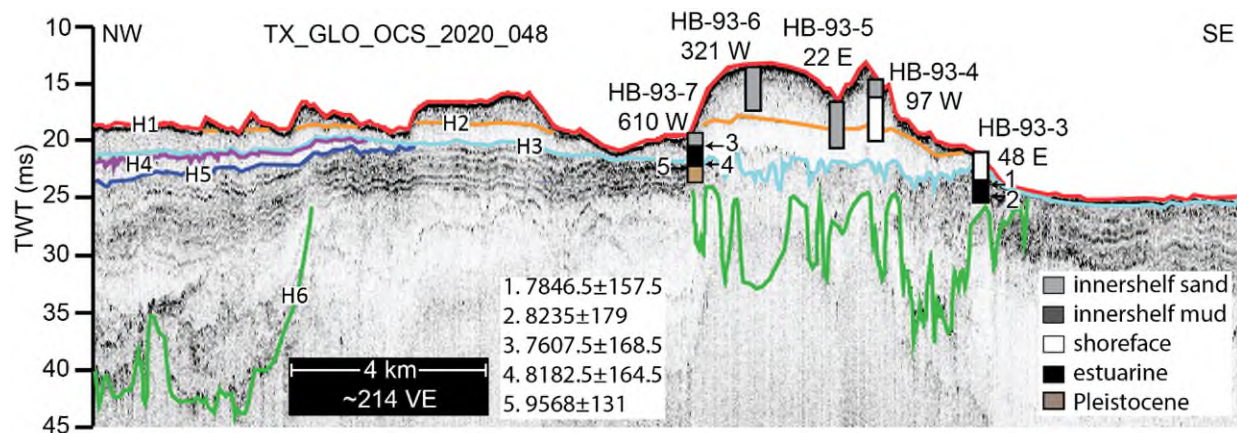
Figure 2.11. Core/seismic integration over Heald Bank.
Seismic line collected by APTIM over Heald bank that correlates to locations of cores presented in Rodriguez et al. (2004); locations and depths of cores are represented by black rectangles. The approximate distance (m) and direction each core is located off the seismic line is noted underneath the core name. Locations and depths of radiocarbon dates are shown with numbered arrows. Recalibrated dates (yr BP) are listed below. Location shown in Figure 2.1.

In Tables 2.2 and 2.3 we compare our seismic units with the seismic and sedimentary facies characterized by Rodriguez et al., 2004, and displayed in Figures 2.10 and 2.11. Cores HB-93-5 and 6 are interbedded shell hash and sand, with a shell assemblage that consists of bay/lagoonal, nearshore/backbarrier, and open marine species (Rodriguez et al., 2001); these sediments correlate with SF1 (low-to-medium chaotic, discontinuous reflections) within U1a (Table 2.3). This low amplitude, chaotic seismic unit lies above an erosional surface that post-dates the transgressive ravinement. We therefore interpret U1a to be post-transgressive remobilized sands, which could be associated with tidal currents that are actively reworking the bank, storm reworking, or erosion of the modern shoreface that is transported offshore. Cores HB-93-5, 6, and 7 are also interbedded shell hash and sand with a shell assemblage containing bay/lagoonal, nearshore/backbarrier, and open marine species. These sediments correspond with SF1 and SF3 (transparent-to-low amplitude, chaotic, discontinuous reflections) and overlie H3 within U1; we interpret these strata to be marine sands (Table 2.3) but could also be shoreface sands that were deposited above the ravinement during transgression (i.e., shoreface progradation from a more landward location after the barrier drowned). Cores SB-93-3, 10, 16, 17, and SB-96-3 are composed of muddy sand with a shoreface/inlet shell assemblage and correlate with SF2 (high amplitude dipping reflections) in the lower amplitude SE portion of U2, whereas cores SB-93-15, SB-96-1 and 2 are interbedded sands and mud with an assemblage consisting of estuarine shells, correspond to the higher amplitude NW portion of U2. Radiocarbon dates from SB-93-17 and SB-96-1, using material sampled from the higher amplitude section of U2 (and Rodriguez et al., 2004 estuarine facies), have median dates ranging from 2,530 years BP ± 172 and 7,238 years BP ± 187, respectively (Figure 2.10). Finally, cores HB-93-3 and SB-96-1 contain interbedded sands and muds with bay/inlet shells and correspond to U4, which we interpret as estuarine.

22

Table 2.2. Radiocarbon dates and shell taxon analyzed

Chirp Line Name*	Core Name	Median Depth (cm)	Conventional Radiocarbon Age ± Error	Calibrated Age (Rodriguez et al., 2004) ± Error	Calibrated 2σ age this study ± Error (Certainty)	Calibrated 1σ age this study ± Error (Certainty)	Rodriguez et al. (2004) facies/interpretation	Taxon analyzed	Taxon environment
013	SB-93-3	190	2346±53	1960±65	1794±187 (1)	1791.5±91.5 (1)	B/shoreface or tidal inlet	*Abra aequalis*	Open bays/marine
013	SB-93-4	360.5	3290±50	3130±75	2951±187 (1)	2945±97 (1)	C/estuarine	*Abra aequalis*	Open bays/marine
023	SB-96-1	172	6578±60	7090±75	6865±212 (1)	6855±104 (1)	C/estuarine	*Rangia flexuosa*	Estuarine/river
023	SB-96-1	230	6735±50	7265±40	7044±187 (1)	7049.5±93.5 (1)	C/estuarine	*Rangia flexuosa*	Estuarine/river
023	SB-96-1	287	6935±65	7440±60	7238.5±186.5 (1)	7248.5±91.5 (1)	C/estuarine	*Rangia flexuosa*	Estuarine/river
023	132A	100	2435±60	2065±75	1904.5±199.5 (1)	1897±102 (1)	B/shoreface or tidal inlet	*Mulina lateralis*	bay/inlet
023	SB-96-3	276	2720±40	2400±55	2252±175 (1)	2250±82 (1)	B/shoreface or tidal inlet	*Abra aequalis*	Open bays/marine
026	SB-93-7	290	4490±50	4695±80	4486±216 (1)	4481.5±101.5 (1)	C/estuarine	*Ostrea equestris*	bay/inlet
026	SB-93-7	431.5	8677±270	8545±90	9666.5±641.5 (0.98867)	9721.5±246.5 (0.782102)	C/estuarine	peat	back-barrier/nearshore
026	SB-93-10	124	1875±40	1420±55	1261.5±142.2 (1)	1270±69 (1)	B/shoreface or tidal inlet	*Abra aequalis*	Open bays/marine
032	SB-93-15	154	1463±40	1000±40	837±146 (1)	844±73 (1)	B/shoreface or tidal inlet	*Abra aequalis*	Open bays/marine
032	SB-93-16	121	1650±50	1210±45	1057.5±165.5 (1)	1038.5±83.5 (1)	B/shoreface or tidal inlet	*Ensis minor*	lagoon/bay margin
032	SB-93-16	208.5	1880±55	1425±60	1271.5±169.5 (1)	1270.5±78.5 (1)	B/shoreface or tidal inlet	*Abra aequalis*	Open bays/marine
032	SB-93-17	286.5	2938±40	2725±25	2530±172 (1)	2553±99 (1)	C/estuarine	*Mulina lateralis*	bay/inlet
048	HB-93-3	279	7965±60	8415±60	8235±179 (1)	8259.5±84.5 (1)	C/estuarine	*Mulina lateralis*	bay/inlet
048	HB-93-3	197.5	7580±50	8015±50	7846.5±157.5 (1)	7857±80 (1)	C/estuarine	*Mulina lateralis*	bay/inlet
048	HB-93-7	330.5	8570±70	9525±40	9568±131 (1)	9518.5±40.5 (0.819657)	C/estuarine	peat	back-barrier/nearshore
048	HB-93-7	310.5	7900±50	8355±45	8182.5± 164.5 (1)	8200.5±90.5 (1)	C/estuarine	*Mulina lateralis*	bay/inlet
048	HB-93-7	154.5	7325±60	7770±65	7607.5±168.5 (1)	7600.5±82.5 (1)	C/estuarine	*Mulina lateralis*	bay/inlet

*The prefix for all seismic line names are "TX_GLO_OCS_2020_"
Ages are in yr BP

Table 2.3. Correlation between seismic units and core facies

Core	U sampled (this study)	Interpretation	Rodriguez et al. (2004) interpretation	Line number*	Distance (m) and direction from line
HB-93-3	U1	marine sand	shoreface	048	48 E
HB-93-3	U4	estuarine	estuarine	048	48 E
HB-93-4	U1	marine sand	shoreface	048	97 W
HB-93-4	U1a	Post-transgressive remobilized sand	innershelf sand, shoreface	048	97 W
HB-93-5	U1	marine sand	innershelf sand	048	22 E
HB-93-5	U1a	Post-transgressive remobilized sand	innershelf sand	048	22 E
HB-93-6	U1a	Post-transgressive remobilized sand	innershelf sand	048	321 W
HB-93-7	U1	marine sand	innershelf sand, estuarine	048	610 W
HB-93-7	U4	estuarine	estuarine, Pleistocene	048	610 W
SB-93-10	U1	marine sand	innershelf sand	026	915 E
SB-93-10	U2	proximal overwash/shoreface	shoreface	026	915 E
SB-93-15	U1	marine sand	shoreface	032	282 E
SB-93-15	U2	distal overwash	estuarine	032	282 E
SB-93-16	U1	marine sand	innershelf sand, shoreface	032	792 E
SB-93-16	U2	proximal overwash/shoreface	shoreface	032	792 E
SB-93-17	U1	marine sand	innershelf sand	032	425 E
SB-93-17	U2	proximal overwash/shoreface	innershelf sand, shoreface, estuarine	032	425 E
SB-93-3	U1	marine sand	innershelf sand	013	262 W
SB-93-3	U2	proximal overwash/shoreface	innershelf sand, shoreface	013	262 W
SB-93-3	U4	estuarine	estuarine	013	262 W
SB-93-4	U1	marine sand	innershelf sand	013	119 W
SB-93-4	U4	estuarine	innershelf sand, shoreface, estuarine	013	119 W
SB-93-7	PL	Pleistocene	shoreface, estuarine	026	426 E
SB-93-7	U1	marine sand	innershelf sand	026	426 E
SB-96-1	U1	marine sand	innershelf mud	023	60 E
SB-96-1	U2	distal overwash	innershelf mud, estuarine	023	60 E
SB-96-1	U4	estuarine	estuarine	023	60 E
SB-96-2	U1	marine sand	shoreface, estuarine	023	126 E
SB-96-2	U2	distal overwash	estuarine	023	126 E
SB-96-3	U1	marine sand	innershelf sand	023	500 E
SB-96-3	U2	proximal overwash/shoreface	shoreface, estuarine	023	500 E
SB-96-4	PL	Pleistocene	Pleistocene	023	102 E
SB-96-4	U1	marine sand	shoreface	023	102 E

*The prefix for each seismic line number is "TX_GLO_OCS_2020_"

2.5 Discussion

2.5.1 Classification of Sand Banks

Heald and Sabine sand banks, off the east Texas coast (Figure 2.1), have been classified by previous research as either marine-derived sand banks (Thomas and Anderson, 1994) or paleo-barrier island deposits (Rodriguez et al., 2004). Originally, these banks were considered marine sand bodies due to the interpretation of a transgressive ravinement present beneath the banks in seismic reflection data (Thomas and Anderson, 1994). A transgressive ravinement is an erosional surface formed during shoreface landward migration and thus deposits overlying this surface regularly formed in a shelfal environment (Jervey, 1988; Nummedal and Swift, 1987, Zecchin et al., 2019). However, both Heald and Sabine banks were later reclassified as paleo-barrier island remnants based on cores that sampled deposits interpreted as estuarine, shoreface, marsh, and back-barrier estuarine facies (Rodriguez et al., 2004), and internal seismic reflections (Rodriguez et al., 2001), although these were collected with water gun and boomer systems, which are considerably lower resolution, but deeper penetration, than chirp records used in this study. Using improved seismic coverage from the integration of several surveys with higher resolution full waveform chirp data, we can test these earlier interpretations.

With these data, we interpret the stratigraphically shallowest seismic unit, U1 as a largely homogeneous marine sand deposit overlying the transgressive ravinement (H3); this deposit makes up the majority of Heald Bank and a small surficial portion of Sabine Bank (Figure 2.7a, Table 2.1). We interpret H3 to be the transgressive ravinement through Sabine Bank and below Heald Bank because it is a regionally extensive, mostly flat, erosional unconformity that caps U4 (estuarine). H3 extends from our study area and farther inshore where Burstein et al. (2023) also recognized this unconformity. U1a is similar to U1 because they both overlie the transgressive ravinement and are composed of chaotic, discontinuous seismic facies (SF3 and SF1, respectively). U1a is a subunit that is interpreted to be post-transgressive remobilized sand deposit that mostly exists on Heald Bank and the small bathymetric highs fronting Sabine Bank (Table 2.1). Sedimentological data show Heald Bank is composed of reworked inner-shelf sand and shoreface and/or tidal inlet sands (Figure 2.11; Rodriguez et al., 2004). Rodriguez et al. (2004) interprets the transgressive ravinement beneath Heald Bank to be between sedimentary facies A (inner shelf) and B (shoreface). Our seismic interpretation places the transgressive ravinement (H3) lower in the section between U3 or U4 (below) and U1 (above) (Figures 2.5, 2.11). In some places, such as core HB-93-3 on Figure 2.11, those two interpretations are not aligned. Such discrepancies could be due to uncertainties in the core seismic integration, which has three sources: 1) a constant velocity is assumed to convert the core depths to TWT, 2) the locations of the cores are projected by hundreds of meters onto the seismic lines, and 3) both studies recognize bedforms on the bank that indicate active reworking and, since the surveys are 28 years apart, the seafloor could have been subjected to significant changes. Alternatively, the core-seismic discrepancies could indicate that additional erosional surfaces are present in the stratigraphy, but absent seismically. For example, H3 is seismically evident as a facies contrast and truncates estuarine strata, whereas the facies A/B boundary in Rodriguez et al. (2004) is the boundary between innershelf sand and shoreface sand, and may not produce a seismic reflection. Since Heald Bank is above what we interpret to be the transgressive ravinement, we interpret it to mostly be a reworked marine sand sheet; however, distal overwash could be present in U4/U2, and during the overall transgression process, shoreface sands could still deposit above the transgressive ravinement if the barrier moves landward, and storms help move sand offshore during a late episode of shoreface progradation (i.e. Wallace and Anderson, 2013; Anderson et al., 2022).

We interpret U2, which is mostly found beneath Sabine Bank, to be a partially preserved, subaqueous overwash deposit based on the low-angle, landward thinning, sheet-like strata that all dip landward, with no change in dip direction across the study area (Figure 2.12). Coastal ground penetrating radar studies,

which were verified with cores, have imaged several sets of landward dipping reflections onlapping lagoonal surfaces (Bennett et al., 2008; Switzer et al., 2006). Bennett et al. (2008) recognizes several internal facies with varying reflection dips and erosional surfaces between facies, whereas Switzer et al. (2006) shows a large sand sheet with an erosional base. Similarly, Shaw et al. (2015) recognizes structureless, ungraded sand at the base of the deposit, with planar, subparallel beds above with a topset-foreset break in slope that both progrades and aggrades landward. While these studies show differences in the internal structure of washover deposits, all deposits consist of landward-dipping reflections with an erosional base. The upper portion of U2, where the amplitude of the reflections decrease, is likely a portion of the sandy shoreface. This geometry and stratification were described by Schwartz (1982), along with smaller bedforms, from overwash deposits in North Carolina. U2 contains two components: 1) a SE portion with lower amplitude, higher slope reflections, and 2) a NW portion with higher amplitude, lower slope reflections. Variability in physical properties of each sedimentary layer, or acoustic impedance, produces seismic reflections for different layers (Dondurur, 2018). The variability in reflectivity is based on the contrast (i.e., differences in velocity, density, porosity, grain size, or sediment composition) between the two substrates (Dondurur, 2018). The interbedding and difference in reflectivity is consistent with cores that sample this highly reflective, low paleo-slope, overwash unit (SB-96-1, SB-96-2, SB-93-15, and SB-93-17), that Rodriguez et al. (2004) identifies as back-barrier estuarine facies characterized by interbedded sands and muds. These classifications are consistent since the interbedding of estuarine muds and thin distal overwash sands produce both the high reflectivity (consistent with the difference in grain size and sediment composition) seen in high-resolution seismic images and a unit that overall has a mud-like, estuarine appearance in cores. Below Heald bank, the estuarine unit below the transgressive ravinement could also contain distal overwash (Figure 2.11: HB-93-3), but this was not imaged in the seismic data. While estuarine is a broad category of sediments, we narrow our classification down to overwash where barrier island sands would be transported into the back-barrier environment and downlap onto estuarine muds (Figure 2.12). These identical overwash facies are observed along nearly every modern barrier along the Texas coast (summarized in Anderson et al., 2022). The cores that sample the less reflective and higher paleo-slope portion of the same overwash package (SB-93-16, SB-93-17, SB-93-3, SB-96-3, and SB-93-10) are classified as shoreface and/or tidal inlet by Rodriguez et al. (2004). This agreement in seismic facies and core classification indicates that the more homogeneous, less-reflective portion of the overwash deposit has a higher sand content than the more distal portion and is likely proximal overwash that grades into shoreface sands (i.e., shoreface progradation after the barrier drowned).

The individual paleo-slopes measured within U2 are higher in the SE portion where there is an antecedent low in the estuarine unit, whereas the NW paleo-slopes are shallower (Figures 2.3 and 2.8). The difference in paleo-slopes may be caused by the antecedent surface but are more likely related to the proximity to the barrier island, where higher paleo-slopes are proximal and lower paleo-slopes are distal. Overwash can deposit both subaerial and subaqueous sands, producing a subaerial sheet on a low slope back-barrier environment, a prograding subaqueous front into a lagoon, and finally a subaqueous deposit on top of estuarine sediments (Schwartz, 1982). These three environments are typically categorized as part of a topset-foreset break when overwash deposits into a standing body of water, where the topset is the subaerial component, the foreset is the gently dipping set of reflections at the prograding edge, and the bottomset is estuarine (Schwartz, 1982). The topset-foreset break is useful in determining the water-level in the estuary as the overwash builds (Kim et al., 2006; Shaw et al., 2015). Here, the topset of the paleo-overwash has likely been eroded by the transgressive ravinement; however, at a minimum, the largest height of the foreset, which would indicate the estuarine depth was 5.5 m (average= 2.6 m). The modern-day slopes represent the subaerial slopes of the overwash deposit, while the paleo-SE slope represents the high slope prograding subaqueous front, and the paleo-NW slopes represent the distal subaqueous deposit on top of estuarine deposits (i.e., Odezulu et al., 2018). The negative slopes seen in 3 transects in the NW portion of U2 are very close to zero and present within the middle bay geographically, therefore, we

interpret the negative slopes to represent minor subsidence. The cores also help solidify this relationship where the proximal overwash is sandier and distal overwash has more interbedded muds. Overall, the paleo-overwash displays similar internal stratigraphy as a single washover fan from Matagorda Peninsula that showed planar, stratified beds that prograde landward that could be traceable from the topset, into the foreset, and finally into the bottomset with the exception near the end of the fan (Shaw et al., 2015). This is also the case for U2, where individual reflectors are traceable from the foreset into the bottomset, with some reflections losing definition landward. Additionally, the difference in paleo-slope could be a result of erosion, where high paleo-slopes were frequently deposited, but not preserved during transgression.

U2 could also be interpreted as a flood-tidal delta, or recurved spit, based on the unit geometry, variability in horizon reflectivity and slope. However, the overall morphology of the unit and the reflections within U2 are not consistent with these environments. While flood tidal deltas are generally dominated by landward-oriented bedforms, within U2 we do not observe any bifurcating flood channels, flood ramps with a seaward facing slope, or lobate structures where variable dips would indicate movement of the delta that we would expect to see in flood-tidal delta morphologies (Hayes, 1980). We also do not observe any evidence of high-angle, shoreward-dipping reflections, crossbedding, flat beds, lateral migration, or a tidal inlet that would indicate U2 is a recurved spit (Hayes, 1980). The lack of flood-tidal delta and recurved spit morphologies and presence of overwash morphologies indicates U2 is most likely a subaqueous overwash deposit.

U3 is interpreted as a transparent, homogeneous unit infilling the remaining accommodation above the estuarine fill (Figure 2.7c). U3 does not display the distinct bedding seen in U2, and instead is a homogeneous unit with no internal reflections. Unfortunately, no cores penetrated this unit (Figure 2.7b), so sediment composition cannot fully be assessed. However, SF3 is found in both U3 and U1, and since every core on Heald and Sabine Banks that penetrates SF3 indicates that it is composed of sand, we suggest that U3 may also be composed of sand, possibly associated with the landward migrating barrier, and possibly tidal in origin. Overwash deposits likely formed in the remaining valley accommodation, but back barrier processes, like tides and wave energy, reworked the deposit, leaving it a featureless unit (Figure 2.12). Shaw et al. (2015) hypothesizes the basin depth must exceed the overwash flow depth (1-3 times the flow depth) to decrease flow enough to produce the deposition of the topset-foreset break. The additional accommodation (~5.3 m) created an estuary that was likely much deeper than if only the shelf was inundated, which could have increased the flow depth beyond a threshold that would allow for deposition and preservation of the topset-foreset break and/or increased the tidal prism and fetch of the estuary. The accommodation plus the water-level height during deposition of the overwash would make the estuarine depth, at a minimum, ~2 times the flow depth, which could indicate the basin was much deeper, or the range of flow depths should be smaller. The increased fetch would allow larger waves (Karimpour et al., 2017) and a larger tidal prism would intensify tidal currents and tidal asymmetry (Picado et al., 2010) This would lead to more energy that could rework back barrier sediments and overwasslayers were not preserved. Based on the internal seismic stratigraphy of U2 and U3 and corresponding cores, and the observation that U2 and U3 lie below the transgressive ravinement (H3), we classify Sabine Bank as consisting of remnants of a paleo-barrier island complex, whereas Heald Bank is mostly a marine sand bank.

T1: Initial valley incision, flooding during SLR, and estuarine deposition. A barrier island may exist offshore
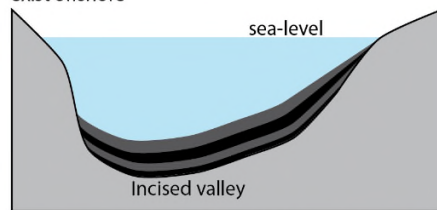
T2: Estuarine sediments fill most of the accommodation as barrier moves closer to the paleo-valley
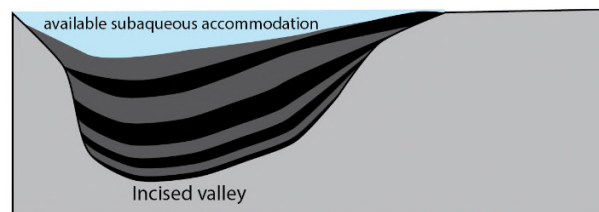
T3: Overwash deposits fill available accommodation, back barrier processes rework the deposits leaving a homogeneous wedge
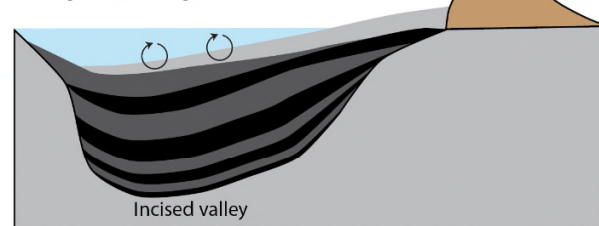
T4: Overwash deposits continue to deposit as sea level rises, and interbedding is preserved on the low slope shelf
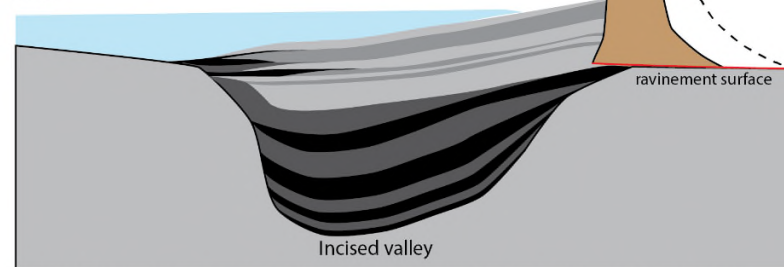
T5: Barrier transgresses leaving behind preserved overwash/shoreface deposits and a ravinement surface
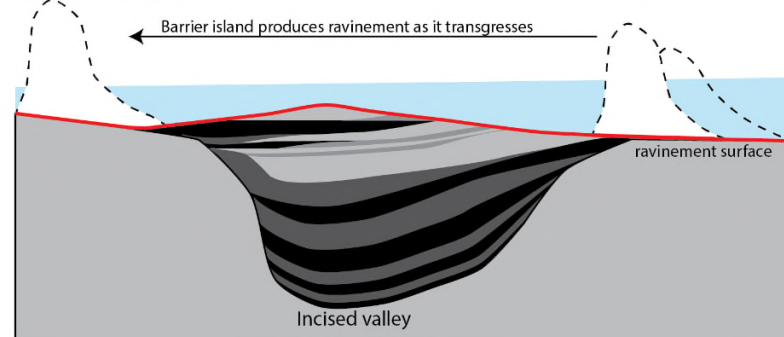
Figure 2.12. Conceptual model of barrier island preservation based on Sabine bank.

2.5.2 Why does Sabine Bank get Partially Preserved?

Since barrier islands are not preserved in the geologic record, proxies found in core and seismic data can be used to locate shoreline positions through time. Estuarine sediments require the presence of a coastal barrier seaward, which could be a barrier island, but other coastal barrier types exist, and an erosional transgressive ravinement suggests a barrier island traversed the area with the shoreface producing this erosional surface. Both estuarine deposits and transgressive ravinements can cover broad areas and thus are imprecise locators of barrier islands through time (Nummedal and Swift, 1987). The presence of other proxies, like overwash deposits, tidal inlets, shoreface deposits, ebb and flood tidal deltas, and marsh peat, all of which form adjacent to a barrier island, can be used to locate and date a paleo-barrier island more precisely (Sanders and Kumar, 1975; Rodriguez et al., 2004; Burstein et al., 2023). In order to identify preserved paleo-barrier island sediments, the transgressive ravinement, estuarine units, and one or more of the precise indicators need to be present, as well as radiocarbon ages, to accurately locate the shoreline through time.

Barrier island lithosome preservation generally requires subaqueous environments that maximize accommodation and sediment supply (Davis, 1994). Preserving transgressive sequences depends on the depth of erosion, wave energy, resistance of the material to erosion, preexisting topography, tidal range, sediment supply, and relative sea-level rise (Belknap and Kraft, 1981). Sea-level and subsidence control the extent of vertical erosion, whereas regional gradients, local wave climate, and sediment thickness control the horizontal translation of a barrier island (Penland et al., 1985). Younger barrier islands are generally thinner than their older counterparts due to the amount of time and space available for sediments to accumulate (Jervey, 1988; Penland et al., 1985).

Increasing accommodation allows for deposits to fall below storm wave base and prevents reworking and erosion, whereas high sediment supply ensures the deposits are not completely eroded from the record (Jervey, 1988). On the east Texas shelf, sea-level, subsidence, wave energy, and tidal range are assumed to affect the study area similarly, and variations in sediment supply and antecedent topography are primarily responsible for alongshore variability (Rodriguez et al., 2004). However, subsidence within compressible estuarine units in the deepest part of the incised valley could locally increase accommodation (Anderson et al., 2022). While barrier island drowning essentially occurs when sediment supply decreases and accommodation increases, preservation can be enhanced by increasing both accommodation and sediment supply (Belknap and Kraft, 1981). Accommodation must be maximized for both barrier island drowning and preservation to occur, however, sediment supply must be minimized for drowning and maximized for preservation. Therefore, the timing of sediment supply fluctuations is crucial for drowning to occur with preservation. This apparent contradiction is why barrier islands are generally not preserved. Five key components were recognized by Rodriguez et al. (2004) as necessary to preserve the barrier island remnants at Sabine Bank: the low-gradient of the shelf, antecedent topography (Sabine paleo-river valley) that provided accommodation, the shore-parallel orientation of the Sabine paleovalley, minimal reworking of the drowned deposits during transgression, and the locally increasing accommodation due to subsidence of the thick estuarine units (Rodriguez et al., 2004).

2.5.2.1 The Role of Sea Level Rise

Radiocarbon dates from the recalibrated samples from Rodriguez et al. (2004) indicate that distal and proximal overwash on the paleo-barrier island was active between ~7.2-4.5 ka and ~4.5-2.5 ka, respectively, and Sabine drowned around 2.5 ka or after. The age of Sabine barrier island drowning also corresponds with the age of Bolivar Peninsula which reached its near present day shoreline position around 2.5 ka (Rodriguez et al., 2004). Sabine Bank was hypothesized to have drowned due to the shoreline being out of equilibrium with the rest of the shoreline, and a reduction in sediment supply or a sea-level threshold was crossed (Rodriguez et al., 2004). Studies suggest that sea-level rise must be rapid

in order to drown barrier islands (Galvão et al., 2023; Emery et al., 2019; Storms et al., 2008; Cooper et al., 2016). In these conditions, back barrier accommodation increases leading to lagoonal drowning, because the bay deepens, ultimately reducing barrier island widths if the excess accommodation cannot be balanced by sediment supply (McBride et al., 1992; FitzGerald et al., 2018; Storms et al., 2008). In contrast, rates of sea-level rise were very low when Sabine Bank drowned (~0.4-0.6 mm/yr; Milliken et al., 2008a), and we therefore look to other coastal mechanisms to explain drowning and preservation.

2.5.2.2 The Role of Antecedent Topography

The accommodation from the Sabine River paleovalley proves to be limited and insufficient to completely preserve a barrier remnant (Figure 2.8). Most of the accommodation available in the river valley is in the NE portion and the aerial extent of the thickest section of accommodation is constrained to a very small area of the paleo-Sabine River valley and reaches a maximum thickness of ~5.5 ms (4.2 m).

Beneath Sabine Bank, the estuarine (U4, lagoonal and bay) sediments did not completely fill the valley and left a shallow depression for barrier island related sediments to fill (Figures 2.4 and 2.8). However, beneath Heald Bank, estuarine sediments nearly completely filled the valley incision, leaving little accommodation or potential for preservation of a barrier shoreline (Figure 2.5); a small area at the confluence of the Trinity and Sabine River paleovalleys is the only exception (Figure 2.7). This observation supports the suggestion of Rodriguez et al. (2004) that the shore-parallel orientation of the valley likely influenced accommodation and therefore preservation of barrier island sediments at Sabine Bank. As the river valley flooded during sea-level rise, the lower southern portion would flood and infill with estuarine sediments first. As sea-level continued to rise, the southern portion would remain flooded and estuarine flooding would continue towards the north. Since the southern portion would be inundated for a longer period, and is deeper, this would allow estuarine sediments to completely fill the accommodation beneath Heald Bank, but not Sabine Bank.

Within the remaining accommodation, U3 fills the depression and mimics the shape of the underlying estuarine fill, displaying a wedge-like geometry where the deposit is thickest seaward and thins landward (Figure 2.3). This pattern has been seen in other studies in the area where the underlying fluvial topography controls the shape of the estuarine fill (e.g., Burstein et al., 2023). The lack of accommodation, homogeneity of the infilling unit, and the shape of the infilling unit suggests that antecedent topography from the paleo-Sabine River valley is providing very little accommodation in this area and other factors are influencing the preservation of the recognizable barrier island proximal features within Sabine Bank.

2.5.2.3 The Role of Shelf Gradients

Modeling studies with different shelf gradient scenarios provide insight into both barrier island drowning and preservation (Shawler et al., 2020; Storms et al., 2008). When shelf gradients are high, barrier islands typically do not form, however once sea-level reaches a plateau or lower gradient, barrier islands can begin to form (Storms et al., 2008). Once established, if barrier islands encountered an increase in shelf slope, back barrier accommodation decreases, and barrier islands can transgress without drowning (thus leaving no remnants) (Shawler et al., 2020) even with no change in sediment supply. Where barrier remnants existed on these more steeply sloping shelfs (<3 m per km), the size of the deposits drastically decrease (Ciarletta et al., 2019). When shelf slopes decrease (negative slope change), remain low, or the barrier island encountered a bathymetric high, barrier islands tend to drown, even under constant rates of sea-level rise with no change in sediment supply (Shawler et al., 2020). As sea-level rises, barriers can maintain subaerial elevations through overwash; however, overwash promotes rapid shoreline retreat unless the shoreface is resupplied with sediment (Ashton and Lorenzo-Trueba, 2018). If sediment does not resupply the shoreface, the barrier experiences 'width drowning', which can occur under moderate

rates of sea-level rise (2 mm/yr) and shallow backbarrier slopes (Ashton and Lorenzo-Trueba, 2018). In all these drowning scenarios, accommodation is too high for barrier islands to persist without supplemental sediment flux (Shawler et al., 2020; Storms et al., 2008).

Additionally, other modeling studies show under wave dominated conditions, overwash deposition is the primary mode of transgression (Storms et al., 2008). Barrier islands that experience higher rates of overwash are more vulnerable to drowning (Ciarletta et al., 2019). Under this scenario, as the barrier island width decreases, the back-barrier depth and width increase leading to overstepping of the barrier island (Storms et al., 2008; Storms and Swift, 2003). In the case of Sabine Bank, the shore-parallel Sabine River paleovalley provides the slight negative slope change that could cause the barrier to drown and for some sediments to be preserved. Shawler et al. (2020) shows in their conceptual model a thin wedge of deposits on the shelf that decreases in thickness landward after the barrier drowns, which is similar to what is seen in U3 (Figures 2.4 and 2.12). Once the accommodation is filled with the initial proximal barrier sands, the gradient switches from negative (landward dipping) to positive (seaward dipping), effectively decreasing back-barrier accommodation; however, this change in gradient may not result in barrier island survival because shelf gradients are still very low (Figure 2.12). As sea-level continued to rise, even at low rates, back barrier accommodation remained high, overwash deposits formed and maintained original internal stratigraphy, and are eventually overstepped (preserved) when sediment supply cannot keep pace with back barrier accommodation (Figure 2.12). With the deposition of U3, back-barrier depths would decrease, and the tidal prism and amplitude would likely decrease the energy in the system allowing the overwash deposits to remain intact (Karimpour et al., 2017). On the low-gradient east Texas shelf, sediment supply must be high for barrier islands to keep pace with sea-level rise without drowning (Rodriguez et al., 2001).

2.5.2.4 The Role of Sediment Supply

Fluvial and longshore sediment supply were high before Sabine drowned producing a very large, stable barrier island. The preserved deposits related to Sabine barrier island are ~5 km wide, which represents barrier associated facies for Sabine barrier island that is much larger than the 500 m wide barrier deposits seen in Cooper et al. (2016) and is greater than the maximum width of modern-day Galveston Island (3.7 km). Additionally, overwash deposits found at Chesil beach, UK showed barrier island growth (5-7 ky BP) during sustained rates of sea-level rise and abundant sediment (Bennett et al., 2008). The large size of the island is likely linked to the eventual preservation of a portion of the barrier island related sediments (Jervey, 1988; Penland et al., 1985). In the time period just before and after Sabine drowned, ~3500-1700 yBP, the bayhead deltas in Calcasieu Lake and Sabine Lake had multiple flooding events as their estuaries were filling with sediment, due to a reduction in fluvial sediment supply during a climate shift (Milliken et al., 2008b; Milliken et al., 2008c). This observation is in line with the central Texas climate being warm and dry when Sabine drowned (Nordt et al., 1994) and an overall reduction of fluvial sediment supply to the coast. Decreasing sediment supply has been attributed to the drowning of Sabine Bank (Rodriguez et al., 2004). However, while fluvial sources decreased, other sources, like sediments coming from the east via longshore transport, could have helped sustain Sabine. For Sabine to maintain its subaerial position, longshore sediment sources would have to compensate for the loss of local fluvial sources.

The Maringouin complex of the Mississippi River delta maintained a ~15,030 km^2 delta from 7.5-5 ky BP (Figure 2.13), which was the westernmost delta complex during the middle and late Holocene (Roberts, 1997; Coleman et al., 1998; Milliken et al., 2008a). This complex was possibly an important sand source for east Texas barrier islands during this time. The Maringouin complex was abandoned and the Teche complex became active between 5.5-3.8 ky BP, representing a shift in the locus to the east (Figure 2.13; Frazier, 1967; Roberts, 1997; Coleman et al., 1998). Moreover the St. Bernard complex's active phase overlaps with the Teche complex 4.0-2.0 ky BP and the St. Bernard complex was the Mississippi's

easternmost lobe (Figure 2.13; Roberts, 1997). Thus, this eastward shift of the Mississippi lobes 5.5 to 2.0 ky BP was shunting sediments away from the Texas coast. While the Lafourche complex began depositing sediment further west around 2.5 ka, this likely occurred after or too close to the time Sabine Bank drowned. Therefore, during the time window Sabine Bank drowned, the remnants of the Teche complex were supplying east Texas, and thus Mississippi delta evolution coupled with the reduction of fluvial input due to climate could provide the necessary reduction in sediment supply to initiate the Sabine barrier island to drown.
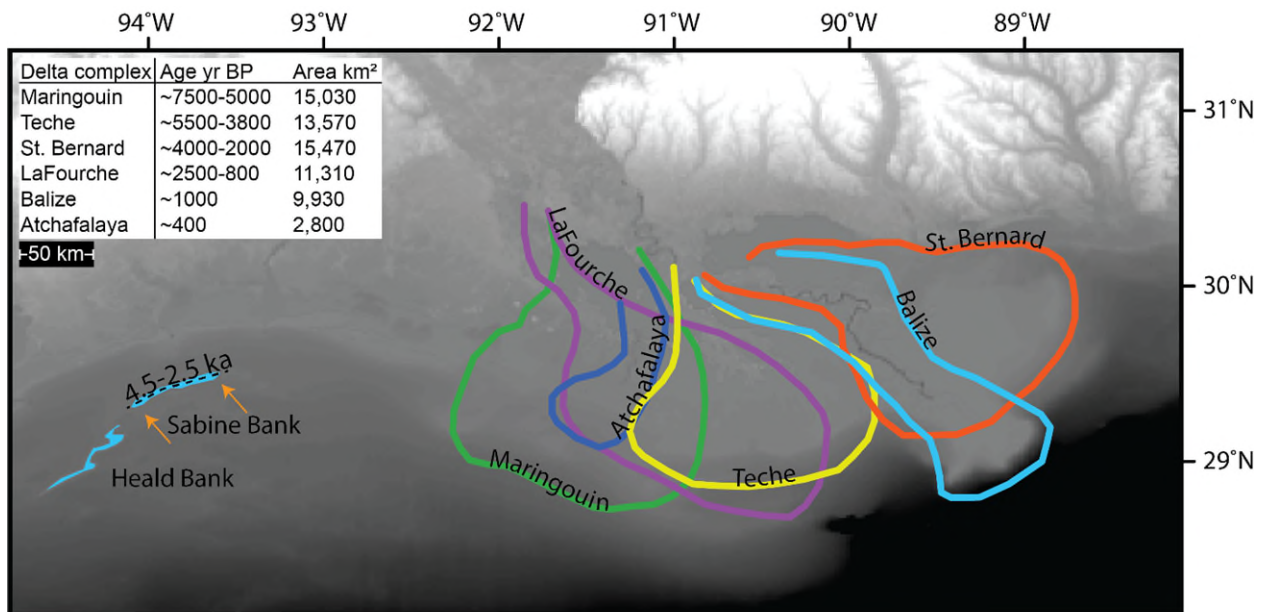
Figure 2.13. Location of Heald and Sabine Banks relative to the Mississippi river delta complexes.
Approximate locations, age, and area of each complex was acquired from Roberts (1997). The shoreline location and age are shown for Sabine barrier island as a dashed black line.

2.5.3 Styles and Timing of Barrier Island Drowning

In general, there are three styles of barrier island drowning that occur under different sediment and hydrodynamic regimes that produce distinct preserved deposits (Cooper et al., 2016; FitzGerald et al., 2006, Emery et al., 2019; Storms et al., 2008). Barrier island rollover is typically described as the most common type of barrier island retreat that only leaves behind a transgressive lag and typically occurs under low sea-level rise and/or low sediment supply conditions (Emery et al., 2019; Mellett et al., 2012, FitzGerald et al., 2016; Nummendal and Swift, 1987; Storms et al., 2008; Zecchin et al., 2019). In-place drowning occurs during rapid sea-level rise that places barrier island sediments below wave ravinement and both seaward and landward barrier facies can be preserved (Emery et al., 2019; Sanders and Kumar, 1975; Cattaneo and Steel, 2003). Finally, overstepping occurs under high- and low-sediment conditions (Mellett et al., 2012). Overstepping is facilitated by small tidal ranges, wave sheltering, and a decrease in sand supply (Galvão et al., 2023; Cooper et al., 2016). Under high-sediment conditions, partial preservation of the barrier island occurs in a limited area due to discontinuous retreat, whereas low sediment conditions preserve landward barrier facies during continuous transgression in a more extensive area (Emery et al., 2019; Mellett et al., 2012; Storms et al., 2008; Cooper et al., 2016).

The Sabine barrier island did not drown from in-place drowning since in-place drowning requires rapid sea-level rise and sea-level rise was low when Sabine drowned (Milliken et al., 2008a; Emery et al., 2019). It did not drown from rollover because rollover reworks the barrier sediments, leaving only a

ravinement behind, in contrast to the partial barrier sediment preservation observed within Sabine Bank. We conclude that the Sabine barrier island was overstepped; however, it could have drowned either by sediment-surplus overstepping, or sediment-deficit overstepping (Mellett et al., 2012; Emery et al., 2019). The remnants of the Sabine barrier island were possibly preserved due to sediment-deficit overstepping. In this case, mostly back barrier island facies are preserved, except for a thin shoreface deposit above the overwash (Emery et al., 2019; Mellett et al., 2012). During wave-dominated conditions and a low rate of sea-level rise, a plateau can abruptly increase barrier accommodation and when sediment supply cannot compensate for the increase in accommodation, overstepping occurs, controlled by the shelf gradient (Storms et al., 2008).

While the majority of Heald Bank consists of a marine sand sheet, estuarine sediments (U4) containing distal overwash, a small fraction of U3 and U2, shoreface deposits, and the transgressive ravinement, are evidence that a barrier island once existed. Additionally, the Heald barrier island drowned earlier than the Sabine barrier island sometime after ~7.7 ka (Rodriguez et al., 2004). Slightly landward of Heald Bank, overwash and inlet deposits suggest that a barrier existed ~8.5 ka, and that by 6.9 ka the barrier had transgressed landward allowing inner shelf muds to be deposited (Burstein et al., 2023). The minimal preservation of U3 and overwash deposits in Burstein et al. (2023) suggest that the Heald barrier island was either overstepped or rolled over. During the time the Heald barrier island drowned, after ~7.7 ka, sea-level rise was ~1.4 mm/yr (Milliken et al., 2008a). Additionally, the Maringouin delta complex of the Mississippi river was still west of the modern-day bird foot delta until 5.0 ka (Roberts, 1997). With these relatively low rates of sea-level rise and the along-shore high sediment supply, sediment surplus overstepping is more likely than rollover. Even though low sea-level rise conditions are met for this be a rollover case, rollover would leave no remnants of a barrier island and requires low sediment supply. In contrast, sediment surplus overstepping requires moderate rates of sea-level rise and high sediment supply and can leave partial preservation of the barrier with partial reworking of the previous barrier (Emery et al., 2019).

2.6 Conclusions

Barrier islands are prominent features across the world; however, sediments directly related to these landforms are rarely preserved in the geologic record. During sea-level rise, barrier islands transgress across the continental shelf. Sediment supply and accommodation are the primary forces influencing preservation potential of barrier islands and are controlled by many processes, like antecedent topography, sea-level rise, and climate. To increase the likelihood a barrier island or its remnants will be preserved in the geologic record, accommodation and sediment supply must be maximized, however drowning barrier islands requires maximizing accommodation and minimizing sediment supply.

Sabine and Heald Banks, on the east Texas shelf, have previously been classified as either marine sand sheets or paleo-barrier islands. Internal seismic stratigraphy of the banks reveal Sabine Bank is primarily composed of coastal facies, like overwash deposits, whereas Heald Bank is mostly composed of a homogeneous marine sand sheet. Radiocarbon dates indicate overwash was active in the back barrier of the Sabine barrier island until 2.5 ky BP when it drowned. Paleo-river valleys are commonly theorized to have provided accommodation for barrier island deposits to accumulate in, in cases of preservation, however very limited accommodation exists in the Sabine River paleovalley. Since the rate of sea-level rise was low during this period it also did not contribute to drowning. Shelf gradients are very low near the former Sabine barrier island, which increased accommodation. This condition combined with low fluvial input during a warm/dry climate, and a decrease in longshore transport from the Mississippi River delta complexes shifting east, likely resulted in the Sabine barrier island drowning. The high accommodation from the shoreface gradient helped both drown and preserve a portion of the Sabine barrier island system. The high sediment supply prior to drowning likely helped Sabine maintain a stable

position, creating a large volume of sand that was not completely removed when sediment supply decreased and the barrier island drowned. The main portion of the Sabine barrier island that is preserved as part of Sabine Bank is the back-barrier, subaqueous overwash deposit that is a potentially important sand resource for coastal protection. In contrast, Heald Bank dominantly consists of a marine sand sheet, although a small fraction may be reworked and preserved overwash. If so, the suggested mechanism for Heald barrier island drowning is sediment surplus overstepping. The fact that far less barrier island material was preserved in the case of Heald, unlike Sabine with extensive subaqueous overwash deposits, may reflect both the style of drowning, amount of sediment supply prior to drowning, and the original size of the barrier island.

3 Stratigraphic Analysis of Sabine and Trinity River Paleovalleys

3.1 Introduction

While the previous chapter focused on stratigraphic analysis of the Texas sand banks and their possible relationship, or not, to preserved barrier island deposits, in this chapter we interpret strata deeper in the chirp data: sediments that were deposited in an estuarine setting in and around the Trinity and Sabine River paleovalleys.

Estuaries are important nursery, feeding and migratory habitats for birds, fish, and other wildlife; they are economically important for commercial and recreational fishing, transportation, and commerce; and they are buffer zones and protect communities from floods and storms (Beck et al., 2003; Bertness, 1999; Daily et al., 1997). Incised valleys have long been recognized as features with high accommodation where transgressive estuarine sedimentary facies form and are well preserved (Zaitlin et al., 1994; Allen et al., 1993). During sea-level rise (transgression), river mouths are flooded, creating an estuary that receives sediment from both fluvial and marine sources and contain facies influenced by tides, waves, and fluvial processes (Dalrymple et al., 1992). Incised river valleys provide a natural laboratory to understand controls on estuarine evolution and preservation during inundation. Estuaries are highly efficient sediment traps with high preservation potential that should be widely represented in the geologic record (Dalrymple et al., 1992; Biggs and Howell, 1984). Generally, estuaries extend from the landward limit of tidal facies (head) to the seaward limit of coastal facies (mouth; Zaitlin and Shultz, 1990; Dalrymple et al., 1992). Since estuaries are primarily transgressive features, they are also ephemeral (Dalrymple et al. 1992).

Estuaries are typically classified as either river, tide, or wave dominated (Galloway, 1975). Near the estuarine head, fluvial energy dominates, and decreases seaward, whereas tidal or wave energy is higher at the mouth and decreases landward (Dalrymple et al., 1992; Roy et al., 1980). This creates three distinct zones within the estuary: the outer bay, which is dominated by marine processes; the central bay, a relatively low energy environment where marine and fluvial processes are equal; and the upper bay which is dominated by river processes (Dalrymple et al., 1992; Roy, 1994). Both types of estuaries have bayhead deltas at their heads (Steel and Milliken, 2013). In the marine portion of the estuary, it can be either wave-dominated or tide-dominated. These two characterizations produce different estuarine facies. Wave-dominated estuaries are typically characterized by coastal barriers (barrier islands, spits, submerged bars) near the mouth due to the high wave energy creating alongshore and onshore sediment transport (Steel and Milliken, 2013). This prevents most marine waves from entering the estuary and therefore any wave action is internally generated (Dalrymple et al., 1992). Small tidal ranges or tidal prisms create lake like estuaries with no inlets, but slightly higher tidal energy allows few inlets to remain open (Dalrymple et al., 1992). Marine sands are typically sourced from inlets, flood tidal deltas, and overwash (Steel and Milliken, 2013). Tide-dominated estuaries have large tidal currents near the mouth that produce elongate sand bars parallel to flow (Dalrymple et al., 1992). These estuaries typically have a funnel shape where the incoming flood tide is cross-sectionally compressed and tidal current speeds increase until friction dissipates the energy, which typically occurs in the central bay (Dalrymple et al., 1992). Fluvial energy, in both tide and wave dominated estuaries, decreases at the head due to the decreasing hydraulic gradient producing two energy maxima at the head and mouth and an energy minimum in the central bay (Dalrymple et al., 1992). The interaction of these processes produces sandier sediments in the upper and outer bays, with the finest grain sediments in the central bay (Dalrymple et al., 1992). In tide dominated estuaries the energy minimum in the central bay is less pronounced than in wave-dominated systems, which creates an overall sandier estuary with most of the mud accumulating in tidal flats and marshes along the estuarine flanks (Dalrymple et al., 1992).

Estuaries can also be classified as underfilled, overfilled, or near equilibrium depending on sediment supply and accommodation (Nichols, 1989; Simms et al., 2006). When accommodation is greater than sediment supply, basins are underfilled resulting in depth increases and ultimately changes in coastal processes, like wave energy and the tidal prism (Nichols, 1989; Deaton et al., 2016). Underfilled basins typically have large volumes and low accumulation rates, resulting in limited sediment supply (Nichols, 1989). In the geologic record they typically exhibit fluvial fill at the base of the valley, an estuarine middle section, and capped by marine deposits (Simms et al., 2006). Wave and tidal energy are often the most important factors controlling internal stratigraphy, however sea-level rise, antecedent topography, and climate variability control overall transgression (Zaitlin et al., 1994; Simms et al., 2006). When accommodation is less than sediment supply, basins are overfilled, sediment is exported from the system, and many processes may not be recorded in the geologic record. Overfilled valleys have active deltaic sedimentation and high accumulation rates indicating they are not sediment limited (Nichols, 1989). Overfilled valleys are mostly filled with fluvial sediment and are laterally unstable producing several avulsion cycles and do not occupy a single valley over their evolution (Simms et al., 2006). Finally, when accommodation is equal to sediment supply, the basin is in equilibrium, coastal processes remain constant, and preservation is the most complete (Nichols, 1989). Most estuaries are near equilibrium and waves and currents primarily modulate depth (Nichols, 1989). Under and overfilling of basins has direct implications for how coastal systems evolve, as well as what and where environments are preserved. Ideally, a basin in equilibrium would be the ideal to understand how processes are preserved in the record, however classifying the basin allows for interpretations that include preservation biases of that systems record.

This analysis presented in this chapter aims to understand the sediment composition and grain size of estuarine units of the Trinity and Sabine River paleovalleys, situated beneath Shepard, Heald, and Sabine Banks (Figure 3.1). Estuarine environments that are closer to high energy environments, like rivers and inlets, are more likely to contain sand deposits than the low energy central bay. Therefore, the bayhead delta, upper bay, and outer bay units could contain sand deposits. Due to transgression, the outer bay unit is closer to the surface than the upper bay and bay head delta. Using high resolution chirp seismic reflection data, we mapped the bay facies throughout the region and used archival cores to determine the likely sediment composition of several bay facies.

3.2 Study Area

3.2.1 Sea-Level History

(This section reiterates key points from Section 2.2.2) Following the last glacial maximum (LGM), global sea-level has been rising at various rates (Shepard and Suess, 1956; Curray, 1960; McFarlan, 1961; Nelson and Bray, 1970; Frazier, 1974; Anderson et al., 1991; Tornqvist et al., 2006). On low gradient coasts, like the Texas coast, even slight sea-level variations can produce inundation of large coastal areas. In Texas estuaries, several flooding events during the early Holocene, ~ 9.8-9.5 ky BP, 8.9-8.5 ky BP, 8.4-8 ky BP, and 7.4-6.8 ky BP, occurred as sea-level was rising rapidly as the West Antarctic Ice Sheet retreated (Milliken et al., 2008a; Anderson et al., 2002). Several of these flooding surfaces coincide with specific early Holocene episodic ice sheet retreat events (Milliken et al., 2008a). For example, the 8.4-8 ky BP event is associated with the collapse of the Laurentide Ice Sheet (Tornqvist et al., 2006). The rapid, 4.2 mm/yr, rate of sea-level rise during the early Holocene ended around 9.6 ky BP. The middle Holocene (8-4 ky BP) is characterized by a relatively continuous rate of sea-level rise of 1.4 mm/yr (Milliken et al., 2008a). Subsidence in the Gulf of Mexico is 1-1.5 mm/yr on the innershelf and is mostly driven by sediment loading of Holocene and Pleistocene deltas (Ivins et al., 2005; Ivins et al., 2007). However, the East Texas shelf is generally outside of the limits of the Mississippi river delta loading (Simms et al.,

2007). During the late Holocene, over the past 4 ky, rates of sea-level rise were 0.4-0.6 m/yr (Milliken et al., 2008a).
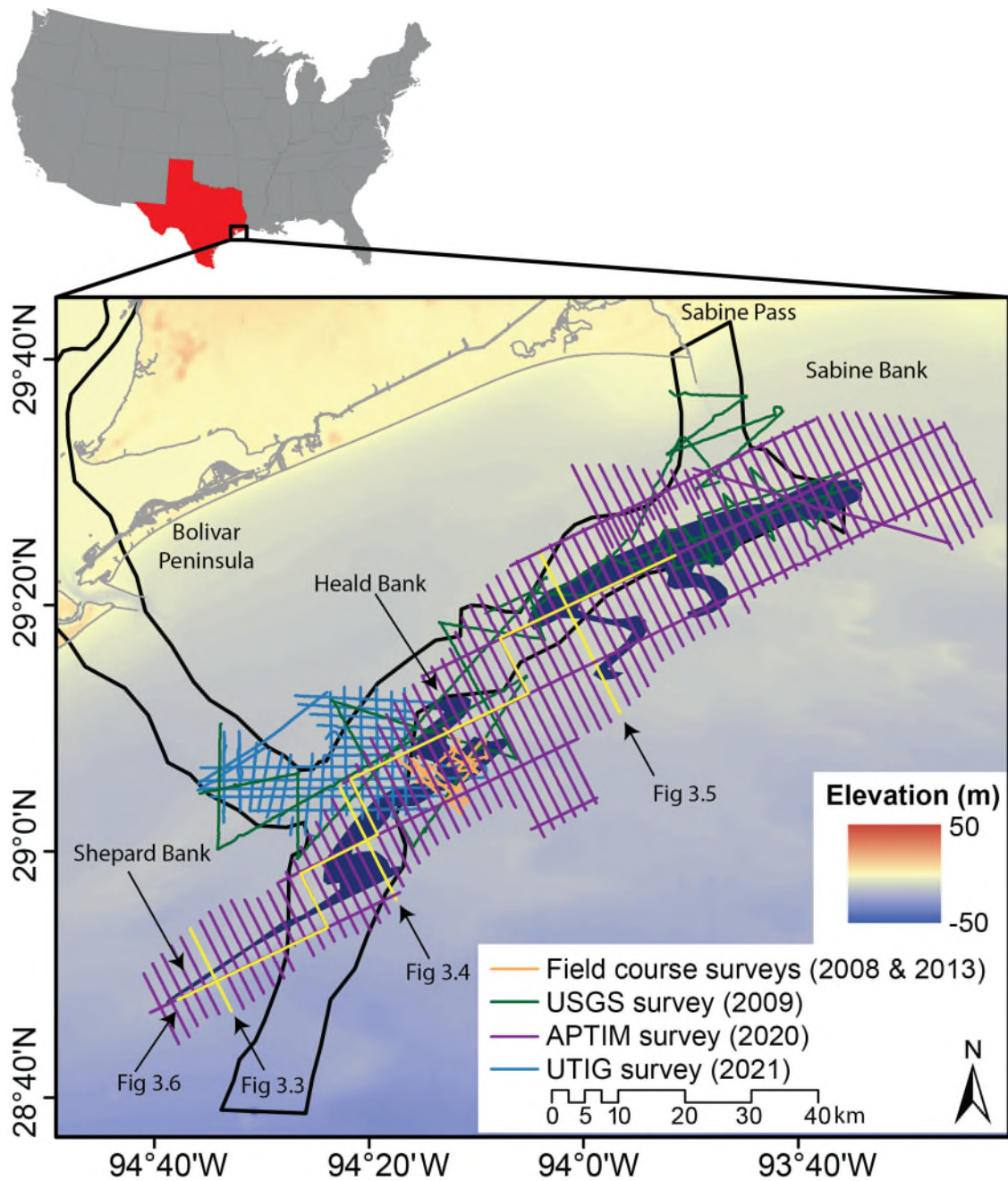
Figure 3.1. Study area map of the Trinity-Sabine incised river valley extent and all surveys.
The black outline is the paleo-Trinity-Sabine River paleovalley from Thomas and Anderson (1994). The dark blue polygons show the extent of Shepard Bank to the SW, Heald bank central, and Sabine Bank to the NE. Yellow lines identify locations of figures as indicated. Background elevation data was obtained from: https://www.gmrt.org/GMRTMapTool/.

3.2.2   Climate History

Globally, the transition from Pleistocene to Holocene is marked by warming and drying of the climate based on several independent datasets (Toomey et al., 1993; Ellwood and Gose, 2006; Nordt et al., 1994; Nordt et al., 2002; Bryant and Holloway, 1985). Overall Holocene climate is warming, but there are variations across the state (Troiani et al., 2011). A shift in vertebrate fossils and pollen between 8.7-6 ka (Toomey et al., 1994; Bryant and Holloway, 1985) suggest desert like conditions were sustained until the middle Holocene when a C4 plant maximum was noted (6-5 ka; Nordt et al., 1994; Nordt et al., 2002). These climate records agree until the Late Holocene (4 ka) when C4 plant biomass decreases and suggest a cooler/wetter climate (Nordt, 1994), but vertebrate records suggest very dry conditions between 5-2.5 ka based on the disappearance of wet climate species. By 2.5-1 ka wetter and cooler conditions were observed again based on faunal assemblages and shifts in pollen (Toomey et al., 1993; Bryant and Holloway, 1985). Finally, ~1 ka, slightly drier or warmer conditions were observed again (Toomey et al., 1993).

3.3   Methods

Methods for chirp processing and interpretation, and core-seismic integrations are given in Section 2.3.

In an effort to understand the sedimentological characteristics of each unit, horizon, and seismic facies, we used previously published cores from the study area (Thomas and Anderson, 1994; Dellapenna et al., 2009). Within the bounds of our seismic track lines, 92 cores and borings exist. However, most of those penetrate <4 m without sampling the estuarine units identified in this study. We used two of the longest cores, and two borings to constrain grainsize and character of three of our units. We converted core penetration depths, contact boundary depths, and radiocarbon age depths to TWT using 1,525 m/s as a conversion, which assumes no variation in velocity down core, although variations exist (Abdulah et al., 2004). To obtain meters below sea-level, we added the TWT of the seafloor at the core location to each depth.

3.4   Results

3.4.1   Seismic Facies

Within our study area, we have identified 7 seismic facies, 13 seismic horizons, and 11 seismic units. Several horizons and units, other than those described below, exist within our study area, however they are highly confined and only span a few lines, we therefore only interpreted horizons that mapped across ≥7 dip lines, which equates to an aerial extent of ~13 km.

Seismic Facies 1 (SF1): SF1 consists of low-to-medium-amplitude discontinuous reflections. This facies can be found in surficial units, and deeper units near the base of the section (Figure 3.2).

Seismic Facies 2 (SF2): SF2 is a low-to-medium and medium-to-high-amplitude, parallel to sub-parallel unidirectional, dipping reflections facies. This facies is primarily found near the surface (Figure 3.2).

Seismic Facies 3 (SF3): SF3 is characterized by transparent-to-low-amplitude, chaotic, and discontinuous reflections. This facies is found throughout the section at many depths (Figure 3.2).

Seismic Facies 4 (SF4): SF4 is composed of medium-to-high-amplitude, draping reflections with occasional truncations. This facies is found throughout the middle units and some deeper units (Figure 3.2).

Seismic Facies 5 (SF5): SF5 contains medium-to-high-amplitude, unidirectional dipping reflections displaying lateral accretion with some truncations. This facies is found deeper units within the section (Figure 3.2).
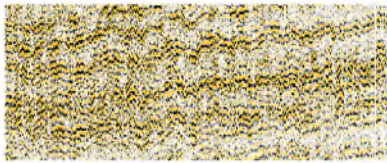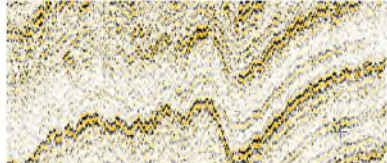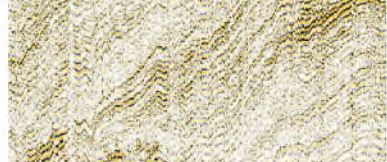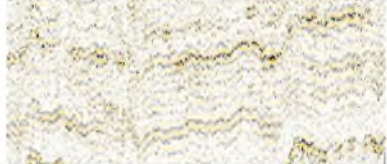
Facies	Example	Description
SF1		Low-to-medium-amplitude with discontinuous reflections
SF2		Low-to-medium and medium-to-high-amplitude, parallel to sub-parallel, unidirectional, dipping reflections
SF3		Transparent-to-low-amplitude, chaotic and discontinuous reflections
SF4		Medium-to-high-amplitude, draping reflections with occasional truncations
SF5		Medium-to-high-amplitude, unidirectional dipping reflections displaying lateral accretion with some truncations
SF6		Low-to-medium-amplitude, draping reflections with occasional truncations
SF7		Transparent-to-low-amplitude, chaotic reflections, occasional medium-to-high-amplitude discontinuous reflections

Fig 3.2. Examples of seismic facies found in the study area with descriptions of each facies.

3.4.2 Horizons

In the previous chapter, which focused on the stratigraphy associated with the sand banks, we identified 6 horizons for stratigraphic analysis. Extending deeper into the estuarine section we expand that interpretation to include 15 horizons in total. They are:

Horizon 1 (H1): H1 is a high amplitude, continuous horizon that exists throughout the entire study area. This horizon is the modern-day seafloor. In the southern portion of the study area, the seafloor reaches 33.32 ms (~25 m) in depth, and in the northern portion of the study area, it is shallowest at 8.84 ms (~7 m) (Figure 3.3, 3.4, 3.5).

Horizon 2 (H2): H2 is a low amplitude parallel horizon that separates SF1 above from SF3 below. This horizon is confined to the sandbanks. It varies in depth from 28.54 ms (~22 m) at the deepest and 15.52 ms (~12 m) at the shallowest depths (Figure 3.4).

Horizon 3 (H3): H3 is an erosive surface that divides a strong facies contrast. In some areas this horizon truncates several other horizons, like H4, H5, and H6. This is generally a well-defined horizon, however in some areas where the facies contrast is not strong, it is inferred based on geologic principles and is always above H4 or H5 and below H1, or H2 if present. Above H3 is SF3 and below are SF2, SF3, and SF4. This horizon is deepest in the SW at 34.42 ms (~26 m) and shallowest near Sabine Bank at 12.82 ms (~10 m; Figure 3.3, 3.4, 3.5).

Horizon 4 (H4): H4 is the boundary between SF2 above and SF3 below. Truncations in SF3 downlap onto H4, which defines this surface. It is present beneath and landward of Sabine Banks and varies in depth from 24.49 ms (~19 m) to 14.40 ms (~11 m; Figure 3.5).

Horizon 5 (H5): H5 is a generally conformable surface that is the boundary between SF3 and SF4. It is found beneath both banks and is deepest beneath Heald Bank at 27.61 ms (~21 m) and is shallowest in the NE at 17.41 ms (~13 m; Figure 3.4, 3.5).

Horizon 6 (H6): H6 is a predominately medium-amplitude horizon that is the boundary between SF2 above and SF3 below. This horizon is beneath Shephard Bank, in the SW portion of our study area, and is truncated by H3 and varies in depth from 34.74 ms (~26 m) at the deepest and 27.49 ms (~21 m) at the shallowest. This horizon likely extends to the W beyond our study area (Figure 3.3).

Horizon 7 (H7): H7 is a high facies contrast boundary between SF3 above, and SF4 below and exists in the SW area of the study area. This horizon varies from 36.13 ms (~28 m) at the deepest and 25.68 ms (~20 m) at the shallowest. This horizon shallows and pinches out to the east and is truncated by H3 (Figure 3.3).

Horizon 8 (H8): H8 is a high-amplitude horizon that designates the boundary between SF3 above and SF4 below in a small portion of the study area and SF6 above and SF1, SF5, SF7 below. This horizon is highly conformable and where it does not designate a facies boundary, can be traced throughout the study area. This horizon is regionally extensive and spans from the SW to the Trinity-Sabine confluence. It varies in depth from 42.62 ms (~32 m) at the deepest and 24.16 ms (~18 m) at the shallowest (Figure 3.3, 3.4).

Horizon 9 (H9): H9 is an erosional surface that designates the boundary between SF1 above and SF4 or SF5 below. This horizon truncates the internal horizons within SF4 and SF5. This horizon is confined to the SW portion of the study area and varies in depth between 41.57 ms (~32 m) at the deepest and 31.22 ms (~24 m) at the shallowest (Figure 3.3).

Horizon 10 (H10): H10 is a medium-amplitude reflection that separates SF4 above from SF3, SF6, and the Pleistocene below. Internal horizons from SF4 frequently onlap onto H10. This horizon is confined to the SW and at the deepest is 41.93 ms (~32 m) and 31.58 ms (~24 m) at the shallowest (Figure 3.3).

Horizon 11 (H11): H11 is the boundary that designates a facies contrast between SF1 above and SF 4 and SF6 below. This horizon is just S of the Trinity-Sabine confluence and varies in depth between 29.67 ms (~23 m) at the deepest, and 24.82 ms (~19 m) at the shallowest (Figure 3.6).

Horizon 12 (H12): H12 is a low-amplitude reflection that designates the boundary between SF3 above and SF1 and SF7 below. This horizon is confined north of the confluence and varies from 35.39 ms (~27 m) and 24.61 ms (~19 m; Figure 3.6).

Horizon 13 (H13): H13 designates the facies contrast between SF4 above and SF1, SF3, SF6, and SF7 below. This horizon is also regionally extensive and spans most of the study area. This horizon continues landward, past the limits of this study area, and joins with H3 from Burstein et al. (2023). H13 varies in depth from 33.73 ms (~26 m) at the deepest and 17.80 ms (~14 m) at the shallowest (Figure 3.4, 3.5).

Horizon 14 (H14): H14 is a high-amplitude horizon that transitions to a low-amplitude horizon towards the N. H14 is confined to the NE portion of the study area. Above H14 is SF5 and below is SF7. At the deepest, H14 is 34.74 ms (~26 m) and 20.58 ms (~16 m) at the shallowest (Figure 3.5).

Horizon 15 (H15): H15, identified as H6 in Chapter 2, is an erosive boundary that cuts into the underlying strata and reaches a maximum of 54.38 ms (~41 m) in depth. The geometry of this horizon produces a channelized feature that runs parallel to the modern-day shoreline. A second valley intersects the parallel valley and runs perpendicular from that valley to shore. Several smaller channels intersect the main parallel valley in multiple locations. H15 is interpreted to be the base of the flooding surface that was created as sea-level infilled the valley. This surface reflects the base of the estuarine section. The chirp is unable to acoustically penetrate H15 to image the base of the incised valley that would likely contain fluvial deposits, like point bars. H15 is the antecedent topography that coastal facies infilled during transgression (Fig 3.3, 3.4, 3.5, 3.6).
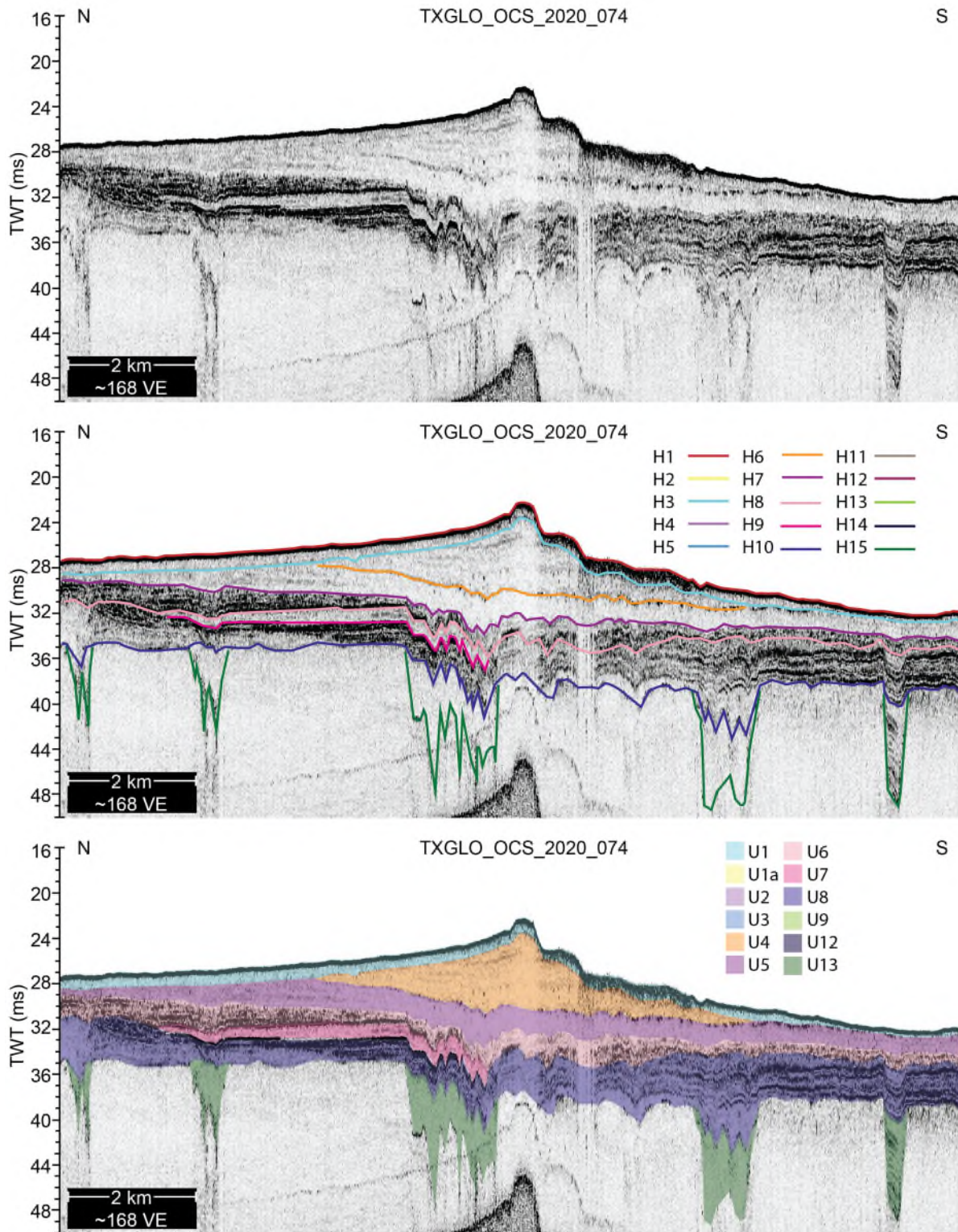
Figure 3.3. Chirp envelope record over Shepard Bank.
The top panel shows the uninterpreted data, the middle shows the interpreted horizons, and the bottom panel shows the interpreted units.
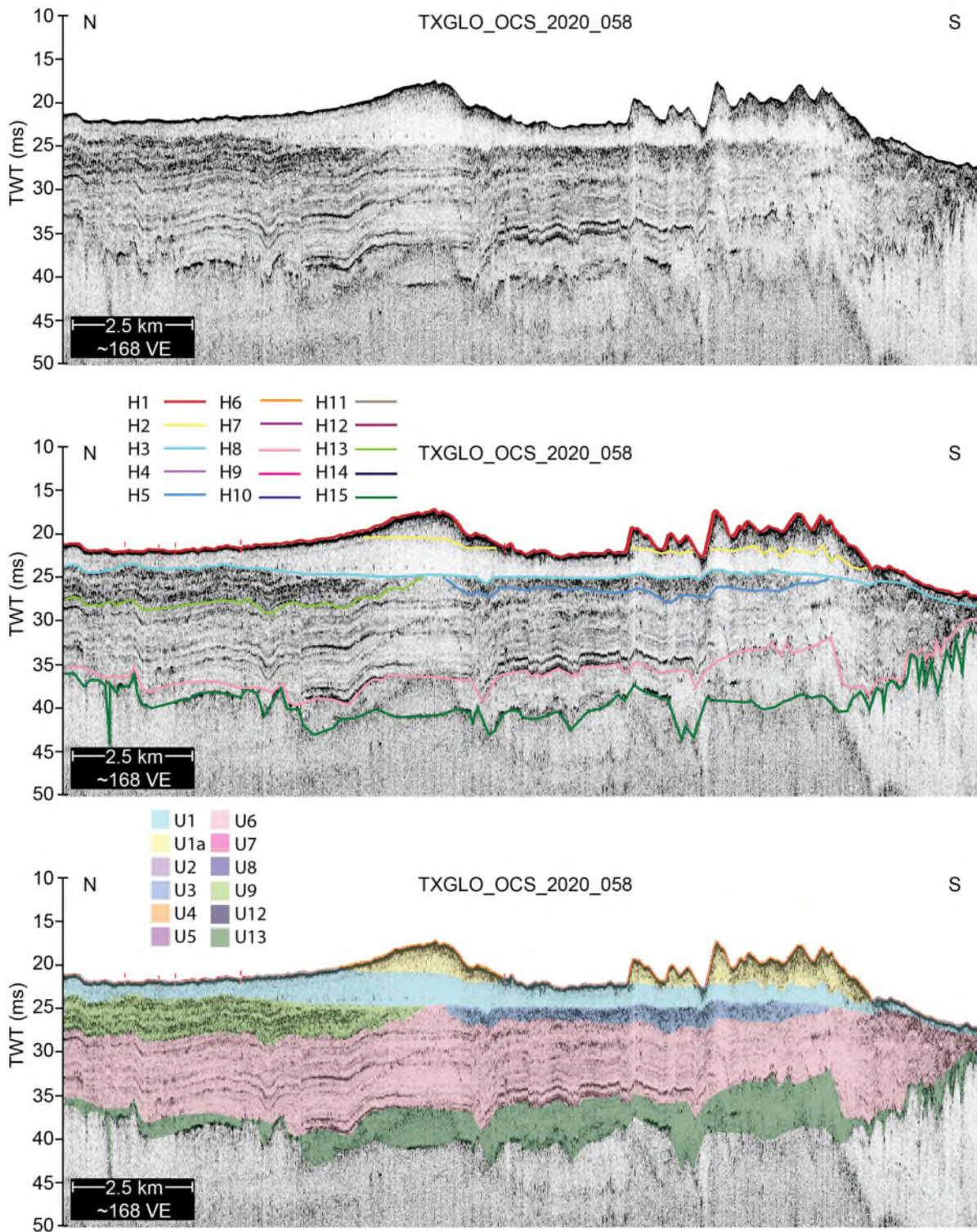
Figure 3.4. Chirp envelope record over Heald Bank.
The top panel shows the uninterpreted data, the middle shows the interpreted horizons, and the bottom panel shows
the interpreted units.
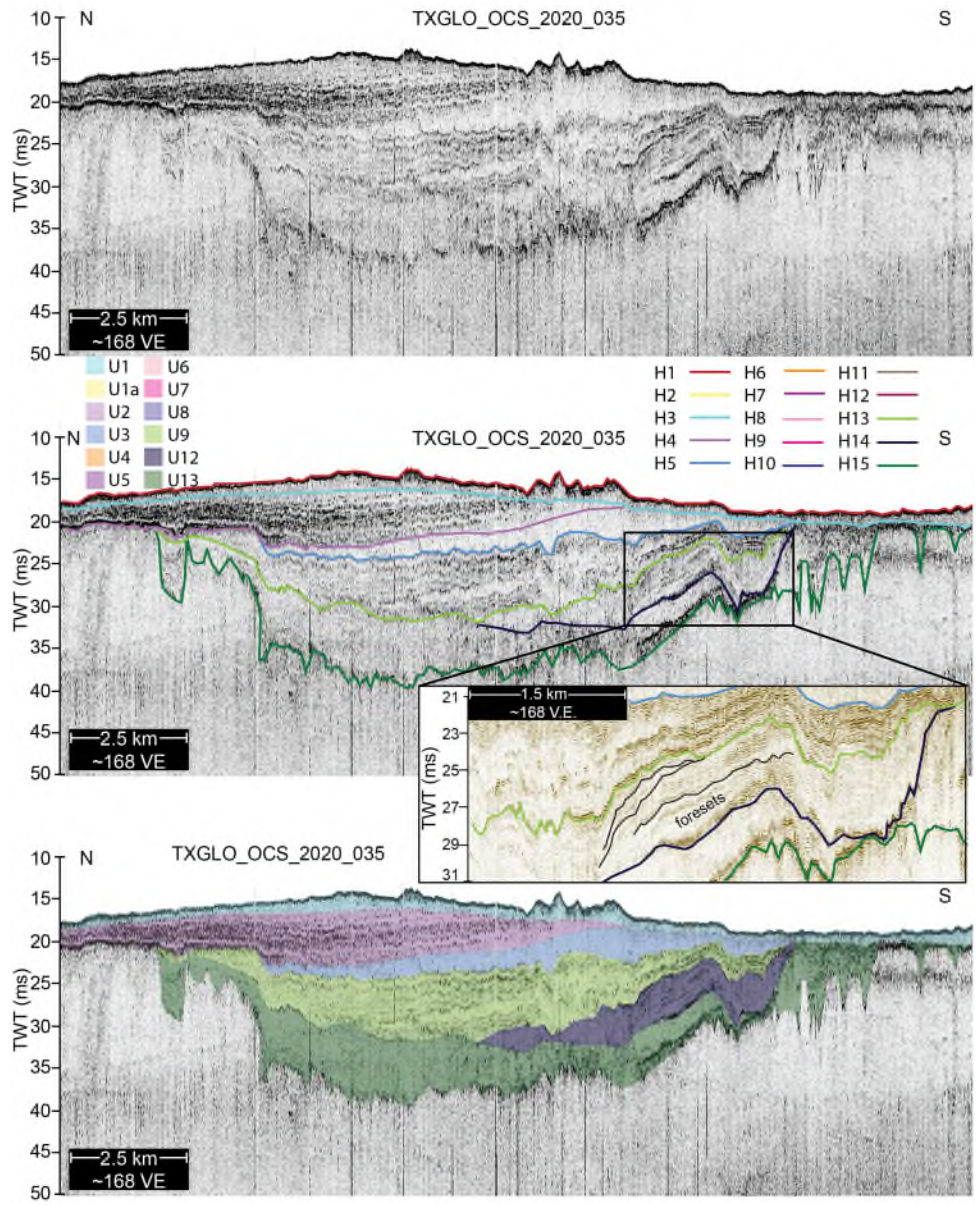
Figure 3.5. Chirp envelope record over Sabine Bank.
The top panel shows the uninterpreted data, the middle shows the interpreted horizons, with inset showing full waveform enlargement of U12 (interpreted as bayhead delta deposits), and the bottom panel shows the interpreted units.
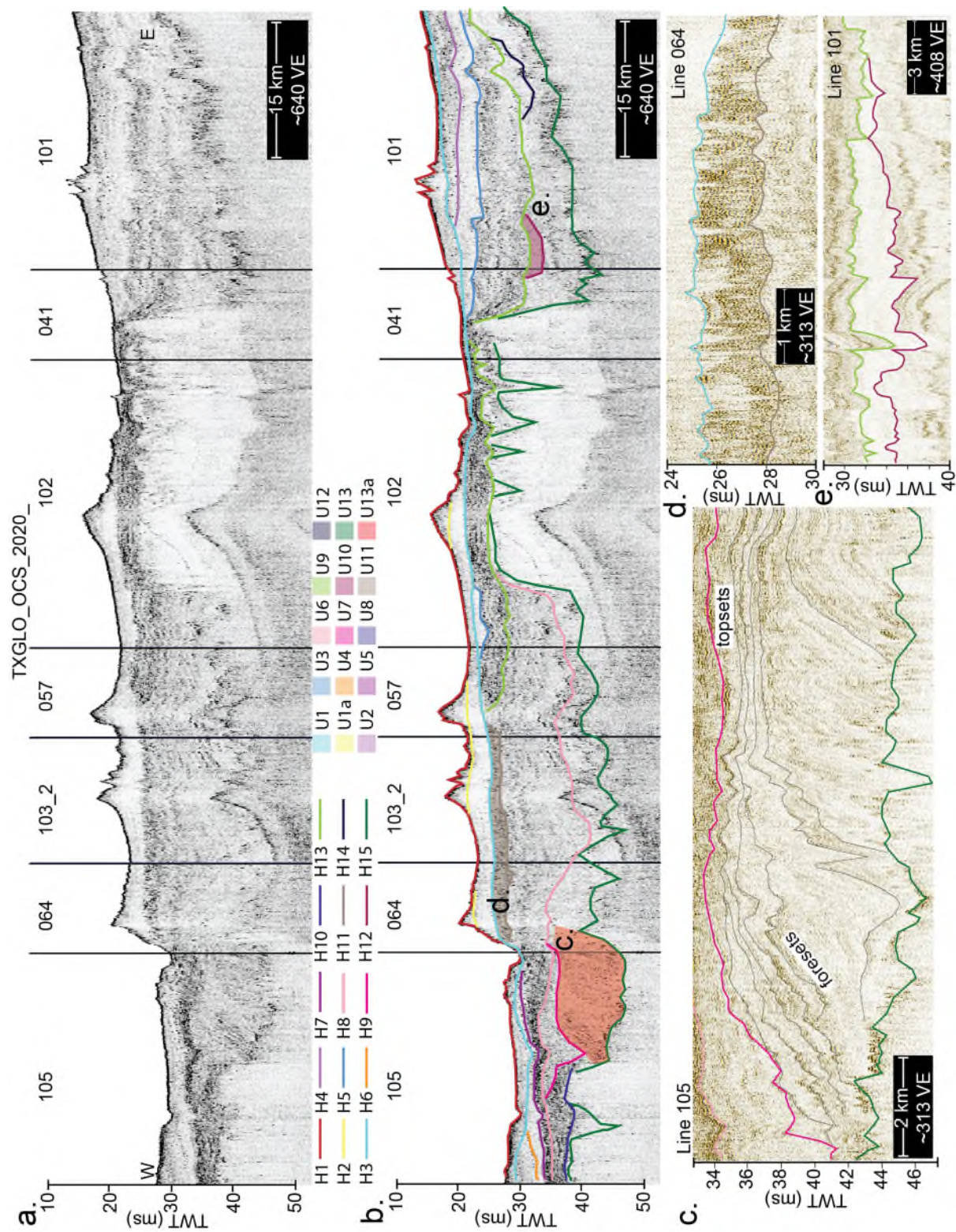
Figure 3.6. Chirp record along a transect crossing the study area.
(a) Uninterpreted envelope data and (b) the interpreted horizons. Location shown in Figure 3.1. Enlarged full-waveform records show (c) bayhead delta strata of U13a, (d) unit U11, and (e) unit U10.

3.4.3 Units

We created an isopach map that shows the thickness of the entire estuarine section comprising units U4-U13 (identified in Chapter 2 collectively as U4). The top of this unit was bounded by H5 if present, then H4 if present, and finally H3. This unit is thickest within the valley and the maximum thickness is 26.88 ms (~20 m) and fills all of the valley accommodation in the SW and most of the accommodation in the NE (Figure 3.7). Additionally, we have generated an updated paleovalley outline (Figure 3.7), including various tributaries, based both on the analysis presented here as well as analysis of data presented in our Texas General Land Office study (Goff and Gulick, 2023). Importantly, within this outline the overall thickness of the estuarine section represents the overburden above the fluvial sands that are known to inhabit the base of the paleovalley. That overburden is notably thinner in the Trinity paleovalley near the confluence with the Sabine, in the Sabine paleovalley closer to the coastline, and within the various tributaries.

Unit 1 (U1): U1 consists of SF1, low-to-medium discontinuous reflections, and SF3, transparent-to-low discontinuous reflections. U1 is present throughout the study area and is bounded above by the seafloor (H1) and below by H3. This unit is thickest, 5.67 ms (~4 m), over Heald Bank (Figures 3.3, 3.4, 3.5).

Unit 1a (U1a): U1a is a subunit of U1 that only consists of SF1. It is bounded by the seafloor above, and H2 below. This unit is constrained to Heald Bank and a small area in front of Sabine Bank (Fig 3.4).

*Unit 2* (U2): U2 is composed of SF2, medium-to-high parallel, unidirectionally dipping reflections and is bounded by H3 above and H4 below. The dipping reflections dip in the landward direction. U2 is found below Sabine Bank but is mostly absent beneath Heald Bank. The thickest portion of U2 is 7.92 ms (~6 m; Figure 3.5).

Unit 3 (U3): U3 is bounded by H5 below and above by H4 if present, or H3 if H4 is not present. This unit is a transparent homogenous unit composed of SF3. At the thickest, U3 is 4.34 ms (~3 m) beneath Sabine Bank and near the confluence of the Sabine and Trinity valleys (Figure 3.5).

Unit 4 (U4): U4 is composed of SF2, low-to-medium, parallel dipping reflections. Unlike U2, these reflections dip in the seaward direction. U4 is constrained to the SW portion of the study area. This unit is 4.18 ms (~3 m) thick and bounded above by H3 and below by H6 (Figures 3.3, 3.9).

Unit 5 (U5): U5 is a thin deposit, 4.02 ms (~3 m), that is constrained to the SW area. It is composed of SF3 and bounded above by H6 where present or H3 and below by H7 (Figures 3.3, 3.9).

Unit 6 (U6): U6 comprises SF4, medium-to-high-amplitude draping reflections to the W, and transitions to SF6 moving towards the E. U6 is an extensive unit and the thickest portion, 17.49 ms (~13 m), is confined to the river valley. The top of U6 is defined as H11, where present, if not, H7 where present, and finally, H3. The base of U6 is H8 (Figures 3.3, 3.4, 3.8).

Unit 7 (U7): U7 is capped by H8 and the base is H9. U7 is characterized by SF1 and is 6.94 ms (~5 m) thick and is confined to the SW portion of the study area (Figures 3.3, 3.9).

Unit 8 (U8): U8 is composed of SF4 and exists almost entirely outside of the main Sabine River valley in the SW area. The top of U8 is defined as H9 where present, then H8 where present, and H7. The base of U8 is H10. The thickest portion of U8 is 6.30 ms (~5 m; Figures 3.3, 3.9).

Unit 9 (U9): U9 is composed of SF4. The top of U9 is H5 if it exists, and if not H3. The base is H13 and the thickest this unit becomes is 9.69 ms (~7 m). This unit is regionally extensive and extends landward

into the study area of Burstein et al. (2023) and Standring et al. (2024) where foraminifera assemblages are dominated by *Elphidium*, which indicates outer bay environments (Figures 3.4, 3.5, 3.8).

Unit 10 (U10): U10 is a small unit just N of the river confluence. The top of U10 is H13 and the base is H12. The thickest portion of U10 is 4.51 ms (~3 m). This unit likely extends landward, beyond our study area (Figure 3.6).

Unit 11 (U11): U11 is composed of SF4 and is confined just S of the confluence. The thickest portion of the unit is 3.28 ms (~3 m). The top of U11 is H7 where present, and H3 when H7 is not present and the base is H11 (Figures 3.6).

Unit 12 (U12): U12 is dominated by SF5 and is 7.89 ms (~6 m) thick. The top of this unit is H13 where it exists and H3 if it does not. The base of this unit is H14. This unit is confined to the northern portion of the study area and at the confluence at a small tributary that joins with the main Sabine River valley (Figures 3.5).

Unit 13 (U13): U13 is characterized by several seismic facies, SF1, SF3, SF5, and SF7, that vary throughout the study area. This unit has a maximum thickness of 20.50 ms (~16 m; Figures 3.3, 3.4, 3.5, 3.6). An isopach for U13 was not generated at this time because of complexities in defining the upper bound, which is characterized by numerous different horizons.

Unit 13a (U13a): U13a is a subunit of U13 that only contains SF5, or the medium-to-high-amplitude unidirectional dipping reflections that display lateral accretions. This unit is constrained to the SW area and the thickest portion is 19.58 ms (~15 m, Figures 3.6, 3.10).
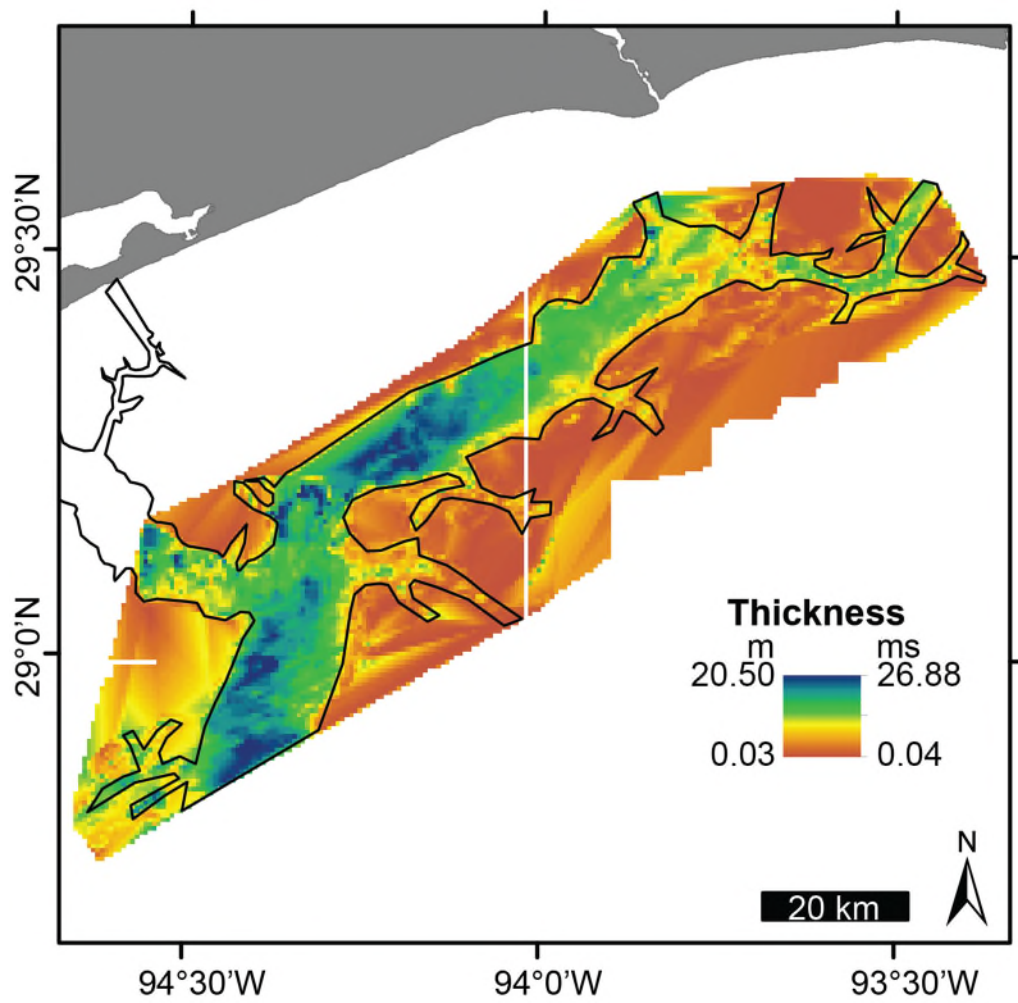
Figure 3.7. Isopach map for the entire estuarine volume.
The estuarine volume consists of Units 4-13. Black lines represent our updated outline of the Trinity/Sabine paleovalley system.
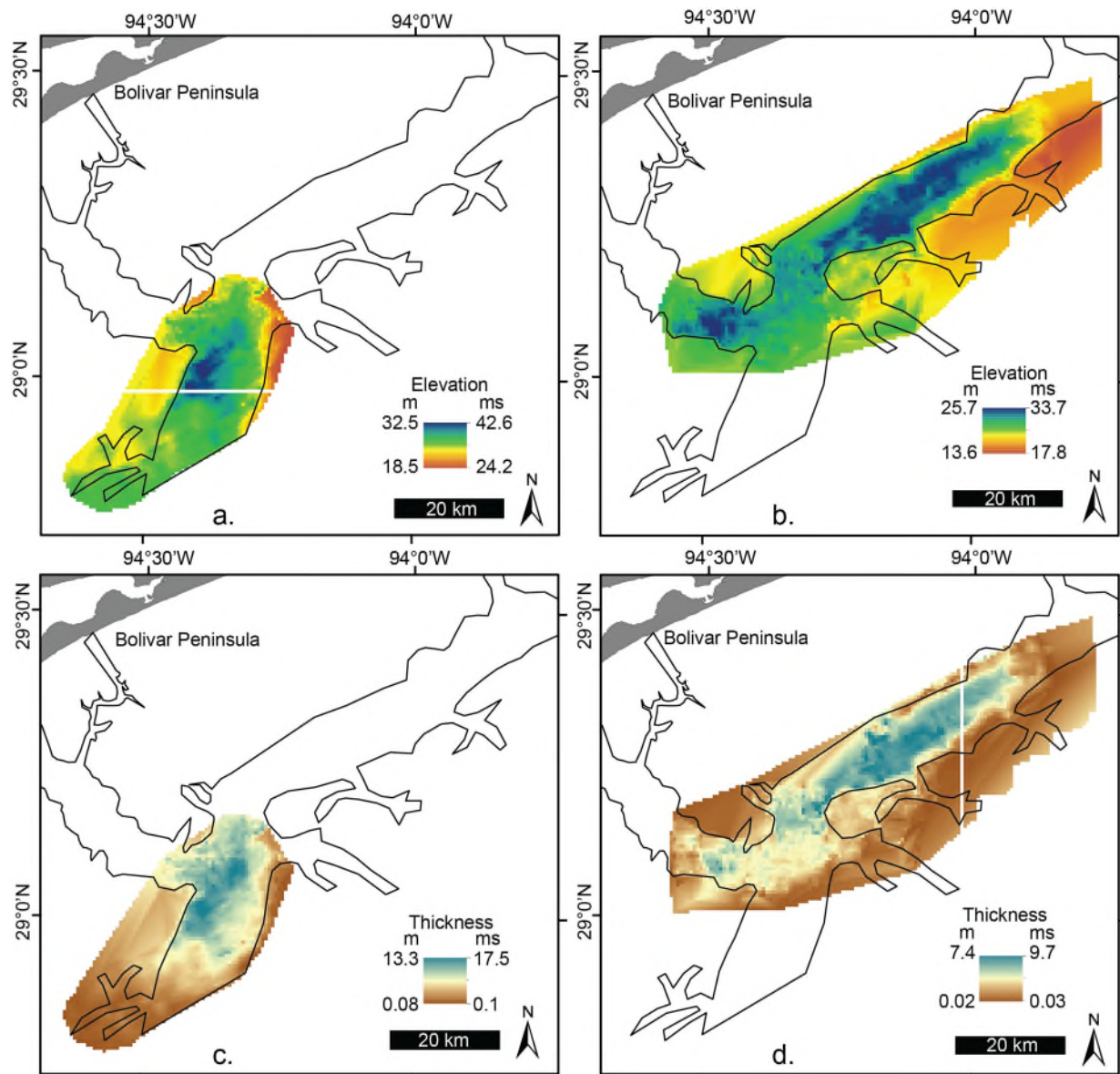
Figure 3.8. Structure and isopach maps for the two largest estuaries in the study area.
Panels a and b show the structure maps for H8 and H13, respectively. Panels c and d show the isopach maps for U6 and U9, respectively.
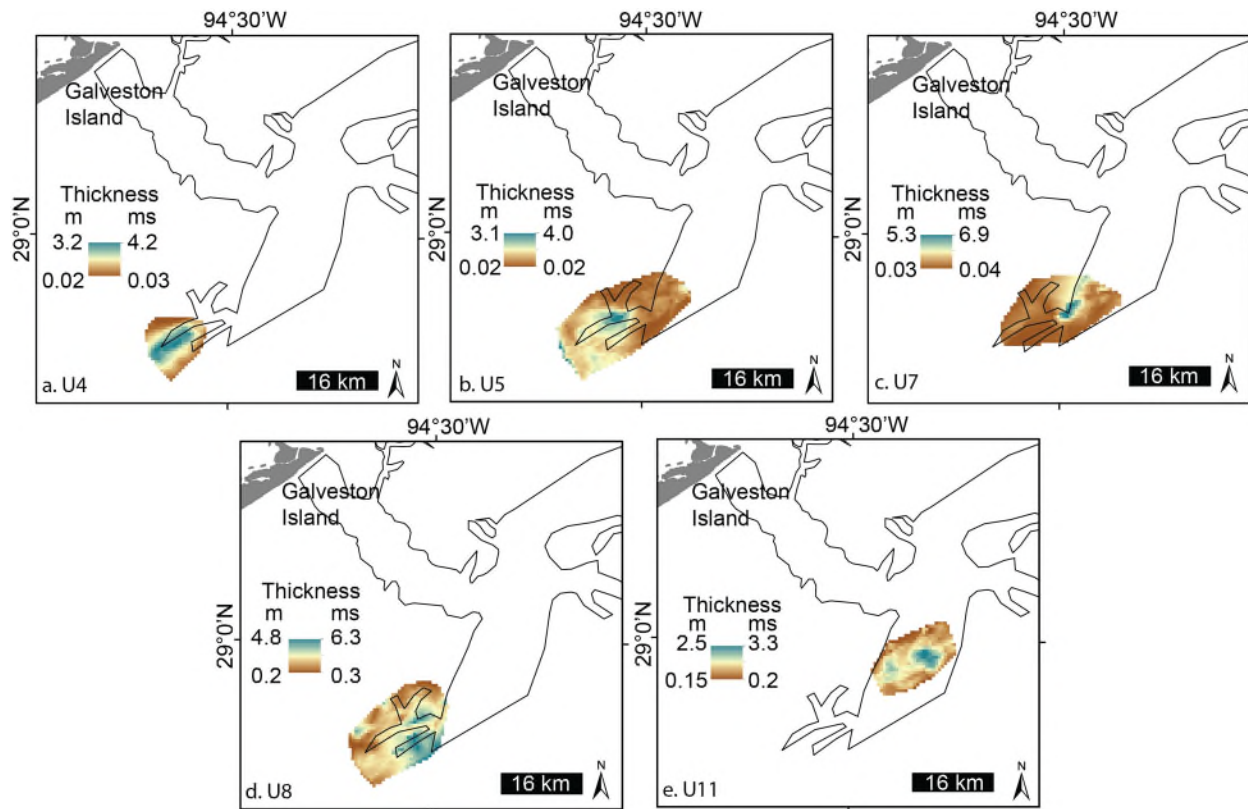
Figure 3.9. Isopach maps of the units in the SW area.
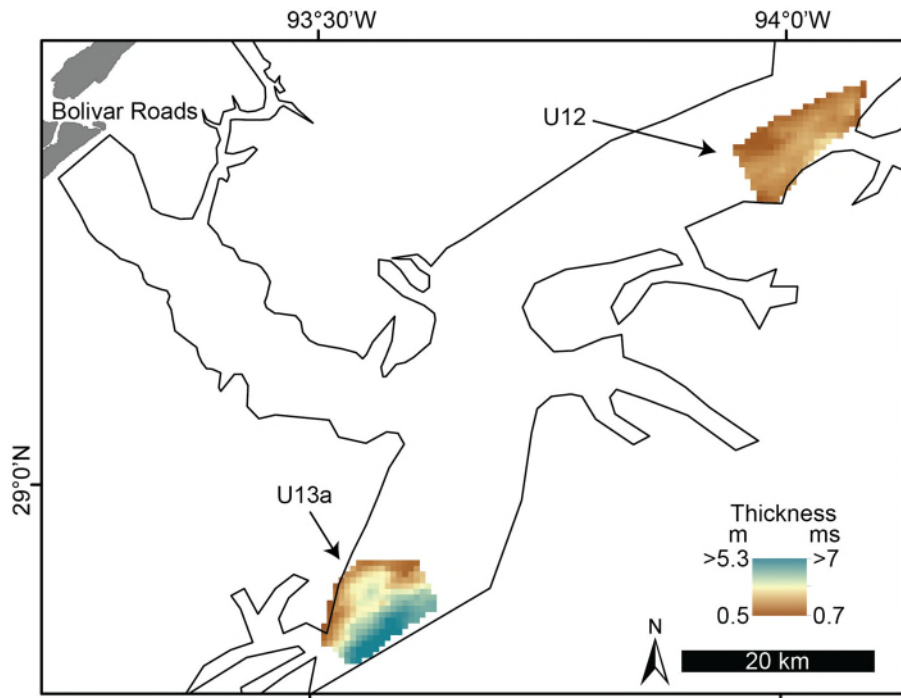
Figure 3.10. Isopach maps of the two potential bayhead deltas (U12 and U13a).

3.4.4 Core-Seismic Integration.

Borings from Thomas and Anderson (1994) and cores from Dellapenna et al. (2009) were used to characterize the grainsize and character of the units. Boring 6 penetrates 42.4 m, boring 9 penetrates 13.7 m, 09cct02-08 penetrates 5.6 m, and 09cct02-21 penetrates 5.64 m. Only the borings sample the entire estuarine section (Fig. 3.11).

Borings 6 and 9 samples U1, U10, and U12. Above H3, boring 6 samples loose silty sand that is shelly, while boring 9 samples very soft clay. U10 at boring 6 consists of soft to firm green-gray clay, however at boring 9, it is very soft clay (Thomas and Anderson, 1994). At 09cct02-08, U10 has a median grain size between 0.020-0.049 mm (Dellapenna et al., 2009; Fig. 3.11). U12 at boring 6 displays soft to firm green-gray clay, that is silty on top of firm to stiff brown-red clay, while at boring 9, this unit is described as stiff-very stiff yellow-brown silty clay on top of yellow-brown fine sand (Thomas and Anderson, 1994) the mean grain size for this unit is slightly higher between 0.030-0.109 mm (Dellapenna et al., 2009; Fig. 3.11). Core 09cct02-21 displays a mean grain size for U1 between 62.03-100.16 μm, U2 has a slightly lower grain size between 0.048-0.082 mm, and U12 has an even lower grain size between 0.032-0.047 mm (Dellapenna et al., 2009; Fig. 3.11).

3.5 Interpretation

Interpretations of H1-H5 and U1-U3 are detailed in Chapter 2 and are horizons and units associated with preserved paleo-barrier island facies. Within the SW area of the study, there are many more horizons and units that designate several estuarine units. U13a also represents a bayhead delta based on the prograding dipping reflections, as well as the location in respect to Anderson et al. (2016), which shows bayhead delta deposits in the same area. Similarly, U12 also displays prograding reflectors and is also likely a bayhead delta. Additionally, U9 represents an outer bay environment based on Burstein et al. (2023) and Standring et al. (2024). Our H13 intersects Burstein et al. (2023) H3, which they classify as the base of the outer bay deposit based on cores from Standring et al. (2024), which recognize the unit above H3 as outer bay based on the abundance of *Elphidium* foraminifera. U6 is likely central bay since it runs below U9, and there is no evidence of erosion between U6 and U9 along H12. Both of these units are regionally extensive. Several smaller estuarine units are present in the SW region. A total of 6 units are present within the SW area. One is the bayhead delta, U13a, and one is likely a shoreface unit, U4. U4 displays seaward dipping reflections that could be indicative of shoreface reflections.

Fluvial valleys in the Gulf of Mexico have the most complete record of coastal Holocene evolution (Anderson et al., 2014; Norfjord et al., 2005) because the strata have a high preservation potential due to the thickness of the deposits relative to other continental margins (Duncan et al., 2000; Anderson et al., 2008). The Trinity and Sabine River valleys are considered underfilled valleys, and likely preserve much of the local geologic past and provides a natural laboratory for understanding how tides, storms, winds, and waves change during inundation. The Sabine River valley varies between 10-15 km wide, and the Trinity is slightly smaller, between 8-10 km wide. The Sabine has many tributary systems joining the main valley; however, the Trinity only has one main tributary that is close to the modern-day shoreline (Goff and Gulick, 2023). Smaller tributary systems tend to have higher gradients, smaller fetch and tidal prisms, and lower sediment supply than their main valley counterparts (Simms and Rodriguez, 2014). These differences in valley size have implications for the environments that infill (Simms and Rodriguez, 2014; Milliman and Syvitski, 1992).
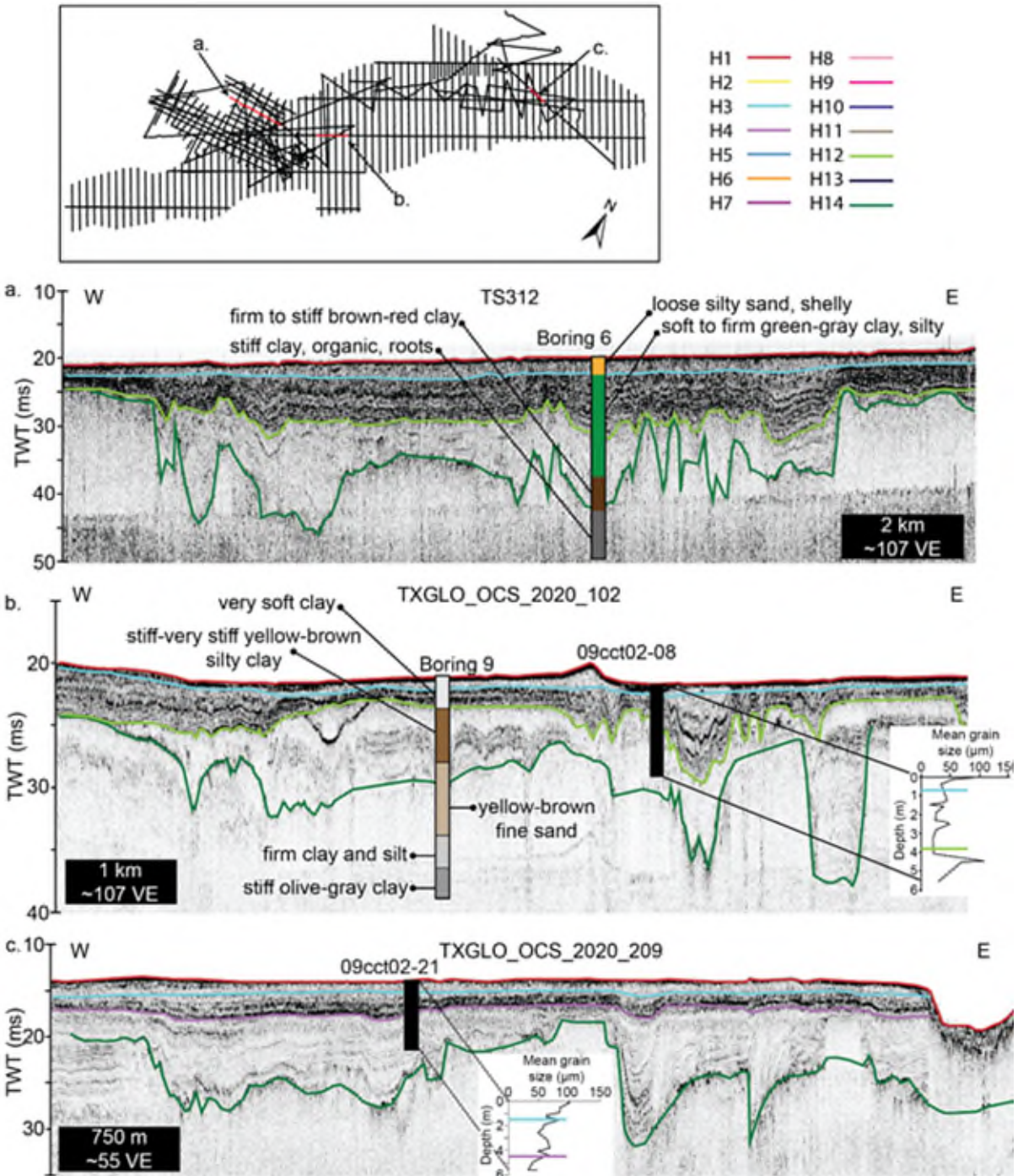
Figure 3.11. Core seismic integration of estuarine units.
Borings 6 and 9 are from Thomas and Anderson (1994). The 09cct02 cores are from Dellapenna et al. (2009).

4 Implications for Sand Resources

Annually, ~5.2 million m^3 are lost to shoreline erosion along the entire Texas coast (Texas Coastal Resiliency Master Plan, 2023). For the 4-year planning cycle, a total of ~21 million m^3 are needed to maintain the current shoreline position (Texas Coastal Resiliency Master Plan, 2023). Early estimates of total sand, including sand, shelly sand, and muddy sand from Sabine were 1.2 billion m^3 and 585 million m^3 for Heald (Morton and Gibeaut, 1995). This estimate was calculated based only on vibracores and used an average length and thickness of each sand bank to calculate a volume (Morton and Gibeaut, 1995). These crude estimates likely overestimate the amount of sand each bank contains. Additionally, even though the quantity of sand was evaluated, estimates based on sand quality were not calculated. The data collected in this study were intended as a reconnaissance level study and are not sufficiently resolved to accurately estimate sediment volumes. Nevertheless, we are able to more accurately map the extent of each sand bank, as well as delineate units that have different sand percentages based on previously collected sediment cores. These units can then be targeted for more detailed geophysical surveys as well as cores that can be measured for sand composition and color.

Paleo-barrier island-associated facies are ideal deposits to extract sand for beach nourishment projects. Based on our results, we identified several deposits that could be possible sand resources and we suggest that these deposits were back barrier subaqueous deposits. Thus, several of these units represent good potential sand resources for coastal protection, as well as prime targets for coring.

U1, U2, and U3 were all identified in Chapter 2 as units possibly containing sand; however, these units can be differentiated by the extent of their homogeneity. U1, which mostly makes up Heald Bank, is highly homogenous and has no overburden. U2 on the other hand, is much less homogeneous: while cores revealed the low amplitude, steeply dipping reflective portion of the unit to be mostly sand, the high-amplitude, lower slope section is predominantly mud. Finally, U3 could potentially be a resource for sand because it has few internal reflections indicating it is homogeneous; however, there are no cores at present that sampled this unit, so we cannot definitively identify the sediment composition. U3 is also beneath a greater overburden than the other two units. Since U1 is the most surficial deposit that is also homogeneous and extensive, it is likely the best sand target. Additionally, in Chapter 3, we identified U4, constrained to Shepard Bank, as a possible shoreface sand deposit, but it has also not been sampled by coring.

Chapter 3 focused on the estuarine sediments contained within and surrounding the Trinity and Sabine River paleovalleys. U9 is interpreted as outer-bay environment which, though primarily muds, should also contain sandy layers associated with storm deposits into the estuary (Burstein et al., 2023). A greater sand potential is contained within the two interpreted bayhead delta deposits (U12 and U13a), representing the deltaic output of fluvial sediments entering the bay, interbedded with estuarine muds. The greatest potential for sand deposits, however, lies within the fluvial deposits at the base of the paleovalleys, below the estuarine section. These sands are, on the other hand, below the greatest overburden. Our estimate of total estuarine thickness, along with our updated map of the paleovalley outline (Figure 3.7), provides a basis for quantifying that overburden. We identify three regions with lower overburden: (1) the outer Trinity River paleovalley near the confluence with the Sabine River paleovalley, (2) the Sabine River paleovalley near the Federal/State line, and (3) in any of the larger tributaries feeding the paleovalley system.

In summary, our stratigraphic analysis has sought to identify sedimentary units that have the potential (proven or otherwise) for high sand content, within both the sand banks on the Texas NE shelf (Sabine, Heald and Shepard Banks) as well as within and below the Trinity and Sabine River paleovalleys. These include:

1) Units U1-U3, which constitute the main parts of the sand banks, including sands that were originally deposited in barrier island as well as marine settings. These units are the most accessible since they are at or near the seafloor.
2) Unit U9, which is interpreted as an outer bay environment that frequently receives sand deposits from storm overwash across barrier islands. This unit is also near the seafloor, but will have a higher percentage of mud mixed in with the sand in comparison to U1-U3.
3) Units U12 and U13a, which are interpreted as bayhead delta deposits, which is where the river empties into the bay and deposits sands that have been transported down the river. These sediments are among the first to be deposited in an estuarine environment and will have greater overburden than the previously-mentioned units.
4) Finally, beneath all the estuarine sedimentary units lies vast amounts of fluvial sand, typically ~10 m thick, across the whole of the main paleovalleys and their several major tributaries. These are the deepest sand resources, however, covered by the greatest overburden. There are regions, however, where the overburden is minimized, including the Trinity River paleovalley near its confluence with the Sabine River paleovalley, within the Sabine River paleovalley close to the federal/state boundary, and within the various tributaries paleovalleys that feed into the main paleovalleys.

Future coring efforts should specifically target the units enumerated above. The upper units have, indeed, already been targeted by a recent APTIM/TWI-lead vibrocoring effort. Accessing the deeper units will require different coring technologies, such as lift boats or platform borings.

5 References

Abdulah, K. C., Anderson, J. B., Snow, J. N., and Holdford-Jack, L. (2004). The Late Quaternary Brazos and Colorado deltas, offshore Texas, USA—Their evolution and the factors that controlled their deposition. In: *Late Quaternary Stratigraphic Evolution of the Northern Gulf of Mexico Margin*, *SEPM Society for Sedimentary Geology vol 79*, p. 237-269.

Adams Jr, C. E., Swift, D. J., and Coleman, J. M. (1987). Bottom currents and fluviomarine sedimentation on the Mississippi Prodelta Shelf: February-May 1984. *Journal of Geophysical Research: Oceans, 92*(C13), 14595-14609.

Allen, G. P., and Posamentier, H. W. (1993). Sequence stratigraphy and facies model of an incised valley fill; the Gironde Estuary, France. *Journal of Sedimentary Research*, *63*(3), 378-391.

Anderson, J. B., and Thomas, M. A. (1991). Marine ice-sheet decoupling as a mechanism for rapid, episodic sea-level change: the record of such events and their influence on sedimentation. *Sedimentary Geology*, *70*(2-4), 87-104.

Anderson, J. B., Shipp, S. S., Lowe, A. L., Wellner, J. S., and Mosola, A. B. (2002). The Antarctic Ice Sheet during the Last Glacial Maximum and its subsequent retreat history: a review. *Quaternary Science Reviews*, *21*(1-3), 49-70.

Anderson, J. B., Rodriguez, A. B., Milliken, K. T., and Taviani, M. (2008). The Holocene evolution of the Galveston estuary complex, Texas: evidence for rapid change in estuarine environments. *Response of Upper Gulf Coast estuaries to Holocene climate change and sea-level rise: Geological Society of America Special Paper*, *443*, 89-104.

Anderson, J. B., Wallace, D. J., Simms, A. R., Rodriguez, A. B., Weight, R. W., and Taha, Z. P. (2016). Recycling sediments between source and sink during a eustatic cycle: Systems of late Quaternary northwestern Gulf of Mexico Basin. *Earth-Science Reviews*, *153*, 111-138.

Anderson, J.B., Wallace, D.J., Rodriguez, A.B., Simms, A.R., Milliken, K.T. (2022) *Holocene Evolution of the Western Louisiana-Texas Coast, USA: Response to Sea-Level Rise and Climate Change*. Geological Society of America Memoir 221, 81 p.

Anderson, J.B., Wallace, D.J., Rodriguez, A.B., Simms, A.R., 2023, Unprecedented Historical Erosion of U.S. Gulf Coast: A Consequence of Accelerated Sea-Level Rise? *Earth's Future, 11*, e2023EF003676.

Aptim Environmental and Infrastructure, LLC (APTIM) and The Water Institute of the Gulf 2022. Texas General Land Office Offshore Sediment Resource Inventory: Geological and Geophysical Data Collection and Processing for Identification of Outer Continental Shelf Mineral Resources Offshore of Texas. Final Report prepared for the Texas General Land Office. Contract No. 18- 127-014: 94 p.

Ashton, A.D., Lorenzo-Trueba, J. (2018). Morphodynamics of Barrier Response to Sea-Level Rise. In: Moore, L., Murray, A. (eds) *Barrier Dynamics and Response to Changing Climate*. Springer, Cham., p. 277-304.

Balsam, W. L., and Beeson, J. P. (2003). Sea-floor sediment distribution in the Gulf of Mexico. Deep Sea *Research Part I: Oceanographic Research Papers*, *50*(12), 1421-1444.

Belknap, D. F., and Kraft, J. C. (1981). Preservation potential of transgressive coastal lithosomes on the US Atlantic shelf. *Marine Geology*, *42*(1-4), 429-442.

Beck, M.W., K.L Heck, K.W. Able, D.L. Childers, D.B. Eggleston, B.M. Gillanders, B.S. Halpern, C.G. Hays, K. Hoshino, T.J. Minello, R.J. Orth, P.F. Sheridan, and M.P. Weinstein. 2003. *The Role of Nearshore Ecosystems as Fish and Shellfish Nurseries*. Issues in Ecology No. 11, Ecological Society of America.

Bennett, M. R., Cassidy, N. J., and Pile, J. (2009). Internal structure of a barrier beach as revealed by ground penetrating radar (GPR): Chesil beach, UK. *Geomorphology*, *104*(3-4), 218-229.

Bertness, M.D. 1999. The Ecology of Atlantic Shorelines. Sunderland, MA: Sinauer Associates, Inc.

Biggs, R. B., and Howell, B. A. (1984). The estuary as a sediment trap: alternate approaches to estimating its filtering efficiency. In J.R. Schubel, V.S. Kennedy (eds.), *The estuary as a filter*. Academic Press, New York, p. 107-129.

Bryant Jr, V. M., and Holloway, R. G. (1985). A late-Quaternary paleoenvironmental record of Texas: an overview of the pollen evidence. In: V.M. Bryant, R.G. Holloway (eds.), *Pollen records of late-Quaternary North American sediments*. American Association of Stratigraphic Palynologists Foundation, Dallas, p. 39-70.

Burstein, J. T., Goff, J. A., Gulick, S. P., Lowery, C., Standring, P., and Swartz, J. (2023). Tracking barrier island response to early Holocene sea-level rise: High resolution study of estuarine sediments in the Trinity River Paleovalley. *Marine Geology*, *455*, 106951.

Cattaneo, A., and Steel, R. J. (2003). Transgressive deposits: a review of their variability. *Earth-Science Reviews*, *62*(3-4), 187-228.

Ciarletta, D. J., Lorenzo-Trueba, J., and Ashton, A. D. (2019). Interaction of sea-level pulses with periodically retreating barrier islands. *Frontiers in Earth Science*, *7*, 279.

Coe, A.L., Bosence, D. W., Church, K. D., Angela, L., Flint, S. S., Howell, J. A., Wilson, R. C. L (2003). *The sedimentary record of sea-level change*. Cambridge University Press, Cambridge.

Coleman, J. M., Roberts, H. H., and Stone, G. W. (1998). Mississippi River delta: an overview. *Journal of Coastal Research, 14*(3), 699-716.

Cole, M.L., and Anderson, J.B. (1982). Detailed grain-size and heavy mineralogy of sands of the northeastern Texas Gulf Coast: Implications with regard to coastal barrier development: *Transactions of the Gulf Coast Geological Society*, *32*, p. 555–563.

Cooke, M. J., Stern, L. A., Banner, J. L., Mack, L. E., Stafford Jr, T. W., and Toomey III, R. S. (2003). Precise timing and rate of massive late Quaternary soil denudation. *Geology, 31*(10), 853-856.

Cooper, J.A.G., Green, A.N., Meireles, R.P., Klein, A.H.F., Souza, J., Toldo, E.E. (2016). Sandy barrier overstepping and preservation linked to rapid sea level rise and geological setting. *Marine Geology, 382*, 80–91.

Curray, J. R. (1960). Sediments and history of Holocene transgression, continental shelf, northwest Gulf of Mexico. In: F.P. Shepard, F.B. Phleger, T.H. van Andel (eds.), *Recent Sediments, Northwest Gulf of Mexico*, AAPG Special Volume 21, p. 221-266.

Daily, G.C., S. Alexander, P.R. Ehrlich, L. Goulder, J. Lubchenco, P.A. Matson, H.A. Mooney, S. Postel, S.H. Schneider, D. Tilman, and G.M. Woodwell (1997). Ecosystem Services: Benefits Supplied to Human Societies by Natural Ecosystems. Issues in Ecology No. 2, Ecological Society of America.

Dalrymple, R. W., Zaitlin, B. A., and Boyd, R. (1992). Estuarine facies models; conceptual basis and stratigraphic implications. *Journal of Sedimentary Research, 62*(6), 1130-1146.

Dangendorf, S., Hendricks, N., Sun, Q., Klinck, J., Ezer, T., Frederikse, T., et al. (2023). Acceleration of U.S. Southeast and Gulf Coast sea-level rise amplified by internal climate variability. *Nature Communications*, *14*(1), 1935.

Davis Jr, R. A. (1994). Barrier island systems—a geologic overview. In R.A. Davis Jr. (ed.), *Geology of Holocene barrier island systems*. Berlin, Heidelberg: Springer Berlin Heidelberg, p. 1-46.

Deaton, C. D., Hein, C. J., and Kirwan, M. L. (2016). Barrier island migration dominates ecogeomorphic feedbacks and drives salt marsh loss along the Virginia Atlantic Coast, USA. *Geology*, *45*(2), 123-126.

Dellapenna, T.M., Cardenas, A., Johnson, K., Flocks, J., 2009, Report of the Sand Source Investigation of the Paleo-Sabine-Trinity Marine Features (PSTMF), Texas General Land Office Cooperative Agreement Number MO7AC12518, Service Contract 09-109-000-3517.

Dobkowski, A. H. (1998). Dumptrucks versus dredges: An economic analysis of sand sources for beach nourishment. *Coastal Management*, *26*(4), 303-314.

Dondurur, D. (2018). *Acquisition and processing of marine seismic data*. Elsevier, Amsterdam.

Donnelly, C., Kraus, N., & Larson, M. (2006). State of knowledge on measurement and modeling of coastal overwash. *Journal of Coastal Research, 22*(4), 965-991

Doyle, L. J., and Sparks, T. N. (1980). Sediments of the Mississippi, Alabama, and Florida (MAFLA)) continental shelf. *Journal of Sedimentary Research*, *50*(3), 905-915.

Duncan, C.S., Goff, J.A,. Austin, J.A., Jr., and Fulthorpe, C.S. (2000). Tracking the last sea level cycle: seafloor morphology and shallow stratigraphy of the latest Quaternary New Jersey middle continental shelf. *Marine Geology, 170*(3-4), 395-421.

Ellwood, B. B., and Gose, W. A. (2006). Heinrich H1 and 8200 yr BP climate events recorded in Hall's Cave, Texas. *Geology*, *34*(9), 753-756.

Emery, A. R., Hodgson, D. M., Barlow, N. L., Carrivick, J. L., Cotterill, C. J., Mellett, C. L., and Booth, A. D. (2019). Topographic and hydrodynamic controls on barrier retreat and preservation: an example from Dogger Bank, North Sea. *Marine Geology*, *416*, 105981.

Fischer, A. G. (1961). Stratigraphic record of transgressing seas in light of sedimentation on Atlantic coast of New Jersey. *AAPG Bulletin*, *45*(10), 1656-1666.

FitzGerald, D. M., Fenster, M. S., Argow, B. A., and Buynevich, I. V. (2008). Coastal impacts due to sea-level rise. *Annual Reviews of Earth and Planetary Science, 36*, 601-647.

FitzGerald, D. M., Hein, C. J., Hughes, Z., Kulp, M., Georgiou, I., and Miner, M. (2018). Runaway barrier island transgression concept: Global case studies. In L.J. Moore, A.B. Murray (eds.) *Barrier dynamics and response to changing climate*. Springer, Chamersburg, p. 3-56.

Forde, A. S., Dadisman, S. V., Flocks, J. G., Dellapenna, T. M., Sanford, J. M., and Wiese, D. S. (2010). *Archive of Digital Chirp Sub-bottom Profile Data Collected During USGS Cruise 09 CCT 01 Offshore of Sabine Pass and Galveston, Texas, March 2009* (No. 526). US Geological Survey.

Fraticelli, C. M. (2006). Climate forcing in a wave-dominated delta: The effects of drought–flood cycles on delta progradation. *Journal of Sedimentary Research*, *76*(9), 1067-1076.

Frazier, D. E. (1967). Recent deltaic deposits of the Mississippi River: their development and chronology. *Gulf Coast Association of Geological Societies Transactions, 17,* 287-315.

Frazier, D. E. (1974). Depositional-Episodes: Their Relationship to the Quaternary Stratigraphic Framework in the Northwestern Portion of the Gulf Basin: The University of Texas at Austin, Bureau of Economic Geology, Geological Circular 74-1, 28 p.

Fruergaard, M., Møller, I., Johannessen, P. N., Nielsen, L. H., Andersen, T. J., Nielsen, L., ... and Pejrup, M. (2015). Stratigraphy, evolution, and controls of a Holocene transgressive–regressive barrier island under changing sea level: Danish North Sea coast. *Journal of Sedimentary Research*, *85*(7), 820-844.

Galloway, W. E. (1975). Process framework for describing the morphologic and stratigraphic evolution of deltaic depositional systems. In: M.L. Broussard (ed.), *Deltas, Models for Exploration*. American Association of Petroleum Geologists, Tulsa, p. 87-98.

Galloway, W. E., and Hobday, D. K. (1983). *Terrigenous clastic depositional systems*. Springer, Berlin (1983). 498 p.

Galvão, W. F. L., da Fontoura Klein, A. H., de Mahiques, M. M., Hein, C. J., de Sousa, L. A. P., Cooper, A., and Green, A. (2023). Holocene barrier overstepping, estuarine rollover and drainage merging in a sub-tropical bay. *Marine Geology*, *462*, 107076.

Goff, J.A., and Gulick, S.P.S. (2023). Identification and investigation of sand deposits in the Trinity River Paleo-valley, offshore Galveston. Final Report: Interagency Contract for CEPRA Project Number 1706, Texas General Land Office.

Hayes, M. O. (1980). General morphology and sediment patterns in tidal inlets. *Sedimentary geology*, *26*(1-3), 139-156.

Ivins, E. R., and James, T. S. (2005). Antarctic glacial isostatic adjustment: a new assessment. *Antarctic Science*, *17*(4), 541-553.

Ivins, E. R., Dokka, R. K., and Blom, R. G. (2007). Post-glacial sediment load and subsidence in coastal Louisiana. *Geophysical Research Letters*, *34*(16), L16303.

Jervey, M. T. (1988). Quantitative geological modeling of siliciclastic rock sequences and their seismic expression. *SEPM Special Publication* 42, 47-69.

Karimpour, A., Chen, Q., and Twilley, R. R. (2017). Wind wave behavior in fetch and depth limited estuaries. *Scientific Reports*, *7*(1), 40654.

Kim, W., Paola, C., Swenson, J. B., and Voller, V. R. (2006). Shoreline response to autogenic processes of sediment storage and release in the fluvial system. *Journal of Geophysical Research: Earth Surface*, *111*(F4), F04013.

Leatherman, S. P., and Williams, A. T. (1983). Vertical sedimentation units in a barrier island washover fan. *Earth Surface Processes and Landforms*, *8*(2), 141-150.

Lorenzo-Trueba, J., and Ashton, A. D. (2014). Rollover, drowning, and discontinuous retreat: Distinct modes of barrier response to sea-level rise arising from a simple morphodynamic model. *Journal of Geophysical Research: Earth Surface*, *119*(4), 779-801.

McBride, R. A., Penland, S., Hiland, M. W., Williams, S. J., Westphal, K. A., Jaffe, B. E., and Sallenger Jr, A. H. (1992). Analysis of barrier shoreline change in Louisiana from 1853 to 1989. *Atlas of shoreline changes in Louisiana from*, 36-97.

McFarlan Jr, E. (1961). Radiocarbon dating of late Quaternary deposits, south Louisiana. *Geological Society of America Bulletin*, *72*(1), 129-158.

McGowen, J. H., Garner, L.E., and Wilkinson, B.H. (1977). *The Gulf shoreline of Texas: processes, characteristics, and factors in use*. University of Texas at Austin. Bureau of Economic Geology.

Mellett, C. L., Hodgson, D. M., Lang, A., Mauz, B., Selby, I., and Plater, A. J. (2012). Preservation of a drowned gravel barrier complex: A landscape evolution study from the north-eastern English Channel. *Marine Geology*, *315*, 115-131.

Miller, C. B., Goff, J. A., Gulick, S. P., Wallace, D. J., and Lowery, C. M. (2024). Internal sand bank seismic stratigraphy provides insight into paleo-barrier island preservation. *Marine Geology*, 107359

Milliken, K. T., Anderson, J. B., and Rodriguez, A. B. (2008a). A new composite Holocene sea-level curve for the northern Gulf of Mexico. In: J.B. Anderson, A.B. Rodriguez (eds.), *Response of Upper Gulf Coast Estuaries to Holocene Climate Change and Sea-level Rise*, *Geological Society of America Special Paper 443*, p. 1-11.

Milliken, K. T., Anderson, J. B., and Rodriguez, A. B. (2008b). Record of dramatic Holocene environmental changes linked to eustasy and climate change in Calcasieu Lake, Louisiana, USA. In: J.B. Anderson, A.B. Rodriguez (eds.), *Response of Upper Gulf Coast Estuaries to Holocene Climate Change and Sea-level Rise*, *Geological Society of America Special Paper 443*, p. 43-63.

Milliken, K. T., Anderson, J. B., and Rodriguez, A. B. (2008c). Tracking the Holocene evolution of Sabine Lake through the interplay of eustasy, antecedent topography, and sediment supply variations, Texas and Louisiana, USA. In: J.B. Anderson, A.B. Rodriguez (eds.), *Response of Upper Gulf Coast Estuaries to Holocene Climate Change and Sea-level Rise*, *Geological Society of America Special Paper 443*, p. 65-88.

Milliman, J. D., and Syvitski, J. P. (1992). Geomorphic/tectonic control of sediment discharge to the ocean: the importance of small mountainous rivers. *The Journal of Geology*, *100*(5), 525-544.

Morton, R.A., and Gibeaut, J.C. (1995). Physical and environmental assessment of sand resources Sabine and Heald Banks second phase 1994-1995. Final Report prepared for the U.S. Department of Interior Minerals Management Service. Cooperative Agreement No. 14-35-0001-30635.

Nelson, H. F., and Bray, E. E. (1970). Stratigraphy and history of the Holocene sediments in the Sabine-High Island area, Gulf of Mexico. In: J.P. Morgan (ed), *Deltaic Sedimentation, Modern and Ancient*, *SEPM Special Publication 15*, p. 48-77

Nichols, M. M. (1989). Sediment accumulation rates and relative sea-level rise in lagoons. *Marine Geology*, *88*(3-4), 201-219.

Nordfjord, S., Goff, J. A., Austin, J. A., and Gulick, S. P. S. (2006). Seismic facies of incised-valley fills, New Jersey continental shelf: implications for erosion and preservation processes acting during latest Pleistocene–Holocene transgression. *Journal of Sedimentary Research*, *76*(12), 1284-1303.

Nordt, L. C., Boutton, T. W., Hallmark, C. T., and Waters, M. R. (1994). Late Quaternary vegetation and climate changes in central Texas based on the isotopic composition of organic carbon. *Quaternary Research*, *41*(1), 109-120.

Nordt, L. C., Boutton, T. W., Jacob, J. S., and Mandel, R. D. (2002). C4 plant productivity and climate-CO2 variations in south-central Texas during the late Quaternary. *Quaternary Research*, *58*(2), 182-188.

Nummedal, D., and Swift, D. J. (1987). Transgressive stratigraphy at sequence-bounding unconformities: some principles derived from Holocene and Cretaceous examples. In: D. Nummedal, O.H. Pilkey, J.D. Howard (eds.), *Sea-level fluctuation and coastal evolution, SEPM Special Publication 41*, p. 241-260

Odezulu C.I., Lorenzo-Trueba J., Wallace D.J., and Anderson J.B., 2018, Follets Island: A Case of Unprecedented Change and Transition from Rollover to Subaqueous Shoals. In: L. Moore, A.B. Murray (eds.), *Barrier Dynamics and Response to Changing Climate*. Springer, Chambersburg, p. 147-174.

Oppenheimer, M., Glavovic, B. C., Hinkel, J., van de Wal, R., Magnan, A. K., Abd-Elgawad, A., et al. (2019). Sea level rise and implications for low-lying islands, coasts and communities. In H. O. Pörtner, D. C. Roberts, V. Masson-Delmotte, P. Zhai, M. Tignor, E. Poloczanska, et al. (eds.), *IPCC Special Report on the Ocean and Cryosphere in a Changing Climate*. Cambridge University Press, Cambridge, p. 321-445.

Paul, M. A., and Barras, B. F. (1998). A geotechnical correction for post-depositional sediment compression: examples from the Forth valley, Scotland. *Journal of Quaternary Science*: *Published for the Quaternary Research Association*, *13*(2), 171-176.

Penland, S., Suter, J. R., and Boyd, R. (1985). Barrier island arcs along abandoned Mississippi River deltas. *Marine Geology*, *63*(1-4), 197-233.

Penland, S., Boyd, R., and Suter, J. R. (1988). Transgressive depositional systems of the Mississippi Delta plain; a model for barrier shoreline and shelf sand development. *Journal of Sedimentary Research*, *58*(6), 932-949.

Perlmutter, M. A., Radovich, B. J., and Matthews, M. D. (1997). The impact of high-frequency sedimentation cycles on stratigraphic interpretation (No. ANL/ES/CP-92288; CONF-9511274-1). Argonne National Lab., IL (United States).

Picado, A., Dias, J. M., and Fortunato, A. B. (2010). Tidal changes in estuarine systems induced by local geomorphologic modifications. *Continental Shelf Research*, *30*(17), 1854-1864.

Pickens, B.A., Christopher Taylor, J., Finkbeiner, M., Hansen, D., Turner, L. (2021). Modeling sand shoals on the U.S. Atlantic Shelf: Moving beyond a site-by-site approach. *Journal of Coastal Research, 3*7(2), 227-237.

Resio, D. T., and Westerink, J. J. (2008). Modeling the physics of storm surges. *Physics Today, 61*(9), 33.

Roberts, H. H. (1997). Dynamic changes of the Holocene Mississippi River delta plain: the delta cycle. *Journal of Coastal Research*, *13*(3), 605-627.

Rodriguez, A. B., Anderson, J. B., Siringan, F. P., and Taviani, M. (1999). Sedimentary facies and genesis of Holocene sand banks on the east Texas inner continental shelf. Isolated shallow marine sand bodies: Sequence stratigraphic analysis and sedimentological interpretation. In: J. Sneddon, K. Bergman (Eds*.), Isolated Shallow Marine Sand Bodies*, *SEPM Special Publication* 64, p. 165-178.

Rodriguez, A. B., Fassell, M. L., and Anderson, J. B. (2001). Variations in shoreface progradation and ravinement along the Texas coast, Gulf of Mexico. *Sedimentology*, *48*(4), 837-853.

Rodriguez, A. B., Anderson, J. B., Siringan, F. P., and Taviani, M. (2004). Holocene evolution of the east Texas coast and inner continental shelf: along-strike variability in coastal retreat rates. *Journal of Sedimentary Research*, *74*(3), 405-421.

Roy, P. S. (1994). Holocene estuary evolution—stratigraphic studies from southeastern Australia. In: R.W. Dalrymple, R. Boyd, and B.A. Zaitlin (eds.), *Incised-valley Systems, Origin and Sedimentary Sequences*, *SEPM Special Publication 51*, p. 241-263.

Roy, P. S., Thom, B. G., and Wright, L. D. (1980). Holocene sequences on an embayed high-energy coast: an evolutionary model. *Sedimentary Geology*, *26*(1-3), 1-19.

Sallenger Jr, A. H. (2000). Storm impact scale for barrier islands. *Journal of Coastal Research, 16*(3), 890-895.

Sanders, J. E., and Kumar, N. (1975). Evidence of shoreface retreat and in-place "drowning" during Holocene submergence of barriers, shelf off Fire Island, New York. *Geological Society of America Bulletin*, *86*(1), 65-76.

Saustrup, S., Goff, J. A., and Gulick, S. P. S. (2019). Recommended "best practices" for chirp acquisition and processing. *US Dept. of the Interior, Bureau of Ocean Energy Management, Gulf of Mexico OCS Region, New Orleans, LA. OCS Report BOEM*, *39*.

Schwartz, R. K. (1982). Bedform and stratification characteristics of some modern small-scale washover sand bodies. *Sedimentology*, *29*(6), 835-849.

Shaw, J., You, Y., Mohrig, D., and Kocurek, G. (2015). Tracking hurricane-generated storm surge with washover fan stratigraphy. *Geology*, *43*(2), 127-130.

Shawler, J. L., Ciarletta, D. J., Connell, J. E., Boggs, B. Q., Lorenzo-Trueba, J., and Hein, C. J. (2020). Relative influence of antecedent topography and sea-level rise on barrier-island migration. *Sedimentology*, *68*(2), 639-669.

Shepard, F. P., and Suess, H. E. (1956). Rate of postglacial rise of sea level. *Science*, *123*(3207), 1082-1083.

Simms, A.R., and Rodriguez, A.B. (2014). Why do coastlines stabilize following rapid retreat? *Geophysical Research Letters, 41*, 1698-1703.

Simms, A. R., Anderson, J. B., Taha, Z. P., and Rodriguez, A. B. (2006). Overfilled versus underfilled incised valleys: examples from the Quaternary Gulf of Mexico. R.W. Dalrymple, D.A. Leckie, R.W. Tillman (eds.), *Incised valleys in time and space, SEPM Special Publication 85*, *p. 117-139.*

Simms, A.R., Lambeck, K., Purcell, T., Anderson, J.B., and Rodriguez, A.B. (2007). Sea level within the Gulf of Mexico since the Last Glacial Maximum with implication for the melting history of the Laurentide Ice Sheet. *Quaternary Science Reviews, 26*, 920–940.

Simms, A. R., Anderson, J. B., DeWitt, R., Lambeck, K., and Purcell, A. (2013). Quantifying rates of coastal subsidence since the last interglacial and the role of sediment loading. *Global and Planetary Change*, *111*, 296-308.

Standring, P., Lowery, C. M., Burstein, J., Swartz, J., Goff, J. A., Gulick, S. P. S., and Miller, C. B. (2024). Foraminiferal analysis of Holocene sea-level rise within the Trinity River Incised Paleo-Valley, Offshore Galveston Bay, Texas. *Marine Geology*, 107345.

Steel, R. J., and Milliken, K. L. (2013). Major advances in siliciclastic sedimentary geology, 1960–2012. *Geological Society of America, Special Paper 500*, 121-167.

Storms, J. E., and Swift, D. J. (2003). Shallow-marine sequences as the building blocks of stratigraphy: Insights from numerical modelling. *Basin Research*, *15*(3), 287-303.

Storms, J., Weltje, G., Terra, G., Cattaneo, A., Trincardi, F., (2008). Coastal dynamics under conditions of rapid sea-level rise: late Pleistocene to early Holocene evolution of barrier–lagoon systems on the northern Adriatic shelf (Italy). *Quaternary Science Reviews, 27*(11)*, 1107–1123.

Stuiver, M., and Reimer, P. J. (1993). Extended 14C data base and revised CALIB 3.0 14C age calibration program. *Radiocarbon*, *35*(1), 215-230.

Stutz, M. L., and Pilkey, O. H. (2011). Open-ocean barrier islands: global influence of climatic, oceanographic, and depositional settings. *Journal of Coastal Research*, *27*(2), 207-222.

Swift, D. J. (1975). Barrier-island genesis: evidence from the central Atlantic shelf, eastern USA. *Sedimentary Geology*, *14*(1), 1-43.

Switzer, A. D., Bristow, C. S., and Jones, B. G. (2006). Investigation of large-scale washover of a small barrier system on the southeast Australian coast using ground penetrating radar. *Sedimentary Geology*, *183*(1-2), 145-156.

Sydow, J., and Roberts, H. H. (1994). Stratigraphic framework of a late Pleistocene shelf-edge delta, northeast Gulf of Mexico. *AAPG bulletin*, *78*(8), 1276-1312.

Texas General Land Office (2023). Texas coastal resiliency master plan technical report. **www.glo.texas.gov/crmp**

Texas General Land Office (2020-2021). Coastal Erosion Planning and Response Act. https://www.glo.texas.gov/coast/coastal-management/forms/files/cepra-report-2017.pdf.

Thomas, M. A., and Anderson, J. B. (1994). Sea-level controls on the facies architecture of the Trinity/Sabine incised-valley system, Texas continental shelf. In R. Dalrymple, R. Boyd, B.A. Zaitlin (eds.), *Incised-valley Systems, SEPM Special Publication 51*, p. 63-82.

Thorne, J. A., and Swift, D. J. P. (1991). Sedimentation on continental margins, VI: a regime model for depositional sequences, their component systems tracts, and bounding surfaces. In D.J.P. Swift, G.F. Oertel, R.W. Tillman, J.A. Thorne (eds.), *Shelf Sand and Sandstone Bodies, International Association of Sedimentologists Special Publication, 14*, p. 189-255.

Toomey III, R. S., Blum, M. D., and Valastro Jr, S. (1993). Late Quaternary climates and environments of the Edwards Plateau, Texas. *Global and planetary change*, *7*(4), 299-320.

Törnqvist, T. E., Wortman, S. R., Mateo, Z. R. P., Milne, G. A., and Swenson, J. B. (2006). Did the last sea level lowstand always lead to cross-shelf valley formation and source-to-sink sediment flux?. *Journal of Geophysical Research: Earth Surface*, *111*(F4), F04002.

Troiani, B. T., Simms, A. R., Dellapenna, T., Piper, E., and Yokoyama, Y. (2011). The importance of sea-level and climate change, including changing wind energy, on the evolution of a coastal estuary: Copano Bay, Texas. *Marine Geology*, *280*(1-4), 1-19.

Van Andel, T. H., and Poole, D. M. (1960). Sources of recent sediments in the northern Gulf of Mexico. *Journal of Sedimentary Research, 30*(1), 91-122.

Wallace, D.J., and Anderson, J.B. (2013). Unprecedented erosion of the upper Texas Coast: Response to accelerated sea-level rise and hurricane impacts: *Geological Society of America Bulletin*, *125*(5-6), 728-740.

Wang, J., Church, J. A., Zhang, X., and Chen, X. (2021). Reconciling global mean and regional sea level change in projections and observations. *Nature Communications*, *12*(1), 990.

Watson, R.L. (1968). Origin of shell beaches, Padre Island, Texas. *PhD Thesis, University of Texas, Austin.*

Weight, R. W., Anderson, J. B., and Fernandez, R. (2011). Rapid mud accumulation on the central Texas shelf linked to climate change and sea-level rise. *Journal of Sedimentary Research, 81*(10), 743-764.

Westerink, J. J., Luettich, R. A., Feyen, J. C., Atkinson, J. H., Dawson, C., Roberts, H. J., Powell, M.D., Dunion, J.P., Kubatko, E.J., and Pourtaheri, H. (2008). A basin-to channel-scale unstructured grid hurricane storm surge model applied to southern Louisiana. *Monthly Weather Review, 136*(3), 833-864.

Wilkinson, B.H. (1975). Matagorda Island, Texas: the evolution of a Gulf Coast barrier complex. *GSA Bulletin 86(7)*, 959-967.

Yin, J. (2023). Rapid decadal acceleration of sea level rise along the U.S. East and Gulf coasts during 2010–2022 and its impact on hurricane-induced storm surge. Journal of Climate, 36(13), 4511–4529.

Zaitlin, B. A., and Shultz, B. C. (1990). Wave-influenced estuarine sand body, Senlac heavy oil pool, Saskatchewan, Canada. In: J.H. Barwis, J.G. McPherson, J.R.J. Studlick (eds.), *Sandstone Petroleum Reservoirs*. Springer, New York, N.Y, p. 363-387.

Zaitlin, B. A., Dalrymple, R. W., and Boyd, R. O. N. (1994). The stratigraphic organization of incised-valley systems associated with relative sea-level change. In: R.W. Dalrymple, B.A. Zaitlin (eds.), *Incised-Valley Systems: Origin and Sedimentary Sequences, SEPM Special Publication 51*, p. 45-60

Zecchin, M., Catuneanu, O., and Caffau, M. (2019). Wave-ravinement surfaces: classification and key characteristics. *Earth-science reviews*, *188*, 210-239.